POLITECNICO
MILANO 1863

SCUOLA DI INGEGNERIA INDUSTRIALE
E DELL'INFORMAZIONE

Laurea Magistrale in Ingegneria Meccanica

# OPERATING STRATEGY OF THERMAL ENERGY STORAGE SYSTEM FOR SOLAR TOWER CSP PLANTS WITH SUPERCRITICAL $CO_2$ CYCLE

Supervisor: Prof. Paolo Silva

Loretta TOMA

878810

Academic year 2017/2018

*A mamma, papà e Fede*

# *ACKOWLEDGEMENTS*

*"Made weak by time and fate, but strong in will*

*To strive, to seek, to find, and not to yield."*

Ulysses - Alfred Tennyson

Ringrazio il professor Silva per la guida e per i preziosi consigli, per avermi fatta appassionare alla sua materia e per essere stato paziente. Ringrazio Mohamed Bahaa, molto più di un supervisor, sempre disponibile e pronto ad aiutarmi in qualsiasi momento. Ancora, lo ringrazio perché ha contribuito nel farmi sentire a casa in una città per me totalmente nuova.

Grazie alla mia famiglia che ha sempre creduto in me.

Un grazie particolare ai miei genitori, Giuseppe e Sonia, che hanno esaudito ogni mio desiderio prima ancora che io lo esprimessi. A loro devo tutto. Senza il loro sostegno, il loro amore e la loro amicizia non sarei potuta arrivare alla fine di questo percorso. Mi hanno insegnato tutto quello che so. Quando penso a loro, capisco di essere una persona davvero fortunata. Li ringrazio perché mi hanno permesso di ritrovarmi tutte le volte in cui mi sono persa.

Grazie a mia sorella Federica, ancora e punto di riferimento da sempre, esempio di grande Donna. Grazie anche a tutti i litigi, che hanno avuto il merito di farmi guardare dentro e capire che in ogni situazione c'è più di un punto di vista e più di una verità.

Ringrazio con tutto il cuore i miei nonni, Gianni e Sofia, che mi mostrano con naturalezza ogni giorno cos'è l'amore, anche e soprattutto da lontano. Grazie perché sono sempre dalla mia parte.

Grazie alle mie bimbe meravigliose, Annachiara e Aurora, perché mi regalano tanta felicità.

Grazie ad Emanuele, sempre presente nel suo modo silenzioso e mai invadente.

Grazie a Giulia, migliore amica su cui so di poter contare, nonostante le nostre scelte ci separino. Grazie ai miei amici tutti, che mi supportano e sopportano.

Infine, voglio ringraziare dal profondo zio Salvatore per le sue poesie, attraverso cui ho scoperto una bellezza che non conoscevo, e zio Antonio.

# *ABSTRACT*

The reduction of the cost of solar electricity is a crucial step to make investments on solar energy economically convenient. In this study, the Concentrated Solar Power (CSP) technology is investigated even if its Levelized Cost of Electricity (LCOE) is still non-competitive, ranging from 89 to 181 $/MWh$_{el}$ (LAZARD, 2017), less than the value estimated by IRENA in 2012 (150 to 200 €/MWh$_{el}$) (IRENA, 2012), but it can be still reduced by enhancing the conversion efficiency or increasing the equivalent hours thanks to a Thermal Energy Storage (TES) system. Solar tower technology has the advantage of enhancing the efficiency thanks to the higher allowable operating temperatures and the easy integration with a TES system. As a matter of fact, storing thermal energy is the key to overcome world dependency on fossil fuels, whose usage is a direct consequence of our failure to collect and store energy from clean renewable sources, which is simply dissipated into the environment (Alva, Lin and Fang, 2018). CSP is the only renewable energy technology that allows an efficient and simple thermal storage, based on the mature molten salt technology, making solar energy dispatchable and, in addition, decoupling it from the electricity production. In this way, it is possible to obtain a baseload supply, that means to ensure the minimum electricity requirement over a period of 24 hours, even in the case of low or absent solar radiation. Along these lines, the capacity factor, defined as the ratio between the produced electricity over a period of time to the maximum producible electric power over that period, is consistently increased. The aim of this work is to evaluate the convenience of coupling CSP with a recompression closed supercritical carbon Dioxide ($sCO_2$) cycle, instead of the usual steam Rankine cycle, and to choose the correct fluid used as Heat Transfer Fluid (HTF) and the best suited for Thermal Storage (TS) medium.

The proposed and analysed system is an indirect configuration, composed of a heliostat field connected to a solar tower which exchange heat with a $sCO_2$ cycle through a primary heat exchanger. It is simulated using Ebsilon® Professional 13.01 for the entire day, taking advantage from the possibility to make the software work in accordance with on-purpose written Pascal scripts. So, the behaviour of the plant characteristic parameters is studied in detail as function of time. The simulation is extended to the four seasons in order to obtain yearly results. Given the objective of designing a flexible plant, a group of sensitivity analyses is carried on to examine the efficiency response to a variable output. With a view to optimizing the system without exceeding materials and molten salt limitations, further sensitivity analyses are performed, through dedicated Pascal scripts. Results show that the

minimum cycle pressure is not mandatory to be close to the critical one, whilst the maximum one together with the Turbine Inlet Temperature (TIT) are heavily affected by the solar loop maximum temperature, fixed at 565 °C for stability and corrosion issues. From the sensitivity analyses, the crucial role of the split ratio emerges: it ensures the correct amount of fluid flowing in both compressors, preventing the cycle heat exchangers from the pinch point problem occurrence, caused by the deep change in the specific heat capacity of the $sCO_2$ near its critical point.

All performance indicators are calculated, such as storage equivalent hours, power cycle thermal efficiency, whole plant solar-to-electric efficiency and capacity factor, after performing an estimation of the real weather conditions affecting the sun incident radiation. In addition, the investigation of the CSP technology when coupled with Combined Heat and Power (CHP) is carried on, for the sake of understanding the advantage of using heat from the sun to generate both electrical and useful thermal power, instead of wasting the potentially advantageous heat that would be rejected to the environment in separate production. Indeed, the adopted cooling system is a wet type, since it allows higher efficiencies, reduced initial costs and it is more robust and well-adaptable to the changeable ambient conditions.

Finally, with a view to comprehending the strong advantages achieved by a recompression $sCO_2$ cycle working under proper operating temperatures and pressures, the power cycle is simulated with Ebsilon® Professional 13.01 decoupled from the solar loop, whose maximum allowable temperature negatively impacts on the thermal efficiency.

The results highlight the absolute necessity of a novel salt compounds with a higher maximum allowable temperature and capable of withstanding higher fluxes for further system efficiency enhancement.

# *TABLE OF CONTENTS*

# *LIST OF FIGURES*

# *LIST OF TABLES*

# 1. INTRODUCTION TO CSP TECHNOLOGY

According to the World Energy Outlook (WEO) edited by the International Energy Agency (IEA) (International Energy Agency, 2017b), in the New Policies Scenario global energy demand grows more slowly than in the past, but still expands by 30 % between today and 2040. Compared with the past twenty-five years, the way that the world meets its growing energy needs has changed drastically: now, the key aspects are natural gas, rise of renewables and energy efficiency. Renewable energy sources meet 40 % of the increase in primary demand and their explosive growth in the power sector marks the end of the boom years for coal. Renewables attract two-thirds of global investments in power plants to 2040 since they represent an economically convenient source of new generation.

The estimated annual potential of solar energy, from the nuclear fusion in the Sun nucleus, may reach up to 49,837 EJ ($49{,}837 \cdot 10^{12}\ MJ$) (Alva, Lin and Fang, 2018), while the generated power is around $3.9 \cdot 10^{20}\ MW$, calculated from Eq. 1.1, where $\dot{\Delta m}$ is the lack of mass flow occurring during the transformation from hydrogen to helium and $c$ the light velocity. From the power, the constant $G$ of the flux reaching the Earth can be computed, based on Eq. 1.2, where the distance between Sun and Earth is considered. It represents the power distribution on a perpendicular surface of 1 m² on the Earth.

$$Power = \dot{\Delta m} \cdot c^2 = 4.3 \cdot \frac{10^9 kg}{s} \cdot \left(300{,}000\ \frac{km}{s}\right)^2 = 3.9 \cdot 10^{20}\ MW \qquad \textit{Eq. 1.1}$$

$$G = \frac{Power}{A} = \frac{Power}{\pi \cdot 1.5 \cdot 10^8\ km} = 1{,}350 \frac{W}{m^2} \qquad \textit{Eq. 1.2}$$

The solar spectrum, that is the distribution of the energy intensity, in other words the solar flux, as function of the wavelength λ, is close to the blackbody notion with a temperature almost equal to 5,500 K, as depicted in Figure 1.1. The wavelength band can be divided into three parts (La Casinière, Bokoye and Cabot, 1997):

1. ultraviolet region: 280 nm < λ < 390 nm;
1. visible light region:  390 nm < λ < 770 nm;
2. infrared region: 770 nm < λ < 900 nm

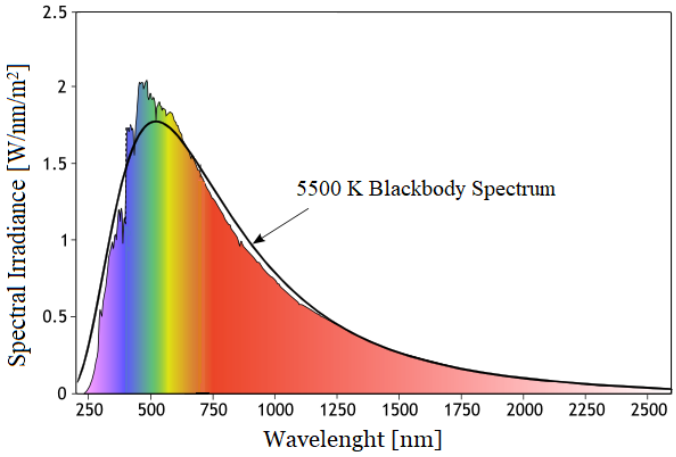


*Figure 1.1: Solar spectrum at the top of the atmosphere*

In Figure 1.1, the extra-terrestrial spectrum is depicted. The spectrum inside the atmosphere, in fact, is different. First of all, the molecules present in the atmosphere absorb a particular wavelength, creating additional peaks and valleys and giving birth to the so-called "Absorption" phenomenon: each molecule has an absorption, and consequentially attenuation, wavelengths band, like $O_2$ and $O_3$ in the ultraviolet and $H_2O$ and $CO_2$ in the infrared region. In the same time, "Scattering" occurs: it is the deviation of the radiation interacting with molecules in the atmosphere, generating the diffuse light. In particular, "Raileigh scattering" regards the small molecules at small wavelength and it is an isotropic phenomenon, while "Mie scattering" occurs when the radiation interacts with bigger molecules and it is not dependent on the wavelength (Figure 1.2).

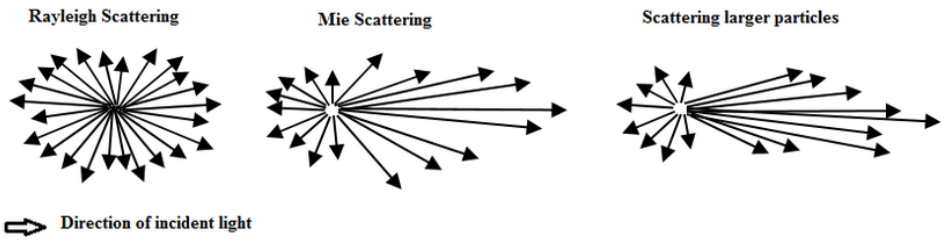


*Figure 1.2: Scattering mechanisms*

All the atmospheric attenuations are well represented by the "Air Mass" parameter (AM), which represents the optical path length of the sun radiation through the atmosphere. It is defined as the ratio between the passed through atmosphere mass and the amount through which the radiation would pass if the surface was perpendicular to it. The AM is well

approximated by Eq. 1.3, where $\Theta$ is the zenith angle and it is function of the time of the day and the period of the year, as well as of the surface position and tilt angle. So, it is affected by the Sun elevation and by the observer latitude, that is the location of the surface (Figure 1.3 (Green Rhino Energy Ltd, 2016)). Minimizing the AM factor, the highest flux is obtained.

$$AM = \frac{1}{\cos \Theta} \qquad \textit{Eq. 1.3}$$

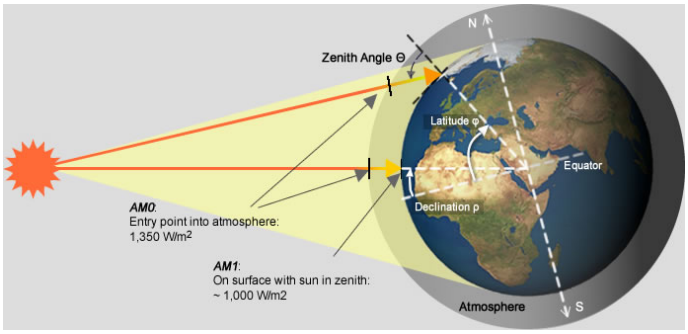


*Figure 1.3: Sun angles (Green Rhino Energy Ltd, 2016)*

Figure 1.4 shows the attenuation on the solar energy reaching the Earth surface, represented by the bright colours.

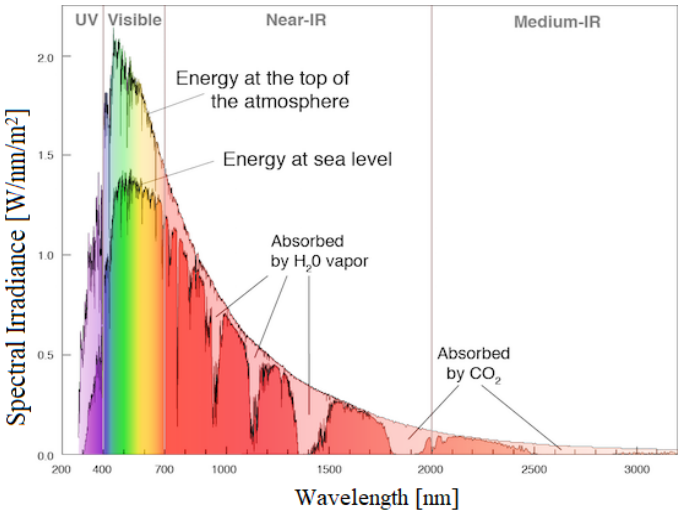


*Figure 1.4: Solar extra-terrestrial and terrestrial spectrum (Rosen and Egger, 2016)*

Apart from the energy of the sea waves, linked with the mutual gravity with the moon, and the geothermal energy, all renewable energy sources are directly or indirectly connected with the Sun. However, electricity could only be generated directly from the Sun power, using concentrated solar power technology (CSP) or photovoltaic panels (PV).

## 1.1. Photovoltaic technology

As earlier discussed, the Sun energy hitting the Earth is composed of direct and diffuse irradiation. Photovoltaic technology enables the exploitation of both quantities, taking advantage of the so-called "Photovoltaic effect", converting directly the energy from the Sun into electricity. The PV cells are made up of semiconductor materials, whose valence and conduction bands are quite close to each other. For the sake of simplicity, Silicon cell is considered. On its crystal lattice, the bond between the electron and the atoms sharing it is strong, so a quite big amount of energy is necessary to break it and move the electron from the valence to the conduction band, where it becomes free to move. If this amount of energy is provided, a positive hole is created in the valence band. However, in order to conduct electricity, a continuous flux of electrons is necessary and, consequentially, a continuous generation of positive holes in the valence band, that can be filled up by other electrons. In this way, an electric field is created inside the cell. An N-type semiconductor is obtained by introducing small amount of Antimony or Phosphorous, negatively charged, in the crystallin lattice and a P-type is achieved using Boron atoms, positively charged. While separated, they are electrically neutral. But if they join together, a P-N junction is created: some electrons from the N-doped side migrate through the junction towards the P-doped side to fill up the holes, producing negative ions. This phenomenon is known as "diffusion". On the N-type material, the concentration of positive charges increases and, as a consequence, the holes migrate through the junction in the opposite direction. As a result, near the junction of the N-type material there is a high concentration of positive charges, while on the P-type material side the negative charges are accumulating, until they reach equilibrium. So, an internal electric field is generated across the junction and, the moving electrons generated by the light (photons) absorption on the N-type material are no longer able to overcome the junction. The same for the positive holes on the P-material. At this point, an external circuit is used to collect the generated electricity, as shown in Figure 1.5 (Hanania *et al.*, 2015).

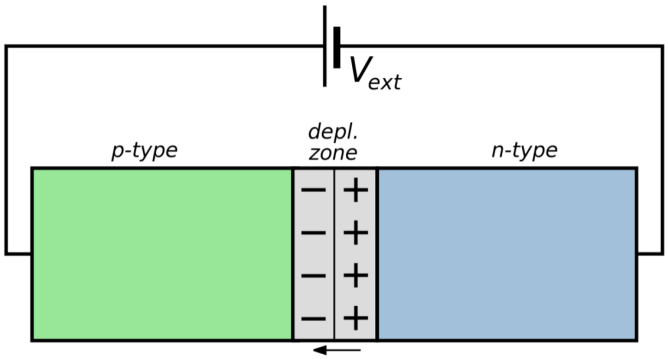


*Figure 1.5: P-N junction (Hanania et al., 2015)*

The laboratory conversion efficiency for photovoltaic cells depends on the used technology: for Si-panels, it is up to 25 % for single junction cells and around 38 % for multijunction ones (Green *et al.*, 2017).

## 1.2. Thermodynamic-based solar system

In this case, only the direct irradiation could be exploited. The aim of the thermodynamic system is to heat up a fluid by solar thermal power and use it to supply a power conversion cycle in order to produce electricity or, sometimes, thermal power as well. A promising advantage offered by this type of technology is the potential reduction of costs thanks to the economy of scale: increasing the plant size, the costs will be reduced, while PV technology costs are proportional to the number of installed modules. In addition, thermodynamic conversion is performed through well-established technologies. The crucial benefit of the thermodynamic system is the possibility to have dispatchable energy: the electricity production can be easily decoupled from the availability of the solar source. This means that the thermodynamic solar technology integrated with a storage system has the potential to increase the equivalent plant hours and to allow for baseload power supply, which all the other technologies cannot ensure. The storage system is a thermal type, so the accumulation of energy is done by physically storing a fluid. In this way, the use of non-environmentally friendly batteries typical of PV is avoided. The biggest disadvantage is represented by the high initial costs which are expected to diminish thanks to the economy of scale impact. By 2020, an initial costs reduction of up to 40 % and more is foreseen (IRENA, 2012a).

# 2. STATE OF THE ART

Nuclear fusion reaction continuously occurring at the core of the Sun produces a huge amount of solar radiation towards Earth. As earlier said, the estimated annual potential of solar energy may be up to 49,837 EJ ($49{,}837 \cdot 10^{12}$ *MJ*) (Alva, Lin and Fang, 2018), much higher than the world annual "total primary energy supply" that IEA estimated as 13,647.37 millions of oil equivalent, amounting to 571 EJ for 2015 (International Energy Agency, 2017a). However, for the same year, the "primary energy supply" from sources including solar, geothermal and wind together is only 8 EJ (1.4 %): clearly, solar energy potential is not exploited (Alva, Lin and Fang, 2018). The IEA target of 630 $GW_{el}$ power generation using CSP by 2050 has been inciting researches to find the best way to optimize power plants and obtain the highest possible efficiency. Given the unique CSP property of making energy dispatchable, many possibilities of reducing its LCOE are under investigation. One possibility consists in finding new and advanced materials with better properties of handling thermal storage, such as withstanding higher temperatures, which is beneficial to improve conversion efficiency. Indeed, the strong advantage of concentrating the solar radiation over adopting photovoltaics lies in the easier and cheaper possibility of storing heat instead of electricity: the plant results more flexible and the power demand can be followed in real time, even during the night, without employing big, costly and non-environmentally-friendly batteries, needed by the photovoltaics panels (Temple, 2017). Another option is acting on the thermodynamic side, trying to enhance the power block efficiency and looking for the best cycle that fits the solar plant and, in particular, the solar tower requirements, which nowadays is considered the most promising technology in terms of performance improvements. Indeed, the overall efficiency of a CSP plant depends on two different conversion processes: the efficiency of the energy conversion from solar to thermal power and the one from thermal power to electricity. Considering a solar tower receiver, which recent studies show to be the best suited technology to reduce LCOE (Bauer *et al.*, 2013; Dieckmann *et al.*, 2017; Eurekalert, 2018), as shown in Figure 2.1: (IRENA, 2012b), the main factor influencing these two efficiency terms is the outlet receiver heat fluid temperature. As a matter of fact, it has a conflicting role: on one hand, the higher it is,

the higher the power block efficiency results, following Carnot Theorem; on the other hand, increasing it, the receiver efficiency is reduced since losses increase and problems related to the HTF stability arise. So, as a direct consequence, the best efficiency point results from a compromise between both terms. Maximizing it, the investment on the CSP technology can be more attractive and money making.

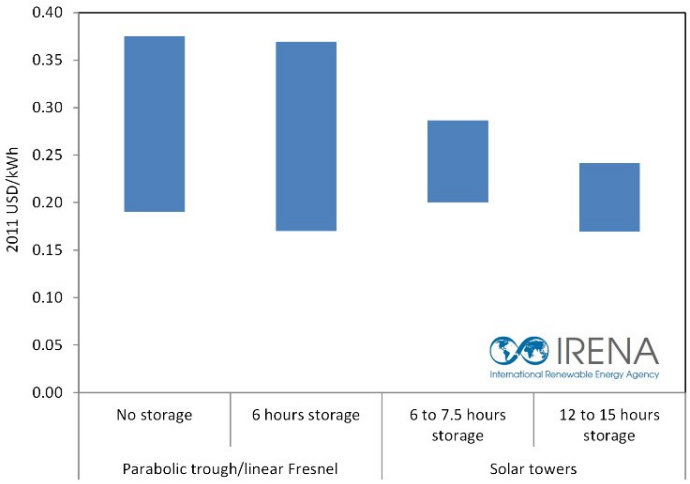


*Figure 2.1: LCOE in CSP plants (IRENA, 2012b)*

## 2.1. Supercritical CO2 properties

When a fluid is heated up under high pressure, a strong change on its physical properties occurs and it is defined as supercritical. Under these particular conditions, the fluid has the solvating power of a liquid and the viscosity of a gas, while physically the two phases are not distinguished. This means that it is characterized by a density similar to a liquid and its surface tension is as low as the one of a gas.

The interest in supercritical $CO_2$ as working fluid for power cycles is due to its critical temperature near to the ambient temperature, 30.98 °C, and a relatively low critical pressure, equal to 7.38 MPa, compared to water, whose critical point is around 374 °C and 22.064 MPa (Ahn *et al.*, 2015). The compressibility factor, *Z*, is defined as the molecular volumetric ratio of a fluid compared with ideal gas (Eq. 2.1) and indicates whether the fluid behaves as an ideal gas or as a liquid. If it is unity, the fluid behaviour is very close to an ideal gas, whilst it is considered to be an incompressible fluid when *Z* is near zero. Regarding $CO_2$ near the critical point, the compressibility factor decreases to 0.2 and 0.5 (Figure 2.2) and it can be considered to act as a liquid, as shown in the figure below (Ahn *et al.*, 2015).

$$Z = \frac{P \cdot M}{\rho \cdot R \cdot T} \qquad \textit{Eq. 2.1}$$

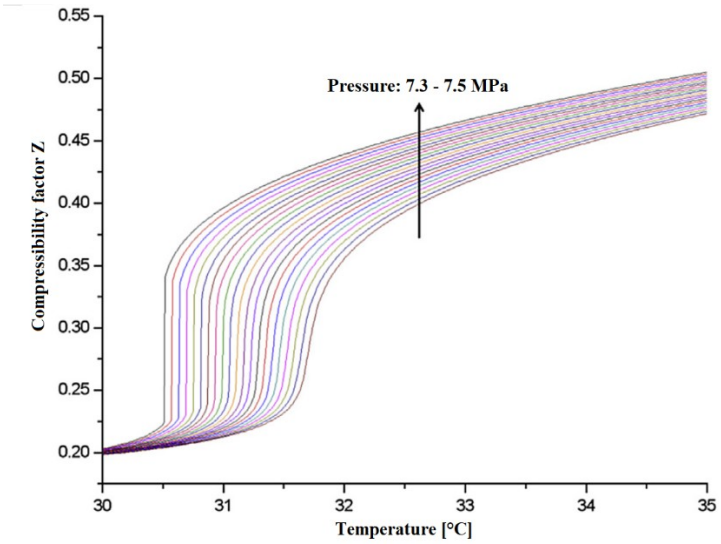


*Figure 2.2: $CO_2$ compressibility factor near the critical point (Ahn et al., 2015)*

These properties have been studied to optimize the closed $sCO_2$ cycle in order to decrease the work needed by the compressor, since the compression process occurs near the critical point, where the working fluid behaves as a liquid, and then it evolves to supercritical conditions, so that the cycle efficiency should increase. Moreover, $sCO_2$ is less corrosive compared with steam at the same temperature: consequentially, the $sCO_2$ cycle can potentially operate with a higher turbine inlet temperature, which is one of the most challenging and affecting parameters of the cycle.

## 2.2. Receiver technology

The aim of the solar field is to collect as much solar energy as possible and to convert it into heat at high temperature which will be use in a power block. CSP technology allows the exploitation of only the Direct Normal Irradiance (DNI), which is the amount of solar radiation received in a collimated beam on a plan normal to the Sun (Blanc *et al.*, 2014). Reflecting surfaces to point the radiation towards a target are used, with a very high reflectivity at all the wavelengths and especially at the lowest, associated to the solar spectrum (see again Figure 1.4). In Figure 2.3 (Vignarooban et al., 2015) the four most common CSP technologies are shown. Linear-focused CSP systems work at lower temperatures than point-focused ones.

The most mature technology for CSP is the Parabolic trough (PT) (E, Kearney and KOLB, 1999), thanks to the well proved plants in California by SEGS (E, Kearney and KOLB, 1999)

and, more recently, in the United States (Gilbert and Cohen for ACCIONA, 2010) and in Spain (Fernández-García *et al.*, 2010; Relloso and Delgado, 2009; Solar Millenium AG, 2008). Up to now, there are more than 70 utility scale power plants operating in the world (Dieckmann *et al.*, 2017). The spread of PT is linked with its inexpensiveness and maturity, even if it has a low concentration factor, of the order of 15-50 suns (concentration ratio is defined as the ratio between the collecting area e the receiver area), with an operating temperature ranging between 50 °C and 400 °C and annual radiative losses at high temperature of around 10 % (Barlev, Vidu and Stroeve, 2011; Binotti *et al.*, 2017).

Another wee-enstablished technology is based on the linear Fresnel reflector (Heimsath *et al.*, 2014), that is easy to be built and cheaper, but its efficiency is strongly penalized by the poor optical efficiency. In addition, it has a lower concentration ratio and a narrow operating temperature range (Barlev, Vidu and Stroeve, 2011), even if it can be economically convenient since it allows the Direct Steam Generation plant configuration, avoiding the costly intermediate heat exchanger necessary for the indirect plant configuration.

One additional possibility can be the Dish-Stirling, consisting in a disc concentrating the heat in one point of the Stirling engine, that uses it as a fuel. It is a recent and expensive technology, with a maximum operating temperature equal to 1500 °C and CR ranging between 100-1000 suns, but it is fundamental to follow the sun accurately in order to exploit the technology potential (Barlev, Vidu and Stroeve, 2011). This technology differs from the others since it does not need a heat transfer fluid, the storage system is very difficult to be integrated and it does not scale-up (while other technologies costs will drastically reduce when the plant dimension increases, following the economy of scale effect). The structure is very heavy and expensive: the adoption of small mirrors to form the huge dish is a way to reduce costs. Using a heat engine and a high energy conversion cycle makes the Dish-Stirling an efficient technology, as well as linking the dish and the power cycle with an intermediate heat pipe receiver, providing a quite isothermal heat and decreasing convective losses (Barlev, Vidu and Stroeve, 2011).

Recently, given the high potential concentration ratio (typically from 500 to 2000 suns) which allows to operate at higher temperatures and to reach more efficient thermodynamic conversion power cycle (Barlev, Vidu and Stroeve, 2011; Moser, Trieb and Fichter, 2013), Solar tower (ST) is seen as the technology that could better reduce the CSP LCOE (Dieckmann *et al.*, 2017; Relloso and García, 2015). In fact, the Solar Tower special design is based on the heliostats, flat movable mirrors with a two-axis tracking system and a surface of the order of 50-150 $m^2$, that face the sun and focus the direct radiation on the top of the receiver, put at a height of about 75-150 m. Compared with linear concentrators, such as PT and LF, concentration capabilities are substantially improved, thanks to the focusing

of a massive sun radiation on a single point, resulting in a considerable reduction of the receiver losses and, more important, in a simplified heat transport and, eventually, storage. CSP plants equipped with ST and heliostats generally have an installed capacity bigger than 10 $MW_{el}$ because they have to take advantage of the economy of scale in order to face their huge initial costs.

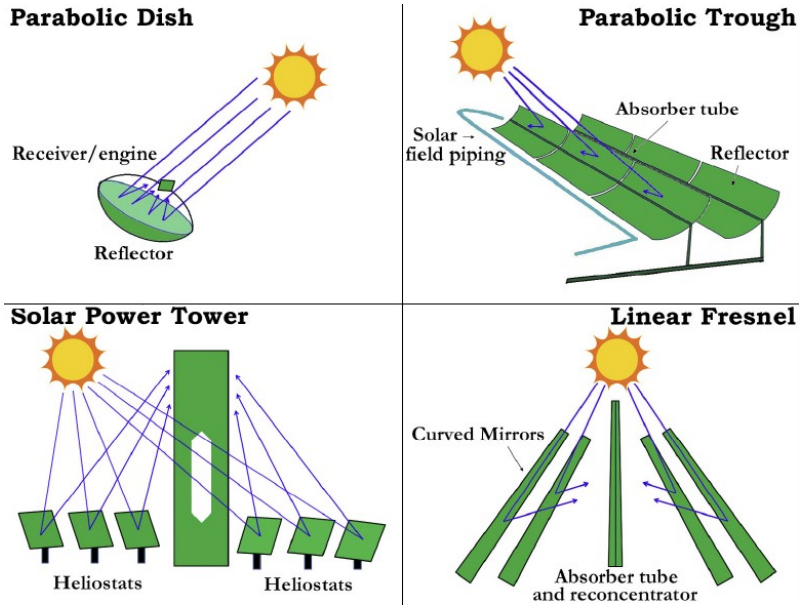


*Figure 2.3: CSP technologies (Vignarooban et al., 2015)*

### 2.2.1 Solar tower configurations

For solar tower, different receiver configurations are presented in numerous experimental studies: the traditional solar receiver installed at the top of the central tower (Ho and Iverson, 2014), multi tower receiver (MTSA), the Solar Concentration Off-Tower (SCOT). The first one is the one evaluated in this study; the second option, multi-tower solar array (MTSA) , is a new concept consisting in more than one solar tower receiver, each closed to the other, so that the heliostat fields partly overlap and the radiation that would not be used by conventional solar tower can be exploited, leading to a consequent more efficient usage of the ground area (Schramek & Millis, 2003); the third configuration is made up of a hyperboloid reflector set on the top of the tower that focuses the incident beam on an array of secondary concentrators (CPC) and then receivers near the ground, allowing better collection optics, a stable flux distribution and reduced costs since the plant is at the ground level, eliminating long pipes and high towers (Kribus, et al., 1998). All the efforts are directed to reach higher operating temperatures and bigger fluxes, so to have better efficiencies.

Nowadays, lots of different receiver designs under research have been proposed (Ho and Iverson, 2014) and tested, but only few of them have been proved in a real plant. In fact, the receiver is one of the most affecting components because solar power is absorbed and transferred to the HTF there, so it has a direct impact on the overall efficiency. According to the previous paper, the most common design for solar tower results to be the tubular receiver with either liquid or gas/liquid fluid, even if improving its efficiency is difficult, given the high costs of nickel-alloys and the long-term operations needed to adapt the tubular receiver at high temperature and pressure. For this reason, it is convenient to choose the best working fluid that manages to improve the receiver efficiency and the receiver design that best suits the properties of the coupled power cycle. Anyway, given the size of these plants (10 MW and above), the beneficial effect of economy of scale is needed in order to offset the high installation costs.

### 2.2.2 Heat transfer system

The choice of the fluid to be heated up (HTF) is crucial to improve CSP performances and maximize efficiency, given that the higher the temperature is at the receiver outlet, the higher the power block efficiency is but, on the other hand, the higher the receiver losses are, too.

Since a large amount of HTF is required, it is necessary to minimize its costs while looking for better performances. The desired properties that a fluid is expected to have in order to be used to transfer heat are (Cordaro, Rubin and Bradshaw, 2011; Pacio and Wetzel, 2013; Vignarooban *et al.*, 2015):

1. low melting point and high boiling point, to allow a large operating range in which it is in the liquid state;
2. thermal stability, since it has to withstand big fluxes and high temperature to maximises the efficiency;
3. low vapour pressure (<1 atm) at high temperature, so that stresses on pipes are reduced;
4. low corrosion with metal alloys used to contain it;
5. low viscosity to reduce pumping losses, high thermal conductivity and high heat capacity, in the case it is used also for energy storage;
6. low cost.

Recently, molten salts, commonly in a mixture made up of 60 % in weight of sodium nitrate ($NaNO_3$) and 40 % in weight of potassium nitrate ($KNO_3$), known as Alkali Nitrate Salts (Carling *et al.*, 1981), are the most used by virtue of their low vapour pressure, the wide operating range (reaching temperatures higher than 500 °C), the high heat capacity that makes them suitable also as storage media, allowing the adoption of a direct TES system,

low corrosiveness and good physical and fluid-dynamic properties at high temperatures (Peng, et al., 2010). Molten salts not only are capable of storing energy and withstand high temperatures, but they are also cheaper than other HTF such as organics, liquid metals or synthetic oils. The main problem related to CSP plants operating with molten salts is the corrosion of piping and container alloys: HTF acts as the electrolyte in a corrosive system that attacks the metal containers, especially at the higher temperatures necessary to increase the CSP efficiency (Bauer *et al.*, 2013). Since molten salts allow operation up to 800 °C, corrosion is enhanced compared to other HTFs and temperatures need to be reduced.

As mentioned before, molten salts are widely used as HTF firstly thanks to their stability at temperatures higher than 500 °C. Secondly, their viscosity and vapour pressure are very low, comparable with water (Peng, et al., 2008). The first molten salt power tower systems were installed in 1984: the THEMIS tower (2.5 $MW_{el}$) in France and Molten-salt Electric Experiment (1 $MW_{el}$) in the United States (Dunn, Hearps and Wright, 2012). Another fundamental advantage that makes utilizing molten-salts in the power tower systems interesting for improving performances, as mentioned before, is their capability for thermal energy storage. In 1996, USA installed the first solar system operating with molten-salts as both HTF and storage media, adopting a direct TES, "Solar Two": 10 $MW_{el}$ power plant with energy storage capability of 3h. Later, in 2008, in Spain "Gemasolar" (initially called "Solar Tres") was established, after the launch of "Andasol-1" (Dunn, Hearps and Wright, 2012), a PT plant with oil HTF in an indirect TES configuration (Bauer *et al.*, 2013), and it was the first one operating commercially with a direct molten salts TES concept: 19.9 $MW_{el}$ with energy storage capability of 15h. All the configurations are coupled with a Rankine cycle.

## 2.3 Thermal energy storage system

As already said, one important concern in CSP designs is the capability for Thermal Energy Storage (TES), to allow the power generation even during low or absent sun radiation hours. After the crisis of 1970s, the world started focusing on renewable energy sources and conserving energy: in this sense, thermal energy storage has a fundamental role (Alva, Lin and Fang, 2018), recovering thermal energy that otherwise would be wasted and rejected to the environment. A notable increase in the use of TES systems is registered: presently, half of the worldwide CSP plants are integrated with a TES system, while the 72 % of plants under construction are projected to have a TES system and the 77 % of the future plants will have this kind storage system.

Table 2.1 explains the feasibility of coupling the existing CSP plants with a TES system (Pelay, et al., 2017).

*Table 2.1: TES integration feasibility for CSP plants in operation (Pelay, et al., 2017)*

| CSP plant type | Solar CR | Operating range temperature [°C] | TES feasibility | Remarks |
|---|---|---|---|---|
| PTC | 15-45 | 20-400 | Possible | Most used |
| LFR | 10-40 | 5-300 | Possible | Very few |
| SPT | 150-1500 | 300-1000 | Possible with lowest costs | Most used with higher Rankine cycle efficiency |
| PDC | 100-1000 | 120-1500 | Difficult | Very few with higher Rankine cycle efficiency |

Nowadays, in Spain all the power plants are equipped with molten salts storage systems: they can cope with stressed conditions and they are cheaper than other materials with comparable properties, such as liquid metal, now under investigation, or synthetic oils. In addition, molten salts are suitable for both HTF and storage media (Vignarooban *et al.*, 2015), so that the direct TES system is adopted, as shown in Figure 2.4 (Alva, Lin and Fang, 2018), avoiding the additional costs related with the intermediate heat exchanger. In direct TES configuration, one single fluid acts both as HTF for the solar field and as HTF for the storage system (Alva, Lin and Fang, 2018). In this case, the molten salt is heated up in the solar tower and sent to the storage loop: when the sun radiation is abundant, one part of the heated salt goes directly to the heat exchanger which realizes the coupling with the power block to heat the working fluid, whilst the left mass flow is stored in the hot tank and it will be used when the sun radiation is too low or absent. After the heat transfer process, the molten salt is sent to the cold tank and pumped back to the tower.

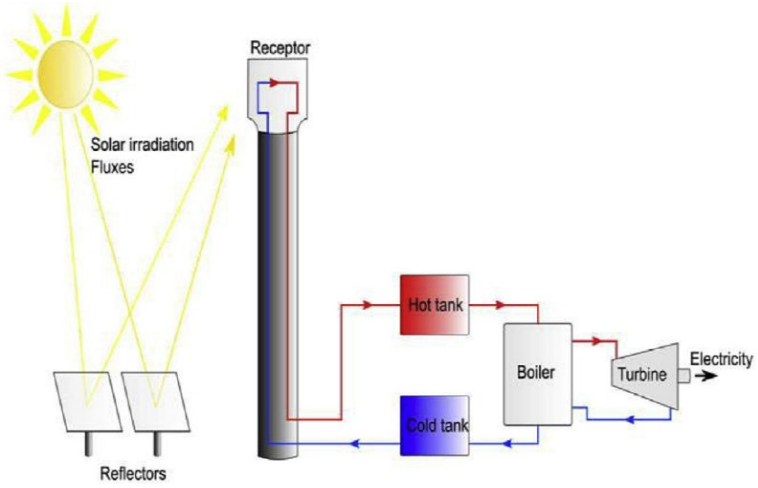


*Figure 2.4: Example of direct TES system (Alva, Lin and Fang, 2018)*

On the contrary, the indirect TES system, depicted in Figure 2.5 (Alva, Lin and Fang, 2018), is necessary when the HTF circulating in the solar field is characterized by a very wide operating temperature, with low melting point of the order of the ambient temperature, but also by a low volumetric heat capacity, for instance in the case of liquid metals, which makes them not suitable for storing energy: an intermediate heat exchanger is needed in order to transfer the heat from the solar field HTF, that is the liquid metal, to the storage media, generally a molten salt. Another example of the indirect TES adoption is the case of PT, when the solar field pipes are so long that their temperature decreases and the molten salts would freeze if used as solar field HTF: as a result, thermal oils are used in the solar field and, through the heat exchanger, they transfer the absorbed heat to the molten salts used only as a storage media (Alva, Lin and Fang, 2018). This choice is due to the minimum temperature (Table 2.2 (Alva, Lin and Fang, 2018; Vignarooban *et al.*, 2015)) of thermal oil (12 °C) much lower than the molten salts one (290 °C), preventing the cycle from circulation of a freezing fluid in the very long pipes.

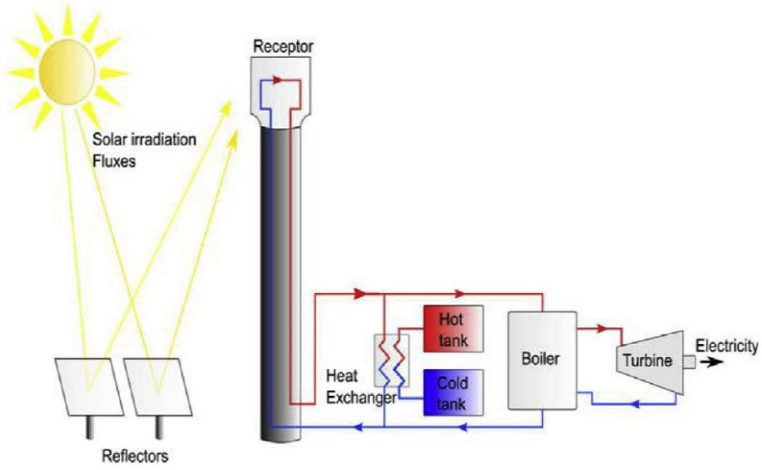


*Figure 2.5: Example of indirect TES system (Alva, Lin and Fang, 2018)*

The heat storage mechanism can be active or passive. The passive technique does not require pumping work for charging and discharging the tanks, but it exploits thermal inertia or natural convection to make the fluid circulate (Heier, Bales and Martin, 2015). It is employed for small applications such as buildings, automobiles, food and textiles and the fluctuant temperature can be mitigated by the latent heat of Phase Change Materials (PMC) to stay in the comfort region. Conversely, the active technique must be applied in the case of big plants characterized by long pipes and large amount of viscous HTF: in these conditions, pumping work is required in order to make the fluid circulate in the storage loop. Thermocline, packed bed, fluidized bed, moving bed, tank systems, concrete block are examples of active techniques (Alva, Lin and Fang, 2018). Table 2.2 shows the main features of the liquids which are currently used as thermal heat storage materials (Alva, Lin and Fang, 2018; Vignarooban *et al.*, 2015).

*Table 2.2: Thermal and physical properties of commonly used storage media fluids*

| Technology | Strengths | Weaknesses | Opportunities | Threats |
|---|---|---|---|---|
| **Sensible heat storage material: *Water*** | Very high specific heat;<br>Non-toxicity, Cheap;<br>Easy availability. | High vapour pressure;<br>Corrosiveness;<br>HTF outlet temperature is not steady. | The best suited for home space heating, cold storage of food products and hot water supply type of applications.<br>In CSP using direct generation, steam accumulators are used | Compatibility with pipeline materials. |

| Technology | Strengths | Weaknesses | Opportunities | Threats |
|---|---|---|---|---|
| | | | (Roubaud, et al., 2017).<br><br>When liquid, it can form a thermocline thanks to the difference in density that generate a temperature gradient (Gil *et al.*, 2010).<br><br>For cold application, water is used in chilled water form or in ice form.<br><br>Very high heat capacity means very high energy density. | |
| **Sensible heat storage material: *Thermal oils*** | Good heat transfer capacity (heat transfer coefficient in the range of 1000-3000 [W $m^{-2}$ $K^{-1}$]) (Benoit *et al.*, 2016);<br><br>Big operative temperature range (12 °C-400 °C) and more heat storage;<br><br>Lower vapor pressure than water;<br><br>Low viscosity; | Low thermal conductivity, so mediocre heat transfer properties;<br><br>Lower specific heat than water;<br><br>More expensive;<br><br>Fire risk if in contact with air;<br><br>Limit temperature is equal to 400 °C.<br><br>HTF outlet temperature is not steady. | They maintain their liquid state at lower temperature than water up to 250 °C under atmospheric pressure. They can form a thermocline and they do not freeze in pipelines.<br><br>Lower vapour pressure means lower pressure in the container and in the pipelines, so that costs are reduced.<br><br>Low pumping losses.<br><br>They fit very well CSP direct configurations as both HTF and TES material. | Above their operating temperature, they degrade and form acids that accelerate corrosion processes.<br><br>In addition, they show degradation with aging after repetitive thermal cycles and many hours under high temperature. |

| Technology | Strengths | Weaknesses | Opportunities | Threats |
|---|---|---|---|---|
| | Good flow properties. | | Possible to improve their heat transfer properties thanks to the addition of nano-additives like graphene, graphite and metal oxides (Wang, et al., 2017). | |
| **Sensible heat storage material:** ***Liquid metals*** | Low melting point and very high boiling point;<br>No freezing problems;<br>Zero vapour pressure;<br>Very large thermal conductivity, hence very good heat transfer properties;<br>Very large heat transfer coefficient;<br>Very high thermal stability. | Expensive;<br>Corrosiveness;<br>Rick of fire (Na);<br>Lower heat capacity;<br>Lower storage density;<br>Higher costs;<br>HTF outlet temperature is not steady. | Best suited HTF for high temperature applications.<br>Solar receiver tube wall temperature gradient will be very low, resulting in lower heat losses to the environment and improving the receiver efficiency.<br>Very efficient heat exchange process (heat transfer coefficient is high) even with small temperature difference. So, higher heat fluxes are possible. | Due to the relatively lower volumetric heat capacity, liquid metals require a higher velocity, so a consequent higher pressure drop, in order to transport the same thermal power, and a bigger tank for storage is required.<br>They are not economically convenient as storage media but only as HTF, so the additional cost of the heat exchanger has to be taken into account. |

| Technology | Strengths | Weaknesses | Opportunities | Threats |
|---|---|---|---|---|
| **Sensible heat storage material:** ***Earth materials*** | Cheap;<br>Easily available;<br>Non-toxic and non-flammable;<br>High thermal conductivity;<br>High thermal storage density. | Lower thermal stability (maximum 300-400 °C).<br>HTF outlet temperature is not steady. | They are used as fillers in single tank thermocline storage system and they act as both heat transfer surface and storage medium, exchanging heat in direct contact so that the contact surface between TES material and HTF is large and costs are reduced. They are usually used as TES material coupled with thermal oil as HTF, but sometimes with air for space heating.<br>Sand or natural rocks as filler material may reduce the quantity of the HTF required for charging and discharging thermal energy up to 80 %.<br>All rocks have almost similar thermo-physical characteristics and are suitable for filler materials with operating temperatures up to 350 °C (Grirate *et al.*, 2014). | Local availability, low cost, density, heat capacity and thermal conductivity, high surface hardness to resist abrasion, low porosity to prevent oil infiltration, high mechanical strength have to be taken into account when choosing rocks and sands for bed filler materials.<br>They can only be the TES material, so indirect configuration in required. |
| **Sensible heat storage material:** | Low costs;<br>Easy construction; | Low specific heat and low | They are suitable for TES up to 550 °C. | |

| Technology | Strengths | Weaknesses | Opportunities | Threats |
|---|---|---|---|---|
| ***Concrete blocks*** | Good mechanical<br>Properties;<br>Non-toxic and non-flammable. | thermal conductivity;<br>HTF outlet temperature is not steady. | Curing and heat absorption make possible to use them as TES materials. | |
| **Latent heat storage systems materials** | Higher energy storage density;<br>Compact TES system;<br>Non-toxic;<br>Steady outlet temperature. | Very poor thermal conductivity, in the range between 0.1 and 1 [$W \cdot m^{-1} \cdot K^{-1}$] | Usually solid-liquid phase change is used. Although for solid-solid phase change specific latent heat is lower, it has the advantage of no leakage.<br>Compared to sensible heat storage material, their specific heat is 50-100 times bigger and therefore the thermal energy storage density is bigger. | Even if liquid-gas phase change has the highest latent heat of phase change, it is not used because of the enormous volume change.<br>During the change of phase, poor thermal conductivity of solid layers is a problem.<br>In liquid phase it is overcome by the convection. |
| **Thermal energy storage materials for chemical heat storage** | Highest thermal energy storage;<br>Long duration of thermal energy storage;<br>Low heat losses. | | Different approaches to increase the charging rate like graphite nanoplatelets composites (Mastronardo, et al., 2016), doping with lithium (Yan & Zhao, 2016) etc are attempted and improvements are observed. | During charging, when decomposition occurs, the storage material like $Mg(OH)_2$ may undergo sintering and grain growth resulting in lower porosity. During discharging, this hinders the rehydration process. The rate |

| Technology | Strengths | Weaknesses | Opportunities | Threats |
|---|---|---|---|---|
| | | | | of dehydration reaction is slow.<br>Still in laboratory phase. |

It is possible to conclude that, for the CSP technology, the most commonly used TES system is the direct one with molten salts, thanks to their wide range of application, their relative low cost and their properties to perform both the HTF solar field and storage media role. In fact, their volumetric heat capacity is very high, as well as their boiling point and thermal stability. They have negligible vapor pressure, like liquid metals and negligible. Molten salts are cheap, non-toxic nor flammable and available. But their lower temperature is above 200 °C, so freezing problems in pipelines are common, especially during night. Their thermal conductivity is around 0.5 [$W \cdot m^{-1} \cdot K^{-1}$] and the heat transfer coefficient ranges almost between 1,500 [$W \cdot m^{-2} \cdot K^{-1}$] and 6,500 [$W \cdot m^{-2} \cdot K^{-1}$], depending on the considered compound. Unfortunately, in general the employment and diffusion of TES system is decelerated by the excessive initial investments, which make the fossil fuel usage economically more convenient, given the actual level of technology development. By the way, researches and experiments have been carried on for the purpose of finding alternative cheaper material for TES (Alva, Lin and Fang, 2018).

## 2.4 Power conversion system

CSP is a versatile technology easily integrable with the most common power conversion systems. So, it takes advantage from well-known and established technologies, without requiring additional increase of costs.

### 2.4.1 Steam Rankine cycle

All the currently operating ST are based on the traditional Rankine steam cycles, made up of a steam generator, a turbine, a condenser and a pump, as depicted in Figure 2.6. In this configuration, firstly the working fluid is pumped from low to high pressure, requiring little work if the fluid is a liquid: the small amount of needed pumping work is one of the essential advantages offered by Rankine cycles. High pressure water is heated in a boiler, where heat collected by the HTF is transferred to the water, at a constant pressure, to become saturated vapor. Here, a disadvantage of the steam Rankine cycle emerges: the steam generator is made up of three stages, that are the pre-heater, the evaporator and the superheater. It is a

big and heavy component, clearly expensive. The vapor is then expanded through a turbine to produce electricity. The turbine inlet conditions are fundamental with a view to obtaining a high efficiency: if vapor temperature is not very high, the fluid is wet vapor and condensation could occur in the turbine, where fast-moving water droplets damage it and reduce its lifetime and efficiency. On the contrary, increasing the TIT, dryer vapor is surely produced, which can thus considerably increase system performance (Barlev, Vidu and Stroeve, 2011). Unfortunately, the fluid temperature at the turbine inlet has a limitation around 600 °C (experimentally, 627 °C if the inlet turbine pressure is equal to 30 MPa) caused by material components issues: steam is corrosive increasing the pressure (Dunham and Iverson, 2014). The main steam Rankine cycle drawback, which makes ORC an interesting possibility, is that it needs high temperature and high pressure to be economically interesting and profitable, that means high installed power. In addition, given the very high pressure ratio and enthalpy drop, multi-stages turbines need to be adopted, causing considerable initial costs and, above all, a huge footprint (Quoilin *et al.*, 2013).

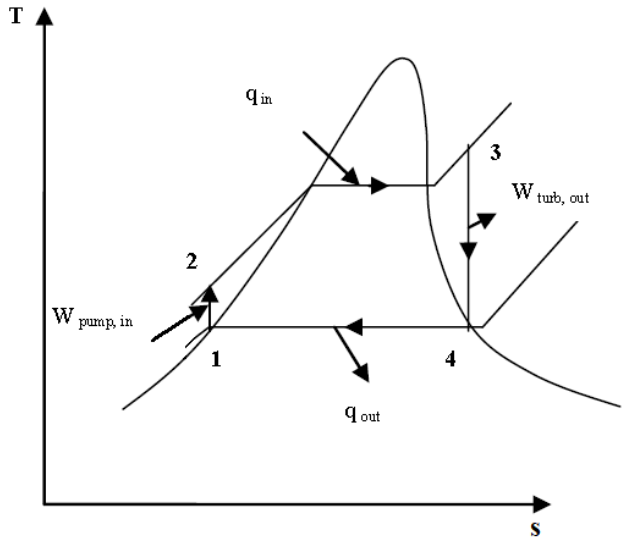


*Figure 2.6: T-s diagram of the steam Rankine cycle*

## 2.4.2 Organic Rankine cycle

Organic Rankine cycles are a valuable option: the process is the same as the steam Rankine cycles, characterized by the vaporization and the expansion of the working fluid from high to low pressure to produce useful work. Then, the condensation and the pumping to high pressure close the cycle, which involves the same components typical of the steam Rankine cycle (Figure 2.7). Though, instead of steam-water, the working fluid is an organic compound, such as n-pentane or toluene, whose boiling point is lower than the water one (Quoilin *et al.*, 2013). As a result, operating conditions are reduced at temperatures of the

order of 70 – 90 °C, causing a decreasing in performances which can be balanced by the smaller amount of needed heat. Compared with the steam Rankine cycle, the organic option results to be convenient for small power and low temperature applications, where the steam Rankine efficiency is low: the power can be scaled down to some kW, maintaining a reasonable plant efficiency. Regarding the turbomachinery, since the enthalpy drop is much smaller than the one required in the steam turbine, single or two-stages turbines are usually employed. By this time, there are few solar field coupled with ORC, all working with linear Fresnel concentrators, given their low investment costs and low operating temperature: 1 $MW_{el}$ plant in Arizona, showing a solar-to-electric efficiency of 12.1 % at design conditions (Canada *et al.*, 2004); 100 $kW_{el}$ in Hawaii, with a collector fluid temperature equal to 120 °C (Quoilin *et al.*, 2013); some very small-scale power plants are under investigation for very remote areas, such as in Lesotho (Quoilin *et al.*, 2011).

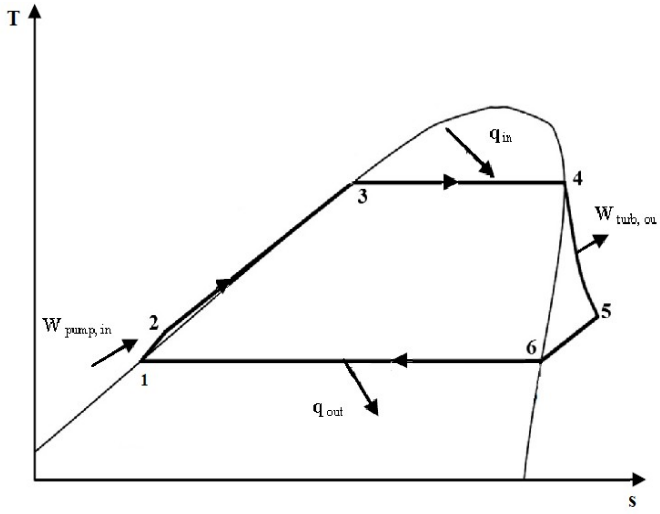


*Figure 2.7: T-s diagram of the organic Rankine cycle*

## 2.4.3 Closed supercritical CO2 cycle

In the last decades, key international energy investors and scientists like the US Department of Energy (Mecheri and Le Moullec, 2016; Rochau, 2014) have been looking at closed supercritical carbon dioxide cycle as a promising technology to increase flexibility and efficiency of CSP plant, especially when ST is considered, given the high HTF temperature at the receiver outlet. The aforementioned cycle consists in a closed loop where the fluid is taken above the critical point, with the purpose of working always with a very dense compound. The components are a compressor, a heat exchanger, a turbine and a cooler, taking advantage of the well-known technology for the Brayton cycle components design, as depicted in Figure 2.8, adapted from (Ahn *et al.*, 2015). The process consists in compressing to the desired pressure the cooled fluid near the critical point, so that it behaves as a liquid and requires less compression work, then it is heated up before entering

the turbine, where it is expanded; the cycle closes thanks to the rejection unit by which the still hot fluid releases heat to the environment before being compressed again.

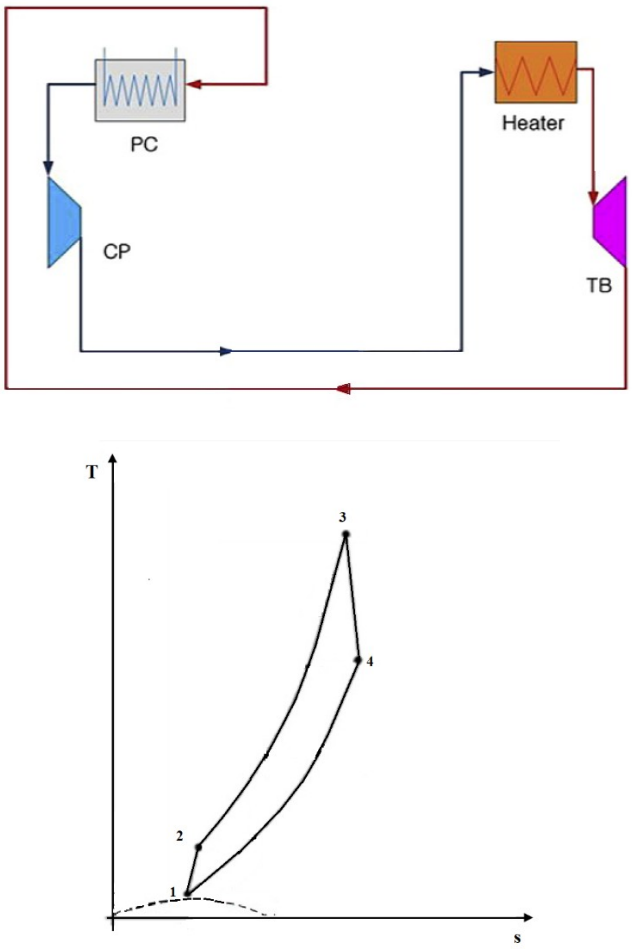


*Figure 2.8: a) Closed supercritical $CO_2$ cycle, adapted from (Ahn et al., 2015); b) T-s diagram of closed supercritical $CO_2$ cycle*

As already explained, operating near the critical point enables the compression work to be drastically reduced, compared with a traditional gas turbine cycle, since the fluid acts as a liquid. Thus, the efficiency is increased even at moderate turbine inlet temperatures. Increasing it, the cycle efficiency is further improved, differently from what happens in the gas turbine cycle (open Brayton cycle), where the advantage of increasing the TIT, obtaining a larger output turbine work, is counterbalanced by the huge work needed to compress the gas. On the other hand, the TIT in a steam Rankine cycle is limited by materials issues related with corrosiveness of water. $SCO_2$, on the contrary, is much less corrosive and enables a substantial rising of the temperature at the turbine inlet, while it still behaves as a liquid in the compression region, so that, at intense turbine inlet conditions, the resulting cycle efficiency is higher than both the steam Rankine cycle and

the open Brayton cycle (Ahn *et al.*, 2015; Crespi *et al.*, 2017; Lee, Kim and Jang, 2014; Was *et al.*, 2007).

Another important advantage of the $sCO_2$ closed cycle is the compact turbomachinery: having the working fluid a high molecular mass and density since it operates beyond the critical point (30.98 °C, 7.38 MPa), which means that the minimum pressure is higher than any working pressure typical of the steam Rankine cycle (few KPa) or Brayton cycle (around hundreds KPa), the volumetric flow rate decreases and allows the adoption of smaller components, reducing initial costs (Ahn *et al.*, 2015). So, the closed $sCO_2$ cycle has smaller weight and volume, lower thermal mass and less complex power blocks due to the higher density of the fluid and simpler cycle design (Angelino, 1969), showing better flexibility, transient and part load behaviour by virtue of the lower turbomachinery heat capacity (Binotti *et al.*, 2017). The expensive multi-stages steam turbine is substituted by a compact few-stages turbine, reducing a lot the plant footprint. Unfortunately, working near the critical point causes some disadvantages, too. As an example, regarding the compressor, the real gas effect is not negligible and the volumetric characteristics are strongly modified, passing from a liquid to a gas behaviour during compression, so the blades design is a crucial issue, even if in the market $CO_2$ compressors are already present (Binotti *et al.*, 2017).

The most attractive $sCO_2$ cycle key feature is the wide range of operating temperatures that makes them suitable for a large number of applications, from stand-alone plants to combined heat and power and waste heat recovery, and for different fuels, both fossil or renewables (Crespi *et al.*, 2017). A meaningful factor for the plant performances is the TIT: it surely impacts on the efficiency of the power block, but also on the solar field one since severe conditions at the turbine inlet mean a higher HTF temperature, which increases receiver losses. Studying and comparing the thermal efficiency (ratio between the net power output to the heat collected by the HTF and given to the $sCO_2$) as function of the TIT, it results that the steam Rankine cycle can achieve high efficiencies under medium-low turbine inlet temperature conditions (Ahn *et al.*, 2015), because the vaporization of liquid water requires a huge amount of heat, coming from the solar field, without causing any increase of the temperature (Irwin and Le Moullec, 2017); but attention must be paid when temperature is low in order to avoid the formation of liquid droplets which would damage and corrode the turbine. Regarding the gas turbine cycle (open Brayton cycle), even if the allowable TIT is significantly higher, the resulting efficiency is not improved too much since compressing a gas requires a huge amount of work and so the needed compressing work compensates the bigger available power from the turbine. On the other hand, using $sCO_2$ cycle the advantage of both the aforementioned cycles are combined and performances are substantially improved: the flow is compressed in the incompressible region, where it behaves as a liquid, leading to lower work needed, and the higher TIT can be exploited

without the material problems that are typical of the Rankine cycle, thanks to the less corrosiveness of $CO_2$ and for the reason that, being the fluid at supercritical conditions, the heat is not used to make the change of phase happen, but only to increase the temperature at the turbine inlet (Irwin and Le Moullec, 2017).

Initially, $sCO_2$ cycles have been developed for nuclear applications (Dostál, 2004), but recently they have been studied to be coupled with CSP technology (Bauer *et al.*, 2016; Crespi *et al.*, 2017; Wang, He and Zhu, 2017), as long as the higher receiver temperature permits to reach higher plant efficiency and a substantial decrease of the costs (Iverson, et al., 2013; Turchi, et al., 2013). As a drawback, the closed $sCO_2$ cycle pressure ratio is much smaller compared with the steam Rankine cycle and the turbine outlet temperature is higher: thus, the simple closed cycle results inefficient compared with the steam one, mainly due to irreversibility and losses, and other configurations have to be considered.

Given that generally the available resources for CSP technology are in desert regions, the necessary amount of water for cooling is difficult to be found, so dry-cooling systems have to be applied (Dunham and Iverson, 2014). The great advantage of dry cooling is the substantial reduction of the amount of water consumption: wet cooled trough systems need approximately 2.8–3.4 t/MWh while solar tower installations about 2.8 t/MWh (Carter and Campbell, 2009). The estimated water consumption reduction is of the order of the 90 % (Holbert and Haverkamp, 2009 - 2009; Pihl *et al.*, 2012), but the beneficial aspect is counterbalanced by the reduction of performances and the increase of costs: indeed, both the efficiency and the electricity production decrease (Azoumah *et al.*, 2010) and the dry cooling equipment is 3.3 times more expensive than the one for wet-cooling (Chung-Ling Chien and Lior, 2011; Mittelman and Epstein, 2010). Overall, the feasibility and convenience of dry cooling systems is not commonly sustained by researches and it needs further technology improvements (Ahn *et al.*, 2015).

#### 2.4.3.1 Recuperative closed supercritical $CO_2$ cycle

As previously said, the temperature at the outlet of the turbine is still high, due to the low-pressure ratio typical of closed supercritical CO2 cycle. Therefore, in order to obtain a high efficiency, it is necessary to recover the large amount of heat that, otherwise, would be rejected to the environment and wasted. Even though several configurations of $sCO_2$ cycles are presented in literature (Angelino, 1968; Feher, 1968), generally the common point is the necessity of the recuperation process: after the turbine, an heat exchanger, the recuperator, enables the exploitation of heat which is used to increase the temperature of the working fluid before entering the main heater (Figure 2.9). Along these lines, cycle thermal efficiency is improved with respect to the simple closed supercritical $CO_2$ cycle because the amount of needed heat as input is substantially decreased.

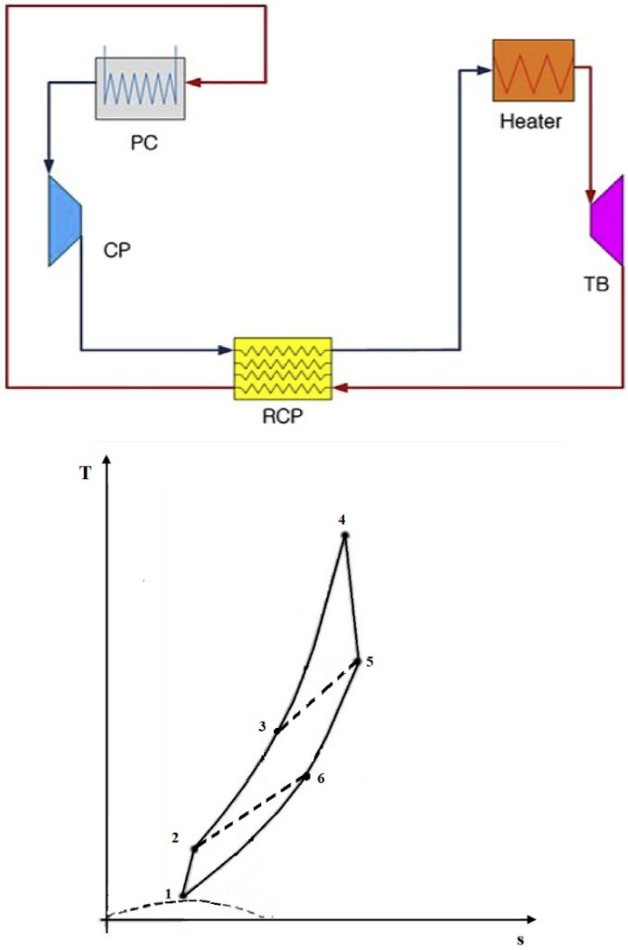


*Figure 2.9: a) Recuperative $sCO_2$ cycle (Ahn et al., 2015); b) T-s diagram of closed supercritical $CO_2$ cycle*

### 2.4.3.2 Recompression closed supercritical $CO_2$ cycle

However, the simple recuperative configuration is inefficient when coupled with CSP, due to the high working temperatures which make also the recuperator suffer the real gas effects. When pressure increases, the gas starts behaving as a real one: in these conditions, the specific heat capacity ($C_p$) does not depend only on the temperature, but also on the pressure. In fact, $CO_2$ shows a deep change in correspondence of the critical pressure, as shown in Figure 2.10. So, the increased specific heat capacity fluid on the cold high-pressure side of the heat exchanger has to exchange heat with the lower specific heat capacity fluid on the hot low-pressure side and this matching leads to a high temperature difference, thus irreversibility, (Binotti *et al.*, 2017). Furthermore, in this condition the so-called "pinch point problem" is very likely to happen in some part of the heat exchanger. The pinch point is the minimum temperature difference place in a heat exchanger and it has to be satisfied for the correct heat transfer process.

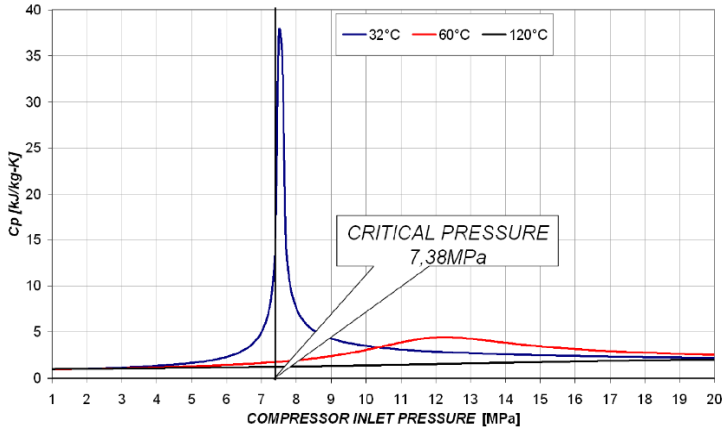


*Figure 2.10: Specific heat capacity of $CO_2$ as function of temperature and pressure (Kulhánek and Dostál, 2010)*

The result is that, to ensure the minimum temperature difference, further heat recover between hot and cold stream is prohibited and the efficiency is still penalised. The violation of the pinch point generally happens in the cold or hot end of the component, but, in this case, given the strong variation of the heat capacity, it may occur somewhere within the recuperator (Kulhánek and Dostál; Ladislav *et al.*, 2016). For this reason, in the recompression layout (Figure 2.11), the low-pressure flow exiting the turbine, still having a considerable temperature, passes through two recuperators: first, the High Temperature Recuperator (HTR) and, secondly, the Low Temperature Recuperator (LTR). After exiting the LTR, the flow is split into two streams: the first one is cooled in the Pre-Cooler (PC) and then compressed to the maximum pressure by the Main Compressor (MC); the second stream is compressed by the Re-Compressor (RC) without being cooled down. In this way, the pinch point problem is avoided until the heat capacity ($m \cdot C_p$) of both sides is the same: the lower $C_p$ of the hot side fluid is compensated by its higher mass flow and it is well matched with the small amount of the high specific heat capacity fluid in the high-pressure side. Then, the two flows are mixed before entering the HTR, where they recuperate heat from the turbine $sCO_2$. Finally, the fluid is heated up to the required temperature in the main heat exchanger, the one connecting the solar loop with the power cycle, and it is expanded in the turbine. In addition, the choice of the proper split ratio enables the exploitation of the residual heat from the LTR, minimizing losses and obtaining the maximum cycle efficiency.

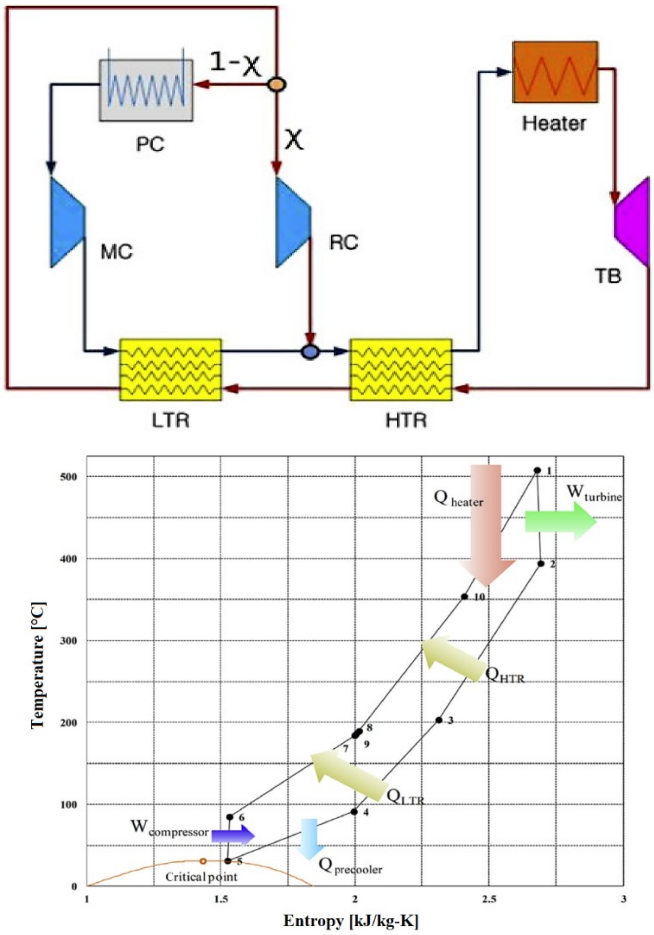


*Figure 2.11: a) Recompression $sCO_2$ cycle components (Ahn et al., 2015); b) T-s of recompression $sCO_2$ cycle (Ahn et al., 2015)*

### 2.4.3.3 Closed supercritical $CO_2$ layouts

Starting from the recuperative set-up, efforts go in the direction of improving efficiency. One attempt to improve the heat recuperation process results in the Pre-compression layout: a second recuperator and an intermediate compressor are added, so that the fluid exiting the HTR is compressed before entering the LTR to enhance the thermal transfer. Other improvements opportunities are given by the re-arrangement of the recompression cycle. For instance, in the Reheat layout the expansion process is completed in two stages and heat is added after the first high-pressure expansion in the secondary heat exchanger, before entering the low-pressure turbine. In this way, the turbine power output is increased. Concurrently, adding an intercooler between the compressors gives an help with a view to reducing the needed work because the temperature of the fluid is reduced. (Binotti *et al.*, 2017; Luu *et al.*, 2017). In any case, even if performances are improved and the resulting thermal efficiency is increased, adding components generate a substantial increase of the costs.

## 2.5 Plant configuration

The most used and efficient heat transfer system between the CSP plant and the power block is the indirect one, given its advantages in terms of flexibility and part load: the solar radiation heats the HTF, which, through a heat exchanger, transfers the thermal energy to the working fluid in the power block. Clearly, this solution, compared to the direct system consisting in the direct expansion in the turbine of the heated fluid to obtain power, requires an additional intermediate heat exchanger, causing additional costs, losses and the decrease of the maximum operating temperature. Concurrently, it allows the stock of a fluid different from the power block one, that is chosen with better storage features, resulting in separated solar hours and electricity production. The dispatchability of the electricity allowed by this set-up comes together with its easy control strategy. Moreover, the $sCO_2$ receiver is still under demonstrations and, up to now, it has been proven in test-lab only; a direct configuration with the $sCO_2$ does not allow an easy integration of a TES system since the gas has not as good storage capability as a liquid or a solid (see section 3.3). As a direct consequence, the indirect configuration leads to more flexible performances (Binotti *et al.*, 2017; Iverson *et al.*, 2013).

Nowadays, about 430$MW_{el}$ of commercial ST plants are operating (mainly in Spain and US), while other 430 $MW_{el}$ are under construction in China, US, Chile and South Africa and other 1,500 $MW_{el}$ are in the planning phase (Binotti *et al.*, 2017). As already said, they are all currently based on traditional Rankine steam cycles to convert the thermal power into electricity and have a temperature operating range between 300 °C and 500 °C, while in the future it is expected to reach 800 °C (Vignarooban *et al.*, 2015).

## 2.6 Technology Development

"Solar One" is the first demonstrational solar-thermal plant, installed in California, working with a solar tower water/steam receiver from 1982 to 1986. It is built to show the feasibility of the solar tower technology and produces 10 $MW_{el}$, coupled with a steam Rankine cycle.

Later, in 1995, it is converted in "Solar Two" by adding more heliostats and, above all, using molten salts as both solar field HTF and storage fluid, instead of water and oil, as in "Solar One". It is the first test plant equipped with a molten salts storage system: in this case, an intermediate heat exchanger is needed to transfer heat from the molten salts to the power block steam, given the adopted indirect configuration.

The previous two projects inspire Torresol Energy that in 2011 started the project "Gemasolar" (GMSP) (Figure 2.12): the first commercial solar power plant based on an

heliostats field with a molten salts tower and a molten salts storage system, coupled with a steam Rankine cycle to produce electrical power. Table 2.3 shows the main characteristics of the plant (Relloso and García, 2015).

*Table 2.3: Main GMSP features (Relloso and García, 2015)*

| **Parameter** | **Value** |
|---|---|
| Owner | TEI (60 % owned by SENER Group) |
| EPC Contractor (main) and Engineering | SENER Ingeniería y Sistemas S.A. |
| Number of heliostats | 2,650 |
| Mirror aperture area | 306,658 $m^2$ |
| Receiver area | 270 $m^2$ |
| Concentration Ratio (avg) | 1,136 |
| Receiver Power | 120 $MW_{th}$ |
| Turbine Net Power | 19.9 MWel |
| Storage capacity | 15 hours |

The molten salts TES provides heat to the power block even during cloudy conditions, so that the number of the steam turbine shut downs and starts up are drastically reduced (Relloso and García, 2015).

It is fundamental to notice that the CR is very high: if all the radiation were focused on the receiver centre, which is tubular type, the peak flux would reach 2,000 $kW/m^2$ and surely the tubes materials would be permanently damaged. Up to now, the maximum peak withstood by molten salts receiver is around 1,000-1,200 $kW/m^2$. So, the concentrated energy is spread all along the receiver surface, in order to have a lower flux and respect the materials limitations. Clearly, in this way the plant performances are reduced (Relloso and García, 2015). Recently, to solve this issue, as explained in section 3.1, researches have been looking at the solid particles receiver, which can withstand higher fluxes and, consequently, the efficiency results improved.

*Figure 2.12: Gemasolar heliostat field layout*

## 2.7 Combined Heat and Power

Combined Heat and Power (CHP) or cogeneration is the combined production of electric and thermal power using the fuel sequentially, so that both the outputs are produced in the same time. In this way, money and fuel can be saved: thermodynamically speaking, cogeneration is an efficient utilization of fuel, by virtue of the possibility of use the amount of heat which, in separate electricity production, would be rejected to the environment and wasted. CHP systems can reach efficiencies of the order of 80 %, while the separated production of thermal and electrical power typically is characterized by an overall efficiency of 45 %, as shown in

Figure 2.13 (Shipley *et al.*, 2009).

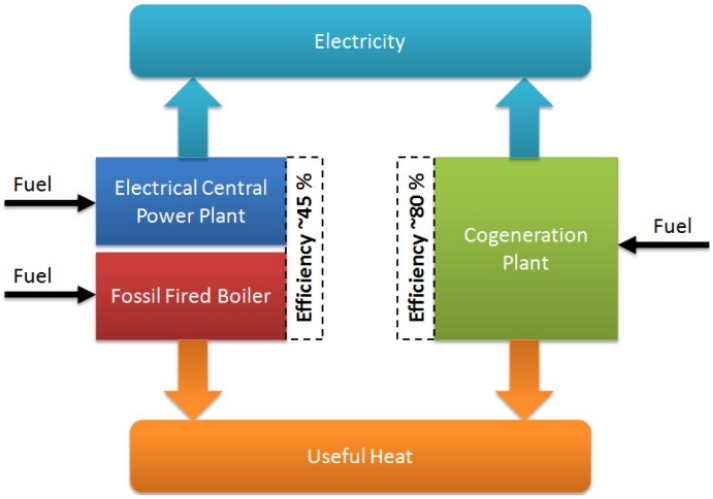


Figure 2.13: CHP process flow diagram (Shipley et al., 2009)

The needed components, such as heat recovery system, electrical generator and controls, are part of the typical power system equipment and so they are well developed and simply established in the CHP configuration, without causing any drastic costs increasing (Gvozdenac, et al., 2017). The CHP convenience is evaluated using the Primary Energy Saving (PES), an index that compare the amount of fuel used by CHP and the one used by actual conventional plants for the separated production of thermal and electric power. An efficient configuration is characterized by a PES equal or higher than 10 % (*Directive 2004/8/EC of the European Parliament and of the Council of 11 february 2004 on the promotion of cogeneration based on a useful heat demand in the internal energy market and amending directive 92/42/EEC* 2004).

In literature, lots of CHP configurations are presented and investigated. For instance (Pantaleo, et al., 2015): the first evaluated configuration is made up of a boiler with a steam turbine and bottoming Organic Rankine Cycle (ORC); the second possibility is formed by a boiler and a steam turbine; the third one consists in a boiler and an ORC; the last configuration is made up of the boiler equipped with the steam turbine and the bottoming ORC with the possibility to switch it on or off, depending on the heat demand. According to the same paper, the ORC is the most suitable for small and micro applications thanks to the possibility of selecting the working fluid, instead of using steam: generally speaking, organic compounds are characterized by a lower boiling point and less heat is required for vaporizing, so that the enthalpy drop is reduced and the turbine can operate with few stages. This enables low temperature applications, such as geothermal, solar, biomass or waste heat (Mohammadi *et al.*, 2017). On the other hand, in the industrial energy demand, where the needed thermal power is high to face the demand, the steam turbine configuration results to be the most suitable because it maximizes the heat available to the load, even if increasing the thermal power causes a reduction in the producible electrical power. Indeed, steam turbine CHP is a configuration which allows to deliver a large amount of thermal power and the electricity is often considered only a by-product, so that the power over heat ratio is usually near 0.2 (U.S. Department of Energy, 2016).

Given the rising in natural gas application, recently gas-steam combined cycle based CHP systems have been attracting lots of investors (Yang, Huang and Ma, 2018), by virtue of the high temperatures at which flue gases are discharged by the turbine, of the order of 300-400 °C. This kind of plant can be divided in two parts, that are the gas cycle and the water/steam one, even if a simpler configuration with only a gas-turbine and a Heat Recovery Boiler (HRB) is possible, to simply obtain heated water. By the way, the link between the aforementioned cycles is the HRSG, which exploits the flue gases and uses their waste heat to generate steam. In order to recover as much waste heat as possible, HRSG can have different pressure levels. The advantage of using a gas-turbine is that the generated electricity is no longer function of the heat load, since it is generated before

producing heat, even though the steam turbine can produce some work, too. In this case, the heat generation regulation has two additional Degrees Of Freedom (DOFs) with respect to the condensing extraction steam turbine (see 2.7.1): the bypass valve, to send directly the flue gases to the stack, and the turbine control stage. The choice of the fuel is not particularly demanding: it can be from renewable sources, such as gasified biomass, or natural gas or fossil fuel (Pantaleo *et al.*, 2015). In any case, the best suited configuration for the desired application strongly depends on the temperature at which the heat from cogeneration is available: compared with the steam turbine case, the temperature of the heat produced by an ORC is significantly lower. For this reason, the choice is often a compromise between a higher electrical efficiency and higher investment costs, adopting a combined cycle (steam turbine and ORC or gas-steam combined cycle), and the less expensive but also less efficient ORC cycle or steam turbine cycle. Another factor to be taken into account is the variable thermal and electrical power demand pattern that, in many cases, makes the configuration with the flexible bottoming ORC operation (which means the possibility to switch it on or off to follow the demand) very interesting and attractive (Pantaleo *et al.*, 2015). To conclude, any time it is fundamental to understand if the higher combined CHP investment cost is counterbalanced by the increased plant operational flexibility and, consequentially, conversion efficiency, remembering that the turbine performances are drastically worsened by partial load operation and PES can show the non-convenient adoption of CHP.

### 2.7.1 Steam turbines

A CHP plant can operate at fixed or variable portion of electricity relative to the output heat. In the former case, the back-pressure steam turbine is used, whilst the latter one is characterized by the adoption of the extraction-condensing steam turbine.

The back-pressure steam turbine consists in expanding the fluid until a higher pressure than the usual condensing pressure of a steam cycle, typically between 0.3 and 0.17 MPa (U.S. Department of Energy, 2016), in order to have heat available at higher pressure and temperature from the condenser. The cycle is the common steam Rankine one. As well-known, the heat grade depends on the conditions at which it is available: the higher the temperature, the better the use. Being the power to heat ratio fixed, the regulation has only one degree of freedom and consists in putting one valve before the boiler, to regulate the fuel flow rate. The main advantages lie in the simple layout, in the small amount of water necessary to cool, the low capitals costs and the overall high efficiency; but the size of the steam turbine increases.

On the other hand, the extraction-condensing configuration (Figure 2.14 (Iodice *et al.*, 2017)) is a turbine from which steam can be extracted at different pressure levels and sent

to heat exchangers. So, in this case it is possible to operate at higher pressures than adopting a back-pressure steam turbine (U.S. Department of Energy, 2016). The mechanical power output decreases as the extraction rate is increased, even if PES is generally improved because the extracted steam from the inlet of the low pressure stage turbine produces thermal power more efficiently than electricity (Yang, Huang and Ma, 2018). Since the power to heat ratio in variable, in this case two DOFs regulation is allowed: one valve to regulate the fuel flow rate in the boiler (component "a" in Figure 2.14) and another one after the hot condenser (component "i" in Figure 2.14), to control the extraction flow rate.

Increasing the outlet turbine pressure is often needed to obtain a certain temperature of the thermal source in the prospective to make heat attractive, but this surely will decrease the amount of mechanical power produced by the plant. The pressure control, in addition, can be obtained using a variable geometry of some turbine stages.

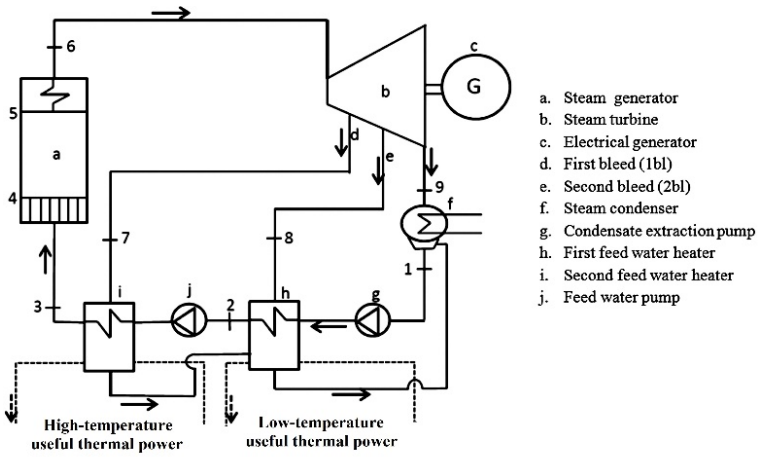


*Figure 2.14: Condensing-extraction steam turbine (Iodice et al., 2017)*

## 2.7.2 Gas turbine

In a gas turbine, that is an open Brayton cycle, the exhaust gases are discharged at a very high temperatures, of the order of 400–600 °C: this condition is favourable with the view to recovering heat, which is a high-grade thermal power. For this purpose, after the turbine, an additional component, the Heat Recovery Boiler (HRB) or Heat Recovery Steam Generator (HRSG) is placed, depending on the amount of available heat and, consequentially, on the possibility to generate, respectively, hot water or steam (Figure 2.15 adapted from (Energy Solutions Centre, 2016)).

The powerful gain of adopting a gas turbine equipped with a recovery component lies in the unchanged generated electrical power produced by the gas turbine. Another important remark is that the outlet temperature of the turbine strongly influences the available useful

heat: increasing it, the heat does the same. If more useful heat is needed, it is possible to add a supplementary fire in order to increase the temperature at the inlet of the recovery component. In this case, in view of flexibility, the DOFs are four:

1. turbine stage control;
2. bypass valve, that can make some flue gases mass flow go directly to the stack, without passing through the HRB;
3. supplementary fire;
4. Inlet Guide Vanes (IGV) to control the air mass flow in the compressor.

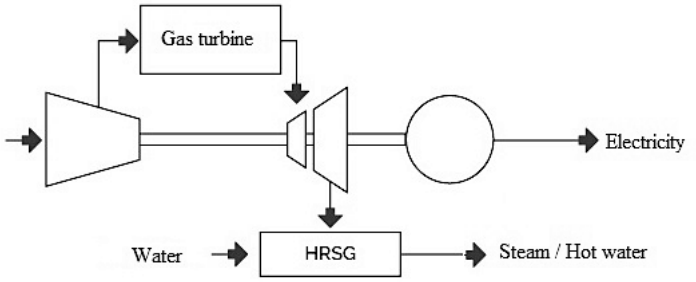


*Figure 2.15: Gas turbine equipped with HRSG/HRB (adapted from (Energy Solutions Center, 2016))*

## 2.7.3 Combined cycle

Another good option, especially in terms of flexibility and cycle control, is the combined cycle, made up of a gas turbine coupled with a steam Rankine cycle through a HRSG (Figure 2.16 adapted from (Energy Solutions Centre, 2016)). The steam turbine is the same discussed in the previous subsection 2.7.1: for instance, considering a condensing-extraction turbine, the degree of freedom of the supplementary fire, the IGV, the turbine control and the bypass valve are added to the DOFs of the previous Rankine cycle. Flexibility is increased and, as already said, it is possible to decouple thermal power from electricity production, without jeopardizing the latter in order to increase the former, as usual for steam turbine configurations.

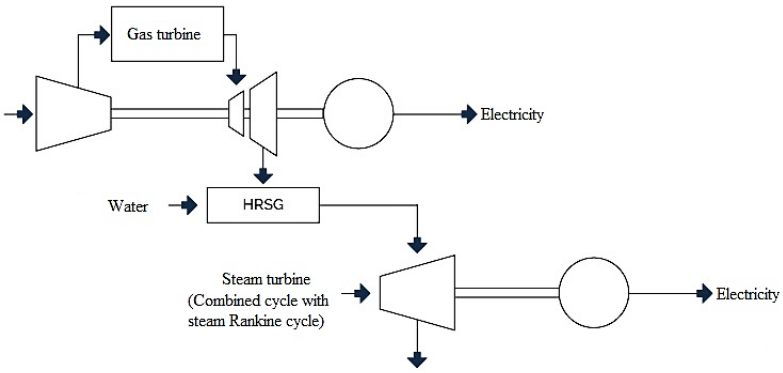


*Figure 2.16: Combined cycle (adapted from (Energy Solutions Center, 2016))*

### 2.7.4 Internal Combustion Engine

Despite the enormous efforts for the purpose of reducing emissions and enhance efficiency, such as variable valve timing or turbocharger, in the Internal Combustion Engines (ICE) around 60-70 % of the energy given by the fuel is lost as heat (Endo *et al.*, 2007). Additionally, actual regulations regarding combustion temperatures and pressure are stricter than in past. For these reasons, Waste Heat Recovery (WHR) has shown to be an effective and economically convenient way to reduce fuel consumption avoiding the increase of emissions (El Chammas and Clodic, 2005).

Internal Combustion Engines (ICE) are a robust and economic choice for CHP, thanks to technology developments and high production level. They offer two main sources of heat to be recovered: one from the exhaust gases, giving medium-grade heat at 350-450 °C, and one from the engine coolants (low-grade), that are water, where a small amount of heat is available at around 50-100 °C, and oil, with a heat temperature of around 100-120 °C (Sprouse and Depcik, 2013). Clearly, the higher the temperature at which the heat is accessible, the higher its quality. Schematic of the system is depicted in Figure 2.17 (Energy Solutions Centre, 2016).

Antecedent studies have demonstrated that the medium-grade and low-grade heat have enough energy to be recovered to justify the coupling of ICE with a secondary cycle, which definitely causes an increase of costs: higher investments are counterbalanced by better efficiency and lower emissions. The most suitable coupling cycle has been proved to be the ORC, thanks to the standard components which it is made up of and to its medium-low operating temperatures (Sprouse and Depcik, 2013).

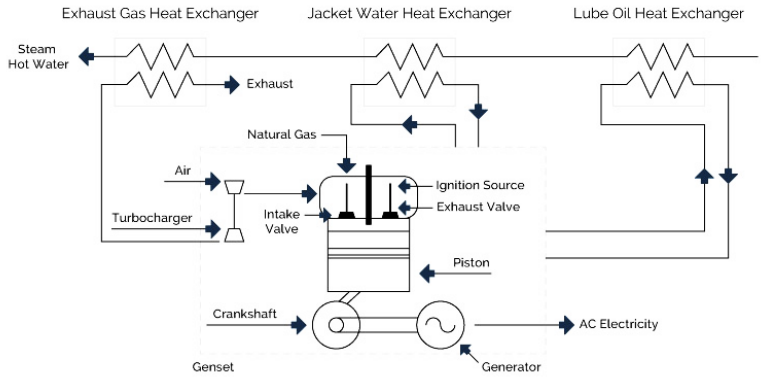


*Figure 2.17: Heat recovery from ICE (Energy Solutions Center, 2016)*

## 2.7.5 CHP as a promising application of sCO2 power cycles

As already widely explained, $sCO_2$ closed loop cycles have the fundamental advantage of increasing the thermal efficiency with respect to the conventional gas cycles or the superheated steam cycles at similar temperatures (Dostal, Hejzlar and Driscoll, 2006) and, nowadays, researches on $sCO_2$ application are directed to the electricity production only. In consideration of the high efficiency and the fuel economy which define CHP configuration, it is attractive to investigate the latter operating with supercritical carbon dioxide as working fluid (Moroz, Burlaka and Rudenko, 2014). In the mentioned study, among the variety of possibilities, fossil fuel is considered for the sake of simplicity. The two selected approaches are:

1. steam Rankine cycle CHP plant with bottoming supercritical $CO_2$ cycle, where heat is produced after the turbine expansion using a steam fraction, subdivided into combined complex steam-$sCO_2$ CHP plant (Figure 2.18) and combined simple steam-$sCO_2$ CHP plant (Figure 2.19);
2. CHP plant with single $sCO_2$ working fluid, subdivided into cascaded $sCO_2$ CHP plant, where heat is produced by the water heating in $sCO_2$ cycle coolers (Figure 2.20), and single $sCO_2$ CHP plant, where the production of heat is done by the cooler and directly in the heater (Figure 2.21).

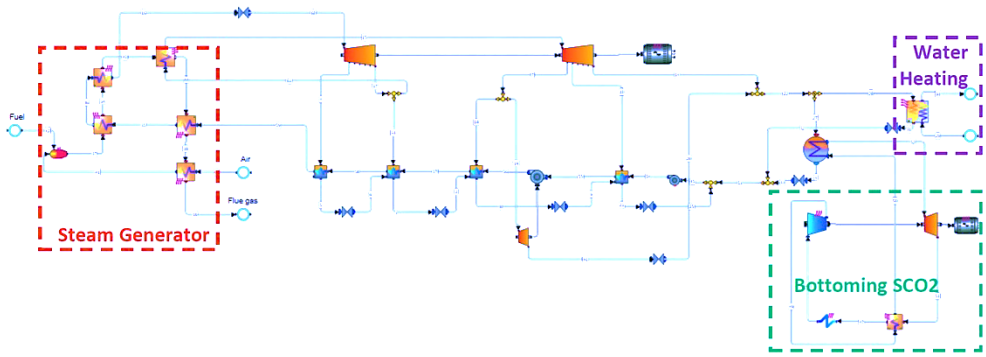


*Figure 2.18: Combined complex steam-sCO₂ CHP plant (Moroz, Burlaka and Rudenko, 2014)*

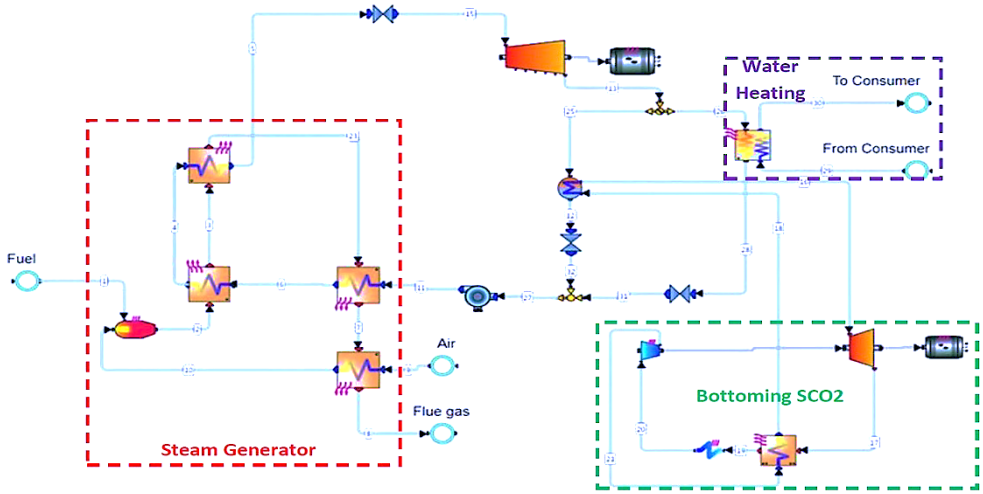


*Figure 2.19: Combined simple steam-sCO₂ CHP plant (Moroz, Burlaka and Rudenko, 2014)*

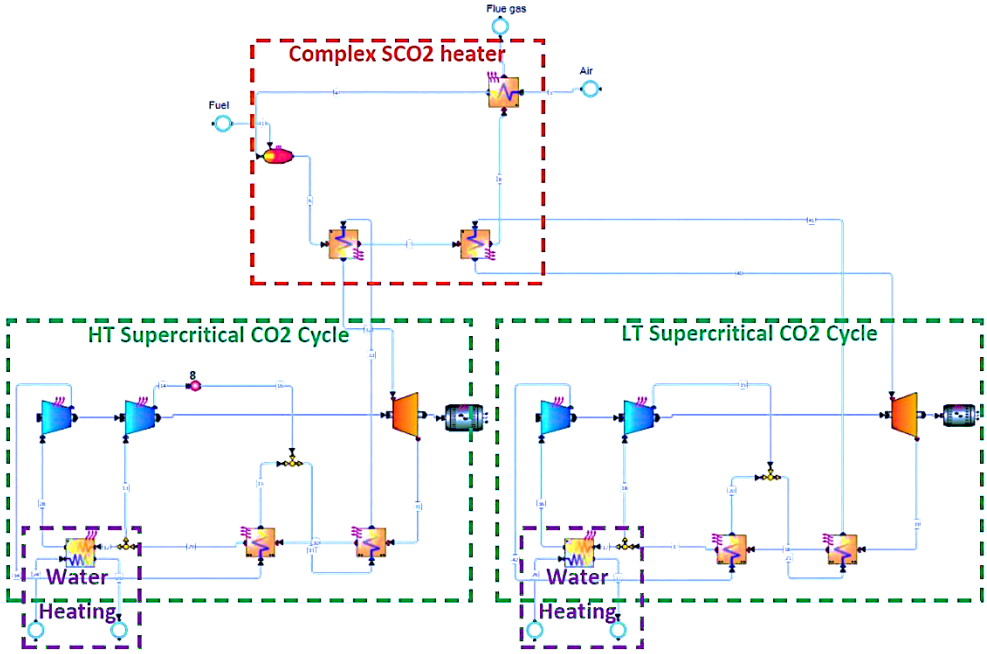


*Figure 2.20: Cascaded $sCO_2$ CHP plant (Moroz, Burlaka and Rudenko, 2014)*

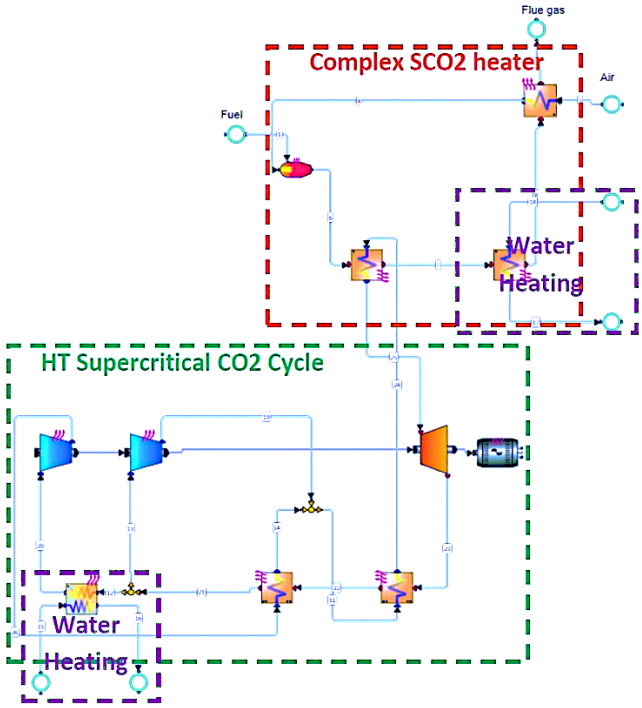


*Figure 2.21: Single supercritical $CO_2$ CHP plant (Moroz, Burlaka and Rudenko, 2014)*

According to the paper earlier mentioned, the first approach, which uses a topping Rankine cycle and a bottoming $sCO_2$ cycle, shows the benefit of maintaining the same boiler, turbine stages and heat exchangers and the advantage of having a small condenser, since the

condensation pressure is higher than a conventional Rankine cycle one. In addition, the bottoming $sCO_2$ cycle layout is very simple thanks to the single recuperator with a low temperature difference and the low working fluid temperature. From the opposite position, CHP plants have the strong advantage of operating with a single working fluid. The highest electric efficiency is reached by the cascaded $sCO_2$ CHP plant. In addition, the electric power produced by steam Rankine cycle CHP plant with bottoming supercritical $CO_2$ cycle depends on the heat load and, in particular, decreases when the thermal power increases, whilst in the CHP plant with single $sCO_2$ working fluid the outputs are completely independent, making this configuration more attractive. On the other hand, the Heat Utilization Factor, which is the ratio between the sum of the net electric power and the useful thermal power to the heat consumption, is higher in the first configuration, but, since electric power is more valuable than the thermal one, the second configuration with the single working fluid remains preferable. In any case, an analysis of the capital costs and specific needs of the users have to be carried out in order to choose the best plant.

# 3. LITERATURE REVIEW

The common interest of investors and researches for CSP technology lie in the attempt to reduce the still high LCOE, in order to produce clean energy in an attractive way for the market. To reduce ST plants costs, it is fundamental to base the studies on GMSP, since it is the only commercial plant in the world operating with a molten salt technology. So, starting from this point, components have to be improved in order to reach better cost/efficiency ratio. The economy of scale is a key feature when dealing with ST plants: increasing the power plant size, the LCOE significantly decreases. Lastly, try to take advantage of the convoy effect: the LCOE of a solar park made up of more than one plant is lower than the LCOE of a stand-alone plant (Relloso and García, 2015). Up to now, there are three possible paths for making finally concentrating solar power economically convenient, acting on the receiver: solid sand-like particles receiver; new molten salts researches; $sCO_2$ receiver. Additionally, the current steam Rankine power cycle has to be changed (Eurekalert, 2018).

## 3.1 Solid sand-like particles receiver

On the view of making CSP affordable, on June 2018 Sandia National Laboratories for the U.S. Department of Energy (DOE) has launched the National Solar Thermal Test Facility (NSTTF) in Albuquerque, New Mexico. The plant solar field is made up of 218 individual Heliostats (National Technology and Engineering Solutions of Sandia, LLC, 2015) which reflect the sun radiation on a 61-meter-high solar tower. Instead of the typical tubular receiver, the one installed on this solar tower is a solid particles type (Figure 3.1 (Ho and Iverson, 2014)): ceramic compounds are continuously heated up by the concentrated sun radiation and reach temperatures 100 °C higher than the typical fluids (Temple, 2017). The heated sand-like ceramic particles could then be easily and cheaply stored in an insulated tank, by virtue of their favourable storage properties, and used to heat the secondary fluid (i.e. $sCO_2$) for the power cycle. Along these lines, since the solar radiation is directly absorbed by the solid particles, the typical constraints of ordinary liquid or gas tubular

receiver are overcome: flux limitations connected with the high thermal stresses of pipes containing the heated fluid are completely avoided and temperatures of about 1,000 °C are allowed at the outlet of the receiver (Ho and Iverson, 2014). Clearly, the efficiency is strongly improved. The main advantages in adopting solid particles receivers are the low costs and the already massive production. On the way round, particles have to be mechanically moved and, concerning big application power plants of more than 10 MW, necessary to take advantage from the economy of scale, the weight becomes a key issue and the aperture extension of the receiver reaches dimensions of 10 $m^2$: this means that an enormous amount of sand has to be moved up, made passing through the heat exchanger, stored in the tank and sent back to the receiver, requiring obviously mechanical devices that provide the needed work. But it is well known that mechanical components are always affected by breakdowns. Anyway, Sandia National Laboratories are investing 9.5 million dollars on sand-like particles receivers, believing that this is the right route to the make CSP affordable and spread up in the market (Eurekalert, 2018).

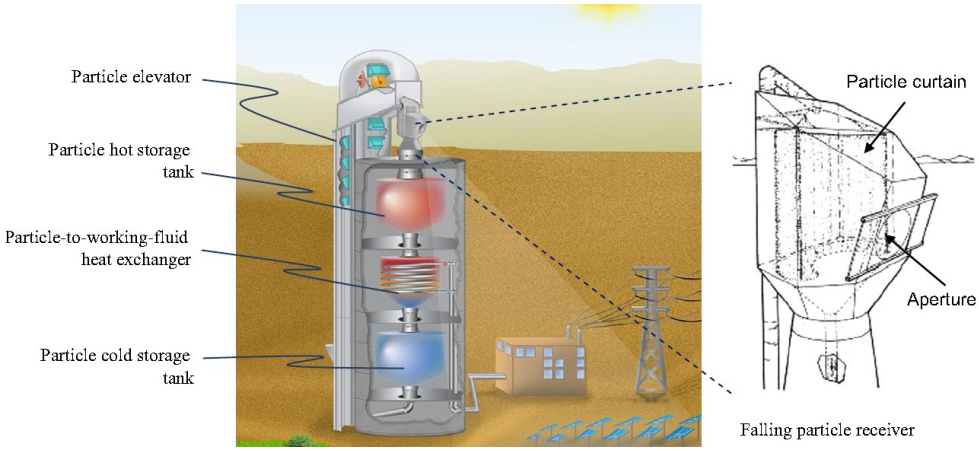


*Figure 3.1: Falling particle receiver system with integrated storage and heat exchanger (Ho and Iverson, 2014)*

## 3.2 Novel molten salt studies

In the last months, National Renewable Energy Laboratory has invested 7 million dollars on researches for new molten salts, having the convenient aspect of being already proved and commercially used (Eurekalert, 2018). Nowadays, in operating plants, corrosion problems limit the upper molten salts temperatures to 565 °C, even though they are stable until 800 °C (Vignarooban *et al.*, 2015). Taking advantage of the existing and well-studied actual technology, researches are going in the direction of understanding the causes of corrosion and trying to attenuate them. Other efforts have been made in order to find different liquid mixture based on chloride that can withstand a temperature of the order of 700-800 °C, so that the molten salts loop can perfectly match the $sCO_2$ cycle, whose best

efficiency is reached with that maximum temperature, avoiding corrosion (Eurekalert, 2018). Recent ongoing tests have shown that the Hastelloy C-276 (Chromium-Nickel-Molybdenum) pipes corrosion rate drastically diminishes at 800 °C in the absence of air when NaCl–KCl–$ZnCl_2$ molten chloride salts are employed (Vignarooban *et al.*, 2015). Obviously, in tests small-lab scale it is easy to seal components and to work in a completely anaerobic environment, but in a real commercial plant complications continuously occur and it is hard to prevent devices from leakages, especially when the plant is started up and shouted down to follow the sun radiation and maintenance has to be carried on, definitely causing the system to face air and water intrusions (Eurekalert, 2018). Besides, new mixtures characterized by a lower melting point are under investigation. For example, the eutectic mixture of five alkali-nitrate salts, $NaNO_3$ (6 wt%)–$KNO_3$ (23 wt%)–$LiNO_3$ (8 wt%)–$CsNO_3$ (44 wt%)–$Ca(NO_3)_2$ (19 wt%), known as Halotechnics SS-500 (Raade and Padowitz, 2011). The caesium-nitrate substantially lowers the melting temperature to around 65 °C, still providing stability above 500 °C amd allowing a strongly wider operating temperatures range (Vignarooban *et al.*, 2015).

## 3.3 Supercritical CO2 receiver

The simplicity of using and transport a gas, the $sCO_2$, has attracted 7.6 million dollars of investment by Brayton Energy. But the first big disadvantage comes up naturally: employing a gas, the receiver efficiency is penalized due to the lower fluid density. The second con to be faced is that an indirect TES system is needed: while solid particles or liquid molten salts are capable of retaining heat, a gas has to transfer the captured heat to another material that can store it. By the way, the last disadvantage can be seen as a possibility to increase the plant flexibility, since the receiver and storage fluid are decoupled and it is possible to choose the best option for each separate role (Eurekalert, 2018). The $sCO_2$ offers the possibility to operate at very high temperatures and to improve the CSP efficiency. Given the high pressure, it is not suitable for PT, whilst it is well compatible with ST technology (Vignarooban *et al.*, 2015). An experimental study directed by Brayton Energy shows that in a solar collector field operating with $sCO_2$, the outlet receiver temperature is 750 °C and the expected receiver thermal efficiency is 92 % (Sullivan *et al.*, 2013; Vignarooban *et al.*, 2015).

## 3.4 Supercritical CO2 power cycle

The interest in adopting the $sCO_2$ arises also thanks to the opportunity of using it both as fluid for the solar field and for the power cycle. Further, all the CSP plants are limited by the steam Rankine cycle to which they are coupled with: extreme conditions make water

corrosive and cause stresses problems on the containing pipes. For this reason, the TIT cannot overcome 600 °C, without exploiting the possible improvements that the solar tower technology offers at higher temperatures and without experiencing the reduction of capital costs leaded by higher TIT: in point of fact, concerning turbomachinery, the best way to reduce the LCOE is to increase its efficiency, which results improved the higher the temperature at the turbine inlet is. In this way, indeed, the capital costs stay the same, but more electricity is produced and the resulting LCOE is lower. So, passing from a steam cycle with a limit of 565 °C to a $sCO_2$ with higher maximum temperatures, an improvement of around 10 percentage points and more on the plant efficiency is experienced and the LCOE is predicted to be reduced of the 20 %. Further, as already explained in the subsection 2.4.3, the $sCO_2$ turbine is much smaller than the steam turbine and this beneficially contributes on the reduction of plant costs. In this view, finally investing in CSP technology coupled with $sCO_2$ power block will be attractive and moneymaking, with an overall efficiency improved of the 30 % with respect to the actual CSP-steam turbine plants (Irwin and Le Moullec, 2017). Millions of dollars have been invested in experiments and tests for this promising technology: Brayton Energy, National Renewable Energy Laboratory, Sandia National Laboratories, Electric Power Research Institute, Georgia Institute of Technology, Georgia Institute of Technology, University of Tulsa, Hayward Tyler, Massachusetts Institute of Technology, Mohawk Innovative Technology, Purdue University, DOE, Idaho National Laboratory, National Renewable Energy Laboratory, Oak Ridge National Laboratory, Oak Ridge National Laboratory, Oak Ridge National Laboratory, Savannah River National Laboratory (Eurekalert, 2018).

## 3.5 Advanced material for sCO2 power cycle application

Currently, the commonly used materials for piping in CSP are stainless steels and nickel-based alloys, for temperatures higher than 500 °C, typical of solar tower plants. The central issues related with contact between pipes and HTF are salts stability and metal corrosion, because the operation conditions are intense, with temperatures up to 800 °C when molten salts are employed. The high temperature is needed to obtain an efficient plant, but the fluid act as an electrolyte and corrodes the metal (Bauer *et al.*, 2013; Vignarooban *et al.*, 2015).

Concerning the standard Solar Salt, 60 wt% sodium nitrate ($NaNO_3$) and 40 wt% potassium nitrate ($KNO_3$) (Carling *et al.*, 1981), thermal stability degrades as temperature increases: according to an experimental recent study, a 3 wt% of mass loss is registered overcoming 530 °C, but during the experimental time frame only the primary decomposition mechanism, by which nitrite is formed, not also the secondary one that releases oxides and

nitrogen, reaches the equilibrium, so it is suggest to continue with the long-term operational tests. This limit is different from the one previously found (565 °C) (Bradshaw *et al.*, 2002) and the reason is that different mass loss definitions lead to different limits. Additionally, the stabilizing role of increased oxygen partial pressure is proven and confirmed. Clearly, the material of tanks and pipes has to be resistant to corrosion at least up to the stability limit of the HTF. Unfortunately, metal corrosion mechanism due to the molten alkali nitrate salts is not well known nor established, so additional studies are required for the purpose of understanding whether there is the presence of Stress Corrosion Cracking (SCC) (Bauer *et al.*, 2013). However, it has been proven that chloride impurities are dangerous by reason of ruining the protective oxide layer of the metal, creating a favourable environment for corrosion to start (Bauer *et al.*, 2013; Goods and Bradshaw, 2004; Kearney *et al.*, 2004). Up to now, it is not enough clear the influence of nitrate/nitrite equilibrium reaction, happening in the operating range temperatures up to 600 °C, on corrosion. Trace moisture increases the corrosion rate, too (Bauer *et al.*, 2013; Kearney *et al.*, 2004). On the other hand, about the actual experimental study on chloride eutectic salt mixture, stable above 800 °C, four types of Hastelloys are tested to find the one that best resists to corrosion: C-276, C-22, N and SS 304. Corrosion rate results to increase in a hotter environment, but a satisfying and favourable Hastelloys behaviour is registered in absence of air, so that it is possible to conclude that the eutectic mixture $NaCl–KCl–ZnCl_2$ is able to work up to 800 °C in pipes and tanks constituted by this advanced material without corroding them, provided an anaerobic environment (Vignarooban *et al.*, 2015).

Conversely, regarding the $sCO_2$ cycle, characterized by extreme conditions that make the fluid work over the critical point, experiments are conducted up to 730 °C and 20.7 MPa. Even though the compact turbomachinery would allow to use costly Ni-based superalloys which show exceptional corrosion resistance, economic considerations limit their usage. Ni-based alloys are the most used for constructing the pipes and the components as this compound does not show considerable change on the oxidation rate connected with the pressure: a protective and stable layer of Chromium is formed which prevents the fluid from corroding the containing pipe and the components passing through. With fine-grain austenitic steel, on the contrary, a Chromium scale is formed at ambient pressure, but then it is substituted by a Fe-oxide layer, whose formation and development is unpredictable, leading to a variable corrosion rate. However, an estimation of long-term austenitic stainless-steel operations in contact with $sCO_2$ shows a beneficial “healing” mechanism, after 10,000–15,000 hours with temperature ranging between 560-650 °C, that slows down the oxidation rate. In any case, further long-term tests are needed to assess the $sCO_2$ (Holcomb, Carney and Doğan, 2016). Age hardened Ni-based alloys represent another possibility for supercritical carbon dioxide cycle elements: they offer an exceptional creep resistance, acceptable ductility and weldability, positive ash corrosion and oxidation

resistance, allowing reduced wall thickness. One of the most used is INCONEL alloy 740H (UNS N07740) (DeBarbadillo *et al.*, 2018), firstly studied and developed for advanced ultra-supercritical steam boilers, characterized by conditions similar to the $sCO_2$ cycle (Holcomb, Carney and Doğan, 2016), so that recently it has been studied for this application, too. The interest in 740H has increased since technology improvements allow to work at HTF temperatures above 700 °C: on such situations, ferritic stainless steel cannot be employed and austenitic stainless steel reduce their resistance, resulting in unfeasible thick walls, as well as solid solution strengthened Ni-based alloys, such as 800HT, 617 or 230. INCONEL alloy 740H is the first age-hardened alloy for pressurized elements construction, showing incredibly superior stress resistance, as shown in Figure 3.2 (DeBarbadillo *et al.*, 2018). But, up to date, only small-scale lab tests have been presented and a full operating system has not been developed, yet.

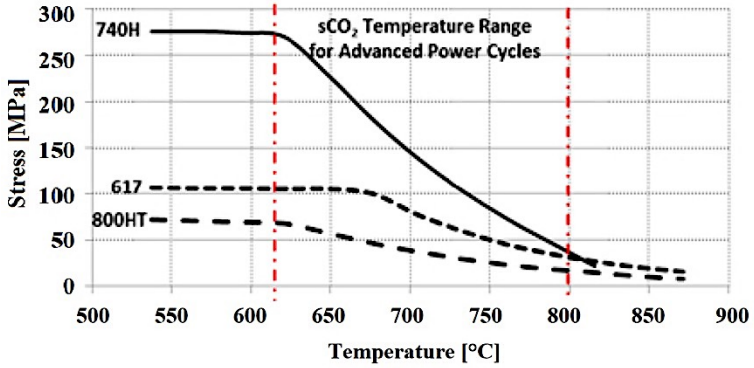


*Figure 3.2: ASME maximum stresses for alloys 740H, 617, 800H (DeBarbadillo et al., 2018)*

# 4. METHODOLOGY AND APPROACH

The focal point of this study is finding an efficient power plant characterized by reduced footprint and emissions, which can supply the baseload power using a renewable energy source and, most importantly, avoiding the adoption of fossil fuels. A fundamental feature of the desired power plant must be the capability to produce dispatchable electric energy and to meet the demand even when the energy source is inaccessible or too low to be exploited, which is a common and recurring issue connected with the employment of renewables. Concerning solar energy, the source is unavailable during early morning, evening and night. As a matter of fact, the feature which all renewable technologies have in common is the expensive, difficult and non-ecological storage system, based on accumulating electricity on batteries. All these reasons have represented the motivation to choose a CSP plant coupled with a recompression supercritical carbon dioxide cycle as object of the presented study. The recompression layout is the best compromise between number and dimension of components and efficiency: it allows a satisfying thermal recover employing the traditional components, so that the footprint and the costs are reduced when compared with intercooling or reheat designs, which need additional intermediate heat exchangers. Concentrating solar power technology is acclaimed to be the only one among renewable sources enabling the adoption of an easy and inexpensive thermal energy storage system, which is more convenient and environmentally-friendly than batteries. The receiver consists in the mature molten salt solar tower: its design allows a significant high HTF temperature which results in a definitely improved plant efficiency. Thanks to the chosen technology, it is easy to incorporate a thermal energy storage system, fundamental to decouple the electricity production from the availability of the solar energy. A molten salt, two-tank direct system has been selected, since up to now it is well established and used in current operating plants, such as “Gemasolar” in Sevilla. Plant characteristics are similar to commercially operating CSP power plants, with the view of comparing the performances of the studied system with the actual state of the art regarding materials and

components: in fact, a key point of this study is to underline the presented plant feasibility and concrete construction. Hence, starting input data for the solar field constraints, such as minimum and maximum salt temperatures, are taken from "Gemasolar" power plant (Relloso and García, 2015), the only solar plant commercially operating with a molten salt TES system, while the power cycle is design based on experimental studies about $sCO_2$ cycles (Ahn *et al.*, 2015; Binotti *et al.*, 2017; Wang and He, 2017), considering the actual equipment limitations and the connection with the molten salt loop that strongly restraints the $sCO_2$ performances.

## 4.1 Plant design

The studied power plant (Figure 4.1) is made up of the solar field, the heat storage system and the power block: Ebsilon® Professional 13.01 is used to design it and to simulate its behaviour along a discretized time of a day, in different periods of the year. Given the aim of simulating the daily behaviour, the system could be thought as composed by two different parts: the first one is needed to replicate the energy production during the period of the day characterized by the presence of the sun, while the second one is used to reproduce the evening and night time. The daily behaviour is simulated in a single model, where all the characteristic parameters change as function of the time and the period of the year. In order to homogenize the whole system and to simulate the strong interdependence of the different parts of the day, switches and controllers are employed: they make the system behaves in accordance with the time being. With a view to understanding the feasibility and the operation scheme of the plant, the "Time Series" tool of Ebsilon is used. After choosing a time span, all the peculiar thermodynamic quantities are obtained as function of the time being. So, as an example, the level of the hot storage tank is constantly monitored, with the purpose of obtaining the amount of molten salt that goes in the stock and the needed mass flow for the $sCO_2$ cycle to produce the required output. Regarding the produced electricity, the system automatically calculates the mass flow of molten salts and, simultaneously, of the $sCO_2$ required to reach the desired rated net power output (NPO) externally chosen. To do that, two controllers are used (C1 and C2 in Figure 4.1) which act as link between the molten salt loop and $sCO_2$ cycle: in this way, the electrical output could be arbitrary varied and, consequently, the mass flow of both fluids changes. Along these lines, flexibility is pursued. In details, the first controller (C1) is the one that, once the value of the required NPO is inserted, calculates the necessary mass flow of supercritical carbon dioxide; the second one (C2), instead, is the real connection between the two plant parts: being applied to the hot side of the primary heat exchanger (4) which enables the transfer of collected heat from the sun by the molten salt to the $sCO_2$, it automatically computes the molten salt mass flow necessary to heat the just calculated $sCO_2$ mass flow rate until the

TIT. The latter controller keeps the outlet temperature of the molten salt constant and equal to 376 °C, according to the considered design, in order to allow the correct transfer of the heat and to prevent the pinch point problem from occurring, always guarantying the minimum temperature difference.

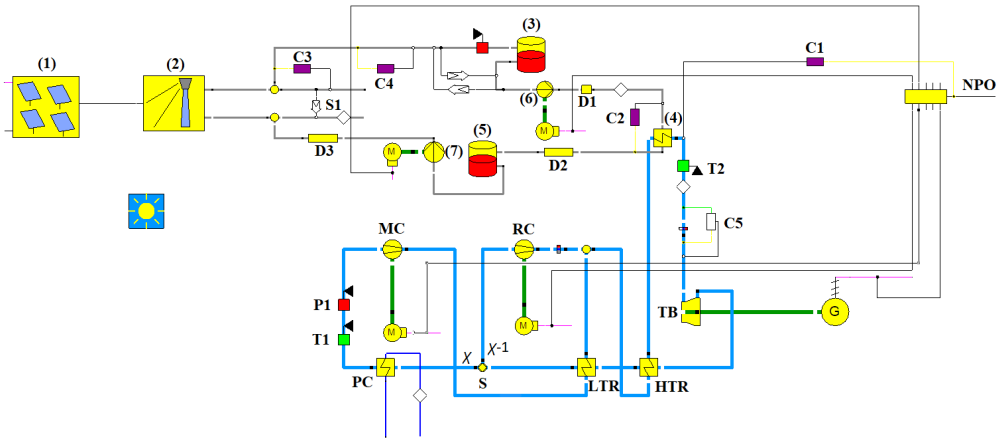


*Figure 4.1: Plant layout*

The efficiencies of each component and effectiveness for the heat exchangers are summarized in

Table 4.1, which in turn refers to Figure 4.1, and they are slightly lower than the obtained in previous studies (Dunham and Iverson, 2014), in order to obtain safer and more reliable results. The effectiveness of the heat exchangers is not given as input, on the contrary of the efficiencies and pressure losses, but they are calculated as the ratio between the actual transferred to the theoretical maximum heat in case of infinite side from the software, as function of the occurring heat transfer process.

*Table 4.1: Components efficiency, effectiveness and pressure losses*

| Cycle Parameter | Value |
|---|---|
| $\eta_{is\_compressors}$ [%] | 85.0 |
| $\eta_{mech\_compressors}$ [%] | 99.0 |
| $\eta_{el\_motors}$ [%] | 85.0 |
| $\eta_{mech\_motors}$ [%] | 99.8 |
| $\eta_{is\_turbine}$ [%] | 88.0 |
| $\eta_{mech\_turbine}$ [%] | 99.8 |

| Cycle Parameter | Value |
|---|---|
| $\eta_{generator}$ [%] | 98.6 |
| $\eta_{is\_pumps}$ [%] | 80.0 |
| $\eta_{mech\_pumps}$ [%] | 99.8 |
| $\varepsilon_{HTR}$ [%] | 96.4 |
| $\varepsilon_{LTR}$ [%] | 80.0 |
| $\varepsilon_{cooler}$ [%] | 93.8 |
| $\varepsilon_{main\_HEX}$ [%] | 98.7 |
| $P_{loss\_HEXs}$ [MPa] | 0.005 |

### 4.1.1 Solar field

The studied system is imagined to be put at a latitude of 30 ° North and longitude 30 ° East, near Alexandria and Cairo, in Egypt. Referring to Figure 4.1, inserting the geographical coordinated and the day of the year in the "Sun" component, then the heliostats field (1) works in accordance with the choice. It is chosen from the standard given by the software ($HEL180\_35N\_100MW_{th}$), but the number of the heliostats is modified in order to meet the desired dimensions. The proposed plant is made up of a 3,000 heliostats field (1) for a total reflective area of 600,000 $m^2$ focusing the sun radiation on a 127 m height tower (2) equipped with a tubular molten salt receiver of an aperture area equal to 247 $m^2$. Here the Solar Salt, composed by, in weight, 60 % of sodium nitrate ($NaNO_3$) and 40 % potassium nitrate ($KNO_3$), is heated up. Through a "General input value", the software is prompted to run with this material. As a matter of fact, the tower characteristics strongly affect the following power block properties and efficiency: the higher the HTF temperature at the receiver outlet, the higher the temperature reached by $sCO_2$ before entering the turbine. Then, enabling a bigger expansion ratio, the power block efficiency is improved. But, on the other hand, with the current technology of molten salt tubular receiver adopted for this project, increasing the receiver outlet temperature will result in a diminished tower efficiency due to the higher losses. Furthermore, to prevent pipes and tanks from Solar salt corrosion, the maximum temperature is set equal to 565 °C. Solar Salt and common tubular receiver have been selected with a view to designing and analysing the performance of a feasible system, which could currently operate with the actual state of the art. As discussed in section 3.2, novel molten salts compounds are under investigation, which could work

under the extreme operating conditions allowing for overall better system performance. But, up to now, they have been studied only in tests small-lab scale.

### 4.1.2 Heat storage system

Given the dimension of the plant due to the required power output, the active storage system represents the best choice, as explained in section 2.3. In fact, long pipelines and HTF viscosity cause pressure losses and, during the charging and discharging processes, pumps are needed to make the fluid circulate the fluid. Chosen a molten salt solar tower set-up, a two-tank direct system is selected: the heat fluid circulating and heated up in the solar receiver is the same that performs the storage role, too. This is another motivation which pushes towards the exploitation of molten salts: they have a high volumetric heat capacity, so tanks are compact, thanks to their high density (from the software, Solar Salt density is equal to 1,728 kg/m$^3$), and high heat transfer coefficient, but the thermal conductivity is low and the resulting exchange process is moderately efficient. Consequentially they are suited to play both the tower HTF and the TES HTF roles. Unfortunately, their viscosity is considerably high as well as the pumping work needed.

Solar Salt (60 wt% $NaNO_3$ and 40 wt% $KNO_3$) maximum allowable temperature range is between 565 °C, due to containing material corrosion, and 290 °C, to prevent the fluid from freezing. To ensure these constraints, as depicted in Figure 4.1, at the tower outlet two controllers are applied on the molten salt loop. The first one (C3) is activated when the temperature is equal to the lower limit and, thanks to a switch (S1), it sends the molten salt mass flow back in the solar tower, so that in the loop there is no circulating mass flow, otherwise it would be frozen and destroy the pipelines. The second one (C4), besides, avoids the circulation of an unstable fluid with a too high temperature, keeping the limit at 565 °C. Even if recently numerous different molten salts compounds are under investigations by virtue of their wider range of application (see section 3.5), in order to assess a power plant that could commercially operate today, using the actual state of the art, the standard and well-developed Solar Salt has been chosen. The heated Solar Salt, depending on the time of the year and of the day, goes through the pump (6) in the hot storage tank (3) and to the primary heat exchanger (4), that connects the molten salt loop to the power cycle. Here, $CO_2$ reaches and overcomes its critical condition, before entering the turbine (TB). The molten salt, after realizing heat, is sent to the cold storage tank (5), where the lowest allowed temperature equal to 290 °C is specified, and then it is pumped (7) back to the solar tower (2), closing the loop. Given the intense conditions and the dimensions of the plant, pumps are needed in the molten salt loop, as already proved by (Alva, Lin and Fang, 2018). The first advantage offered by the selected configuration clearly appears: the utilized tanks are compact. Indeed, the lowered dimensions are an explicit consequence of the molten salts high heat capacity that implies a very high energy density. For the sake of obtaining

realistic results, losses in pipes, especially regarding pressure and heat, are taken into consideration using the “Dummy piping” components (D1, D2, D3).

The crucial key of the developed study is the capability of the plant to supply baseload power and to operate 24 hours per day during the entire year, without being switched off because of the unavailability of the solar source, apart from the worst case simulated by the “Storage Empty” off design, described in subsection 4.3.2. This is an assumption made with the intention of choosing the maximum electrical power which guarantees the needful amount of stored mass flow in the hot vessel during a normal day operation to generate the rated electricity also during the night. In fact, as earlier discussed, referring again to Figure 4.1, necessary Solar Salt and $sCO_2$ mass flow rates are automatically calculated through controllers C1 and C2 as function of the required electricity. However, some days of stop are definitely needed during the year in order to perform the scheduled plant maintenance, but they are not considered at this design step because they do not happen during the ordinary day operation. In order to achieve the result of a continuous power supply, it is crucial to implement an HTF loop integrated with a storage system which, depending on the amount of the available solar radiation and the time of the day and year, allows the storing or the direct exploitation of the hot molten salt. In light of this, a design condition (full load) has been created, where the rated nominal electrical power is produced, and then two different sub-profiles have been realized on top of this main On Design configuration:

1. for the daily behaviour, running during the ordinary sun hours and during the evening and night period;
2. for the worst-case scenario, when solar radiation is absent and there is no stored hot molten salt anymore.

These configurations are essential to properly simulate the most probable cases that could occur during the routine plant operation: each one is characterized by distinct switches and controllers that in turn are activated and deactivated, according to a script suitably developed to such purpose (see section 4.3). The plant is designed to work without any scheduled stop connected with the unavailable sun radiation: in other words, during the normal operation, the output electricity is externally selected first in order to obtain, through the controllers C1 and C2 in Figure 4.1, the necessary molten salt mass flow rate that will be used and stored, enabling the uninterrupted electricity supply even during the night; then, with the aim of maximizing the thermal efficiency, the power output is chosen equal to the highest value allowing the complete charge and discharge of the storage tanks. Additionally, in order to obtain a more realistic simulation, the “Storage Empty” configuration is developed and performed: it takes into account the necessity to switch off the plant when the hot storage tank is completely empty while the sun radiation is too weak to produce hot molten salt with an exploitable temperature.

### 4.1.3 Power block

Instead of the commonly used steam Rankine cycle to produce electrical power, in this study the advanced recompression closed supercritical $CO_2$ is considered. The choice derives first from the compactness and potentially lower costs, thanks to the complete operation above the critical conditions (30.98 °C, 7.38 MPa) which leads to a dense fluid and higher efficiency, deriving from the superior heat recovery process; secondly from the non-toxicity and less-corrosiveness of $CO_2$, that enables the use of smaller components and potentially higher operating temperatures. Again, the software is calculating all parameters referring to the $sCO_2$ properties and limitations thanks to a "General input value" where the fluid is inserted. In Ebsilon® Professional 13.01, the $sCO_2$ is specified as "REFPROP 1013": this means that the characteristics of the fluid are taken from the database available online (NIST, 2013). As said before, this power plant set up has been chosen in the prospective of possible operation with the current state of the art. In this view, taking advantage from the experimental studies and the technology already developed for the common Brayton cycle, the recompression layout is adopted. Indeed, the latter leads to comparable or higher efficiencies than the supercritical or superheated steam Rankine cycle, with the strong advantage of the reduced components dimensions and the wider pressure ratio range of application. So, even if many other configurations are now under experiments, such as with intercooling or reheat or split flow in the turbine, the recompression cycle is selected thanks to the simple layout and the economic advantages deriving from its compactness (Wang and He, 2017). As a first attempt, starting from data used in previous studies and in "Gemasolar" power plant, the power cycle (Figure 4.1) has been developed with a minimum pressure equal to 10.0 MPa (100 bar) inserted through the component P1, a bit higher than the critical one: as reviewed in previous sections, the lowest pressure which maximizes the cycle efficiency is not exactly the critical one (Wang and He, 2017). Regarding the inlet turbine pressure, 22 Mpa (220 bar) is found to be a value leading to high thermal efficiency. The cycle maximum pressure is slightly higher, 22.08 MPa, since pressure losses are always present in power plants and taken into account in the heat exchangers and pipes. This pressure range is in accordance with previous studies regarding the $sCO_2$ power cycle (Ahn *et al.*, 2015; Binotti *et al.*, 2017; Wang and He, 2017), highlighting once again the real possibility of having this plant in operation with the current technology. The minimum temperature of the cycle in the design condition has been set to 35 °C (set by the component T1 in Figure 4.1) in consideration of the opportunity of making the hot water from the cooler (PC) interesting for a possible CHP configuration. In addition to the higher efficiency that a wet cooling system provides, the possibility of a CHP configuration is contemplated: hence, the minimum cycle temperature is chosen in accordance with experiments discusses in subsection 2.7.5 (Moroz, Burlaka and Rudenko, 2014). In this way, the outlet temperature of the water, in the cold side of the cooler, can be used for building heating

purposes, being in the range between 20 °C and 100 °C (Alva, Lin and Fang, 2018). Considering the Heat Utilization Factor (HUF), defined as the ratio of the sum of the net power output and the useful heat to the heat consumption, it is clear that the thermal energy from the sun is better exploited: in the design condition, the thermal efficiency is about 33.4% at a net power output of 45 $MW_{el}$, while the HUF is around 94%, in accordance with (Moroz, L., Burlaka, M. and Rudenko, O., 2014). Nevertheless, the main output of the plant is considered to be the electricity and the thermal power is regarded as a secondary advantage that the developed system offers, like a by-product. In this experiment, the turbine inlet temperature is set to 525 °C through the component T2 in Figure 4.1, even if it is well known that the higher it is, the better the efficiency. This is a strong penalization of the performance but, as already explained, the analysed plant is thought to operate with the current commercial technologies and Solar Salt does not allow operating temperatures higher than 560 °C. Moreover, changing one single parameter in the cycle greatly affects the behaviour of the whole system, so it is not allowed to arbitrary change a physical value without considering the consequences on the whole plant output performances, including the molten salt loop, too. For example, once the maximum Solar Salt temperature is fixed to 565 °C due to stability and possible corrosion, the pinch point problem will surely occur if the TIT is increased more than 560 °C: this is the main reason penalizing the thermal efficiency of the analysed plant with the earlier described temperatures and pressures, equal to 33.4 % in the design condition.

One of the biggest problems related with the $sCO_2$ cycle is the deep change of the specific heat capacity near the critical pressure: in this case, it depends on the temperature as well as on the pressure. For this reason, the recuperators are very critical components and the split ratio $\chi$ is a crucial parameter to attain maximum efficiency and avoid the so-called “pinch point problem”. It occurs when the minimum temperature difference between the hot and the cold stream in the heat exchanger is violated. As already explained in subsection 2.4.3, when the working fluid is supercritical carbon dioxide, the pinch point can be disrespected also in certain regions within the heat exchanger and not only at the inlet or outlet of the component, as depicted in

Figure 4.2: Pinch point occurrence in a sCO2 heat exchanger (Ladislav et al., 2016) (Ladislav *et al.*, 2016). A possible solution is to split the flow, so that the smaller mass flow of fluid characterized by a higher specific heat capacity in the cold high-pressure side is well matched with the bigger mass flow of low specific heat capacity fluid of the hot low-pressure side. The optimal split ratio $\chi$, whose definition is the ratio of the main compressor mass flow to the total mass flow, in the first attempt power cycle is found to be equal to 0.699: looking at Figure 4.1, this means that almost 70 % of the total flow is first cooled down by the component PC and then compressed near the critical point in the main compressor (MC) until the maximum pressure, while the other 30 % is directly compressed by RC to

the maximum cycle pressure. The two flows mix before entering the heat exchanger (4) which performs the link between the Solar Salt loop and $sCO_2$ cycle. In the latter component, the energy balance and the pinch point problem, as well, are two crucial issues: all possible efforts are done with the purpose of transferring to the $sCO_2$ all the heat collected by the molten salt, so that the power cycle is as efficient as possible. But, since the $sCO_2$ has already been heated up in the recuperators, first in the LTR and then in the HTR, it enters the heat exchanger (4) with a quite high temperature. For this reason, the outlet molten salt temperature cannot be too low to respect the pinch point and it is constrained by the controller C2 that, as already explained in subsection 4.1.2, calculates its required mass flow, too.

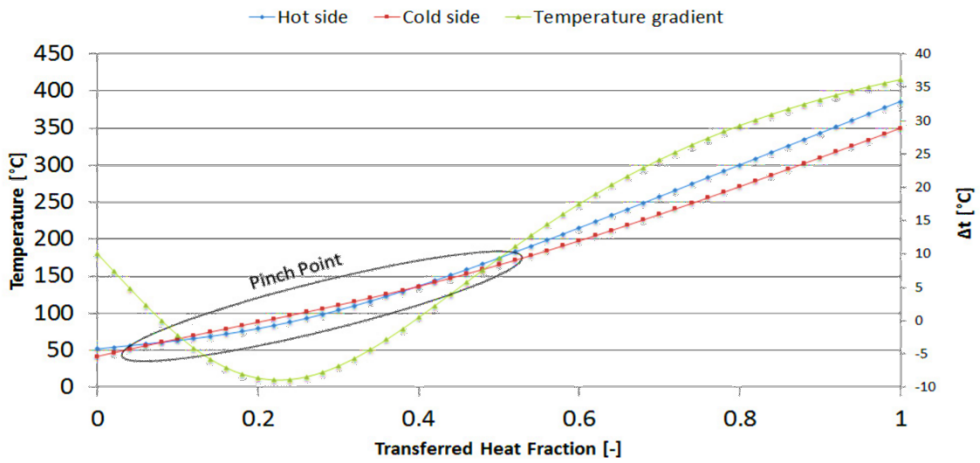


*Figure 4.2: Pinch point occurrence in a $sCO_2$ heat exchanger (Ladislav et al., 2016)*

### 4.1.4 Split ratio, TIT and thermal input vs thermal efficiency

The split ratio (χ) is generally defined as the ratio of the main compressor mass flow to the total mass flow. Mathematically, a split ratio equals to 1 indicates that the total fluid mass flow is going to the main compressor, avoiding the re-compressor, while 0 splitting means that no mass flow is cooled down, which is impossible in thermodynamic terms because, in order to have stable operations, heat must be rejected to the environment. Since it determines the amount of fluid passing through the cooler and through the re-compressor, it has an important effect on the efficiency: the heat recuperation process depends on the matching of the flows with different specific heat capacity and mass flow. When it is too low, the cooling process is insufficient, and heat is accumulated in the cycle: the re-compressor is forced to deal with a hotter stream and the compression work is increased, so that the turbine has to produce a larger output which can be reached only through a larger thermal input. Surely, the thermal efficiency is penalised. On the contrary, when the split ratio approaches the unity value, advantages of recompression layout are eliminated,

and the thermal efficiency strongly decreases. So, there is an optimum value which minimizes the required thermal input to reach the given TIT and maximizes the thermal efficiency. However, it is worth to underline that these mentioned parameters are intrinsically bounded: they have to be changed together in order to find the optimum point of operation (Luu *et al.*, 2017). Before performing the sensitivity analyses, a first cycle attempt is simulated with a TIT equal to 525 °C and the best split ratio results to be 0.699, with minimum and maximum operating pressure respectively equal to 10 MPa and 22 MPa.

One of the pursued objectives of this study is the flexibility of the plant: the inserted controllers enable plant to operate at different power outputs, with the consequent automatic calculation of the molten salt and $sCO_2$ mass flow rate. However, the turbine inlet temperature is fixed, in order not to violate the actual material components limitation and to avoid the occurrence of the pinch point problem. The heat source is time-dependent whilst the power output is imposed by the user, so the resulting calculated mass flow rates are not optimal, they just make the cycle run and produce the externally required energy. For these reasons, it is not possible to fully optimize the plant since the best split ratio value strongly depends on the turbine output and on the circulating mass flow rate: in other words, given the required output to be obtained, without acting on the thermal input nor on the TIT, one value of the split ratio exists that enables the minimum thermal input and the maximum thermal efficiency. In this case, as a first attempt, a splitting ratio of 0.699 is found to optimize the plant operation with a net power of around 35 $MW_{el}$ during summer and 25 $MW_{el}$ during winter, at a TIT of 525 °C. The required output is absolutely demanding and ambitious: it is the maximum value which enables the system to operate during the whole day, in the sense that the plant generates enough hot molten salt to directly produce electrical energy during the day and to use the stored mass flow to supply the high demand also during the hours of absent sun radiation. In consequence of the pushed and stressed required performances connected with fixed non-optimized thermodynamic conditions, such as limited maximum temperature and narrow pressure ratio, the system thermal efficiency results almost equal to 33 %. From Figure 4.3 (Dunham and Iverson, 2014), it is clear that the studied cycle has a lower thermal efficiency than the one found for the same layout with the same thermodynamic parameters (TIT=525 °C, $P_{max}$=22 MPa, wet cooling), but without all the constraints used to reach the necessary plant flexibility. This is due to the fact that all the chosen thermodynamic quantities are not optimized to maximize the efficiency, but they are a compromise among thermal efficiency, flexibility and whole-day plant operation. For clarification, during winter the solar field concentrates the sun radiation on the tower from 8:00 am to 17:00 pm. For the remaining hours, 25 MW of net electrical power are continuously produced to supply the demand. However, it is interesting to notice the big difference in the efficiency as function of the pressure, especially 10 MPa, 20 MPa and 30 MPa. In particular, at a maximum pressure of 10 MPa, only a small amount

of the fluid at the compressor inlet is in the supercritical region, so the advantages are not gained. Increasing the pressure, the fluid becomes totally supercritical and its properties can be fully exploited.

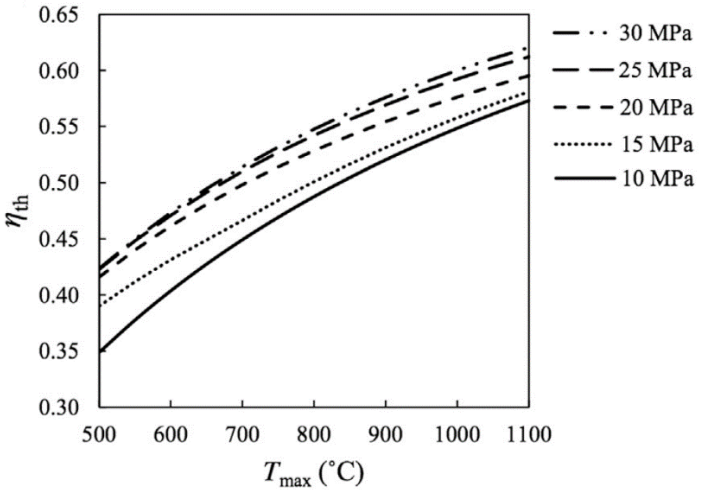


*Figure 4.3: Thermal efficiency of $sCO_2$ cycle as function of the maximum pressure and temperature (Dunham and Iverson, 2014)*

## 4.2 Sensitivity analysis

The described cycle is designed with operation conditions based on literature review, in order to obtain a realistic and feasible system. The software Ebsilon® Professional 13.01 offers the possibility to work in compliance with dedicated scripts, written in Pascal language. Taking advantage of this opportunity, on-purpose scripts are created which, in turn, generate different sub-profiles where some operating conditions are changed. In this way, the response of the system is studied as function of the parameters variation. At the design step considered in this project, the dynamic of the components is not considered: the system is studied as a series of steady-state conditions.

### 4.2.1 Design optimization

The previously described model leads to 33.4% thermal efficiency at design condition. This value is lower than the one found in experimental studies working in the same conditions (Dunham and Iverson, 2014), since during the plant development flexibility and whole day operation have been the most important features to be satisfied. After the first attempt, which however shows feasible performance and results, the cycle is optimised using a series of sensitivity analyses. Hence, the main aim is to improve the thermal efficiency while taking into consideration the current state of the art and technological limitations, i.e. materials that could withstand the cycle maximum pressure and temperature stresses,

maximum allowable temperatures and so on. A first group of sensitivity analyses is conducted aiming to find the proper range of variation for each parameter, in order to obtain physically meaningful results for the whole day operation: starting from values of the first attempt cycle, one single parameter is varied keeping the others constant. Then, a unique analysis is carried out varying all the parameters simultaneously in the just founded values interval. This is necessary since the best efficiency does not depend only on one single thermodynamic quantity, but it is extremely affected by the combination of variable parameters. The sensitivity analysis is carried out taking advantage of the possibility offered by the software to create sub-profiles, starting from the design profile, in agreement with inserted Pascal scripts. The examined thermodynamic quantities are:

1. the turbine inlet temperature;
2. the minimum cycle pressure;
3. the turbine inlet pressure;
4. the split ratio.

The $sCO_2$ mass flow is still calculated by the software through the power output controller in order not to lose flexibility. At the beginning, a script has been written with the aim of creating different sub-configurations, each one characterized by a change in a single parameter, the one whose influence has to be investigated, while all others are kept constant and equal to the values used in the first trial cycle. After finding the proper range of variation for each quantity, another on-purpose script has been written to create sub-configurations characterized by the simultaneous change of all the four parameters. It is fundamental to highlight that all the previously discussed constraints which enable the plant operation during the whole day and the entire year are still present and, as a consequence, they negatively affect the thermal efficiency once again. First, the maximum Solar Salt temperature fixed at 565 °C prevents the $sCO_2$ from working at higher temperatures, which are needed to reach improved efficiencies. In fact, in a heat exchanger fixing the inlet temperature of the hot fluid means limiting the outlet temperature of the second fluid, in order to respect the minimum temperature difference. Secondly, the actual material limitations impose a maximum pressure at which the cycle could operate that has to be respected in order not to exceed the allowable pipes stresses. In addition, the controllers used to calculate the circulating mass flow rates based on temperature and required power output contribute to restrict even more the thermodynamically feasible range of variation for the tested parameters, summarized in Table 4.2. For the sake of understanding, a TIT of 600 °C is studied even if errors due to pinch point violation are expected.

*Table 4.2: Range of variation for 4-parameter sensitivity analysis*

| Parameter | Minimum value | Maximum value |
|---|---|---|
| Minimum pressure [MPa] | 9.5 | 10.5 |
| Maximum pressure [MPa] | 20.0 | 30.0 |
| Turbine inlet temperature [°C] | 500 | 600 |
| Split ratio [-] | 0.65 | 0.75 |

All the imposed restrictions limit the system from operating at high efficiencies, even after performing the sensitivity analysis: the maximum optimum is 35.7 %, reached at 550 °C TIT, minimum and maximum cycle pressures respectively 9.5 MPa and 28.0 MPa and 0.75 as splitting. In this case, increasing the net electrical power up to 45 $MW_{el}$ and the TIT until 560 °C, with an approaching temperature difference of only 5 °C in the primary heat exchanger (component (4) in Figure 4.1) connecting the solar and the power cycles, which is an extreme and risky condition, the thermal efficiency reaches values of around 36.5 %. An important remark is the fact that the maximum efficiency is not reached with the maximum pressure (30.0 MPa in this analysis): this result can be justified with the relatively low employed TIT which does not enable improved performances when coupled with an increased inlet turbine pressure. With maximum pressure in the range of 20.0 MPa and 22.0 MPa, the energy balance in the main heat exchanger (4) is very luckily to be violated, as well as the pinch point. The selected data set for input values is validated by recent experimental studies (Holcomb, Carney and Doğan, 2016) about the current materials used for $sCO_2$ power cycle components, as shown in Table 4.3, where it is underlined that the turbine inlet temperature could be further increased to obtain improved performances, but the examined cycle is strictly limited by the Solar Salt maximum allowable temperature equal to 565 °C.

In conclusion, after accepting the reduced performances of the power cycle, referring again to Figure 4.3, due to the constraints applied with a view to enhancing the plant flexibility and allowing the whole day operation during the entire year, the design configuration is chosen to be the one allowing a thermal efficiency of 36.5 %, with a net electric power output of 45 MW, reached through a TIT of 560 °C, a splitting of 0.75 and a maximum and minimum pressure respectively of 28.0 MPa and 9.5 MPa. This is the starting point for the subsequent analyses of the plant. Considering now the whole system efficiency, it is clear that the TIT is a crucial parameter, since its intensification positively affect the power cycle efficiency, but jeopardized the tubular receiver performance because it causes an increase

of losses. In this view, Figure 4.4 (Dunham and Iverson, 2014) highlight the contrasting role of the maximum cycle temperature. The reached efficiency of 36.5 %, obtained considering also the solar loop constraints, is in line with the aforementioned study.

*Table 4.3: Representative temperatures and pressures of components in sCO2 power cycles (Holcomb, Carney and Doğan, 2016)*

| Cycle | Component | Inlet T [°C] | Inlet P [MPa] | Outlet T [°C] | Outlet P [MPa] |
|---|---|---|---|---|---|
| **Indirect** | Heater | 450–535 | 1.0–10.0 | 650–750 | 1.0–10.0 |
| | Turbine | 650–750 | 20.0–30.0 | 550–650 | 8.0–10.0 |
| | HX | 550–650 | 8.0–10.0 | 100–200 | 8.0–10.0 |
| **Direct** | Heater | 750 | 20.0–30.0 | 1,150 | 20.0–30.0 |
| | Turbine | 1,150 | 20.0–30.0 | 800 | 3.0–8.0 |
| | HX | 800 | 3.0 – 8.0 | 100 | 3.0–8.0 |

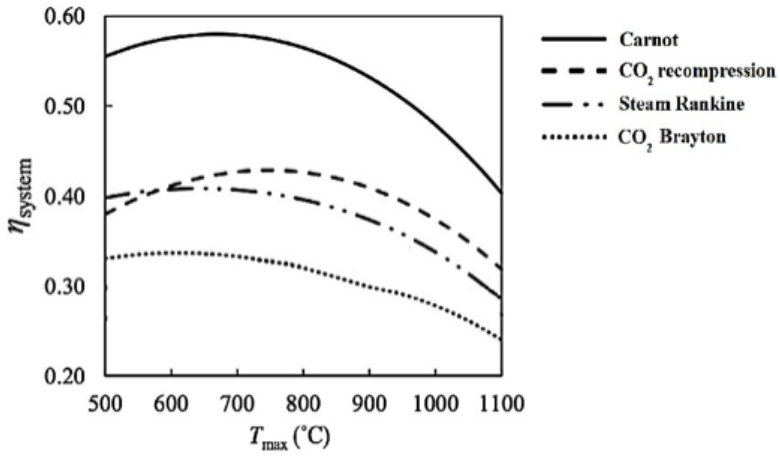


*Figure 4.4: System efficiency for different power cycles at 30 MPa as maximum pressure, wet cooling (Dunham and Iverson, 2014)*

## 4.2.2 Flexible plant operation

After the group of sensitivity analyses made with a view to optimizing the plant and to enhancing the thermal efficiency, further sensitivities are conducted in order to fully exploit the flexibility of the designed system. Starting from the optimum condition, it is wanted to understand how the cycle reacts to the change in the required power output, in case this is decreased and increased. Hence, a script is written which creates sub-profiles with the same

optimized thermodynamic parameters, varying only the required output. In this case, the analysis is not done changing all the affecting parameters simultaneously, as previously done, even if it is well-known that they are interdependent and act together on the plant behaviour and efficiency. On the contrary, it is intentionally chosen to start from the cycle optimized for 45 $MW_{el}$ in the design operation, to select its thermodynamic features as the standard for the plant, and then to study how the variation of the required output affects the installed plant, whose parameters have already been designated. The main result is that the thermal efficiency is improved by the increasing of the demand until 45 $MW_{el}$, after which the thermal efficiency stays quite constant. This is an expected result, since the examined cycle is optimized to reach exactly 45 $MW_{el}$. This analysis is necessary to understand how the plant reacts to a sudden increasing or decreasing of the demand, which is not the ordinary daily operation. Obviously, if more power is required, the necessary $sCO_2$ and molten salt flow rates increase, since the temperatures are fixed, the solar field has already been selected and it produces the same HTF flow rate. The needful flow rates are automatically calculated by the inserted controllers (see the following subsection 4.3.1 for details), so the software is able to compute all the new quantities as function of the changed required output. As a consequence, if the demand increases during the "Day" hours, when the hot tank is accumulating, it will not be able to store all the mass flow that is needed to supply the rated power during the night, because a considerable part of the amount that would be stored is instead used to supply the higher power. Given the fact that it is strongly wanted to prevent the plant from being switched off in order to avoid the transients of the components, one feasible solution could be supplying a lower amount of electric power for a short time interval in order to compensate the previous higher demand. Flexibility of the proposed plant allows this kind of regulation. Of course, also increasing and decreasing the power output all the components will run in a non-optimal situation and will experience a transient operation, but qualitatively the effects will be for sure less influent than the ones caused by the complete plant shut down. The dynamic of the components is not studied at this design point, but the system is viewed as a succession of steady-state conditions. If during the "Day" hours the demand is decreases, the abundant mass flow of produced Solar Salt could be stored in the hot tank, since it is designed slightly bigger in order to have a safety margin. It is assumed that in any case the increasing and decreasing of the demand will compensate. Concurrently, if the regulation is needed during the night, a higher demand implies the usage of a larger amount of the stored molten salt, that has to be compensated by a subsequent decreasing in the produced power; if the demand is lowered, the unused molten salt mass flow can be kept in the hot tank, thanks again to the safety margin of the component. The allowable regulation ranges from 10 $MW_{el}$ to 60 $MW_{el}$, after which the necessary water flow rate is larger than 400 kg/s. It is fundamental to underline object of this analysis is not the dynamic and the transient study, but the demonstration

that the inserted controllers and the on-purpose written scripts allow the plant to adapt and to operate in different conditions only by changing the demand, that is the plant flexibility. Then, a dynamic analysis is absolutely necessary to assess the feasibility of these changes, but it is not object of this project.

## 4.3 Model description

The simulation is performed starting from the design condition, at midday on the 21st of June, during the summer solstice, when the sun radiation and the produced molten salt mass flow are maximum. Then, with the purpose of simulating a 24-h daily behaviour, the design condition is replicated in two models, each characterized by a particular Off-Design (OD) condition: (a) for the daily operation, accounting for the charge and discharge of the tanks; and (b) for the case of absent radiation, having the molten salt storage empty at the same time. So, each model is made up of:

1. the design condition, which is common for both models and gives the same results;
2. a peculiar OD working in accordance with a special on-purpose written script.

In this way, the software is being informed if accumulating is necessary or whether the hot molten salt has to be used directly to produce $sCO_2$ and in turn electrical power or, further, if the molten salt from the hot tank has to be used and hot tank has to be emptied when the sun radiation is absent. The OD sub-profile is required to perform the Time Series calculation, where the time is discretized (t) and all the parameters are calculated in a one-hour time interval, having the conditions of the previous one (t-1) as input.

The design condition is a static configuration, needed as a starting point for the Time Series calculation. Here, the value found thanks to the previous sensitivity analyses, a TIT of 560 °C, a splitting of 0.75 and a maximum and minimum pressure respectively of 28.0 MPa and 9.5 MPa, are given as inputs.

### 4.3.1 "Daily behaviour" off design

In order to perform the Time Series calculation and to analyse the amount of molten salt that the power plant can store in the hot tank during the hours of maximum radiation and how this is discharged during the evening and the night, the "Daily behaviour" off design profile is created. Hence, it performs the ordinary operation of the plant during an entire day. Figure 4.5 represents the initial time for the "Day", which is the period characterized by the presence of the sun, while Figure 4.6 shows the state of the plant in the first hour of the "Evening", when the sun does no longer heat the molten salt. For the sake of clearness, the two periods of the day are described separately, even if they are both obtained in the

same model, the “Daily behaviour”, in order to perform a homogenous and continuous simulation.

During the “Day”, the amount of hot molten salt produced by the solar field is larger than the mass flow required to produce the rated electrical power: the abundant mass flow is accumulated in the hot tank (3), which is empty at the initial time (Figure 4.5). The stored solar salt is then used during the evening and the night, when the sun radiation starts decreasing and becomes absent. Since this simulation is performed during the presence of the sun, the mass flow needed to produce the nominal power (NPO) has to be calculated. Indeed, despite the fact that this profile runs starting from the early morning, the large installed solar field allows to activate the accumulation process in the very early hours of solar radiation. This is a consequence of the first aim of the proposed plant: to supply always the rated power, chosen as the maximum allowable by the selected system configuration. During the “Day” hours, the Solar Salt is accumulated in the hot tank (3), while the cold vessel (5) is emptied in order to always respect the mass balance of the solar tower component (2). In fact, the outlet tower mass flow of salt is larger than the one needed to release heat, so the mass flow entering the cold tank is lower than the amount at its outlet and it results in unloaded condition, in conformity with what was expected. This result will be largely explained in section 5.2 and shown in Figure 5.3. In accordance with the developed set up, the circulating mass flow rates are computed based on the temperature for the correct heat transfer process and on the power output. First, the $sCO_2$ amount is calculated, based on the NPO externally chosen. Then, looking at Figure 4.5, on both sides of the main heat exchanger (4), which links the storage loop and the power cycle, the controller C2 acting on the outlet molten salt temperature is activated in order to maintain its temperature equal to 376 °C. In this way, after obtaining the necessary mass flow of $sCO_2$ to generate the electrical power through the controller C1, the solar salt amount that avoids the violation of the pinch point is calculated by the second controller. Hence, two objectives are pursued simultaneously: the correct heat transfer process between the solar salt and the $sCO_2$ is ensured and, in the same time, the indispensable amount of molten salt is calculated. In line with the chosen methodology, the “Daily behaviour” configuration has to replicate the best and optimised conditions at midday: in fact, the turbine and main compressor inlet temperature and pressure at 12:00 are the same as the design configuration. However, in order to run the Time Series and observe the plant behaviour changing with time, an OD configuration is required by the software. Regarding the power cycle, contrary to what happens in the design condition, in this case it is not possible to set the enthalpy at the inlet of the turbine and the main compressor by giving temperatures and pressures as input: the pressure is still given as an input value by the component P1, but the temperature is calculated by the software and both the components T1 and T2 are deactivated. In fact, since it is a closed cycle, the temperature distribution cannot be known

a priori and has to be calculated in the simulation depending on the heat exchange process. Therefore, a fictitious controller C5 is inserted before the turbine, which is deactivated in the design case, to ensure the calculation of the enthalpy taking into account the common pipe losses. Notice that C5 in the OD configurations becomes purple, while, in the design condition, it is white. Its connection lines are placed on both side of a separator, activated again only in OD, that allows a slightly change of enthalpy values and makes it converge. In the OD configuration, at midday of the 21st of June, the calculated enthalpy results are exactly equal to the obtained one in the design. These results are in line with the expectations.

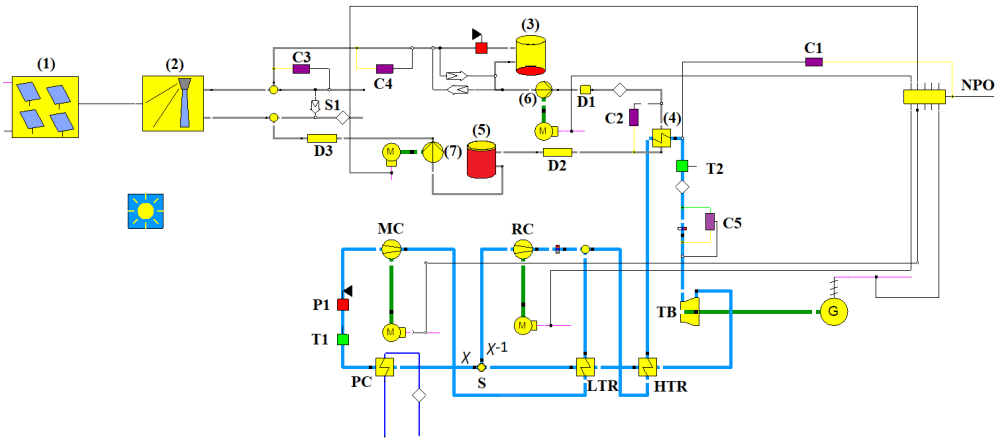


*Figure 4.5: "Day" configuration*

The “Evening” (Figure 4.6) starts to operate after the last hour of the “Day”, that is the last hour characterized by the presence of the sun. Since they are performed in the same model, “Evening” and “Day” are consistent, where the starting data set for the “Evening” simulation is exactly the output of the last hour of the “Day”. This is just to remind that the two parts, “Day” and “Evening”, are not separated, but they are performed in the same model. They are separately described for the sake of clearness and simplicity. During summer, the molten salt mass flow stored in the hot tank is sufficient to satisfy the rated demand of 45 MW for all the night, until 6:00 in the morning. At this time, the hot storage tank is empty and the heliostats (1) begin to reflect the direct solar radiation to the receiver (2), where Solar Salt is heated up and one part goes into the hot tank (3), which starts to be filled up again, and the majority of the mass flow goes directly to the main heat exchanger (4) in order to make $sCO_2$ produce the rated power. During winter, this shift occurs at 8:00 am, since the sun radiation is weaker than in the summer case. An important feature of the “Evening” is the activated component “Value transmitter”, the switch S1 in Figure 4.6, just after the tower (2): it prevents the system from operating when the temperature is equal to or less than 290 °C, which is the freezing point of the Solar Salt. In this way, when the radiation is weak, typical condition during the evening and night hours, the small mass flow

of molten salt characterized by a low temperature and negligible enthalpy is sent back to the tower to respect the mass balance of this component and, in the same time, to avoid the circulation of a freezing fluid in the pipes of the system. Hence during the "Evening", the mass flow before the hot storage tank is null, while after it there is a constant flowing of the fluid which empties the hot vessel and heats the $sCO_2$. Accordingly, before the cold storage tank (5) there is the same flow, while after the container it is null, to always balance the mass on the input and output of the tower. So, during the evening and night hours, the hot storage tank is emptied while the cold one is filled up, whilst the opposite happens during the "Day" hours.

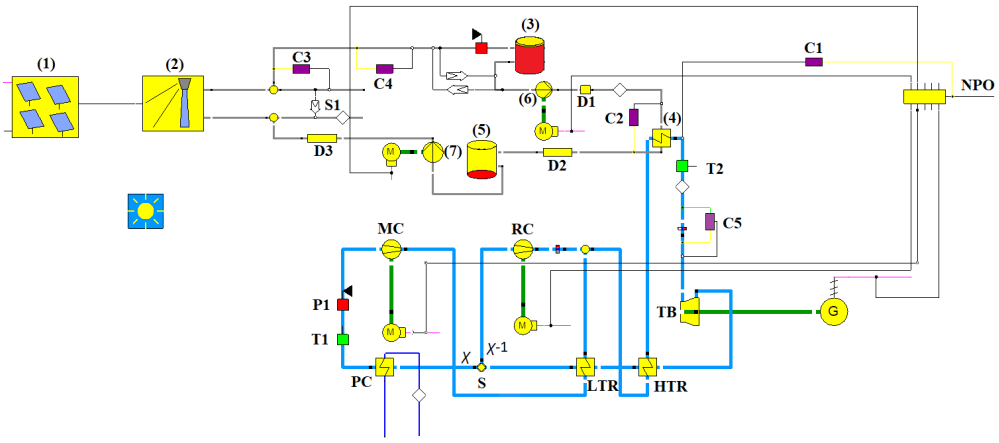


*Figure 4.6: "Evening" configuration*

## 4.3.2 "Storage Empty" off design

"Storage Empty" configuration (Figure 4.7) is necessary to simulate the worst-case scenario: it occurs when the hot storage tank is empty and the sun radiation is too weak to produce the molten salt with the required features to transfer thermal energy. In this case, the amount of molten salt has a too low temperature and it could freeze inside the pipes. Hence, in this configuration the "Value Transmitter" S1 after the solar tower is activated: when the temperature goes below 290 °C, which is the freezing limit for the used Solar Salt, it prevents all the molten salt mass flow from circulating in the loop. Obviously, as a direct consequence, in the power cycle no output is produced, since the heat in the heat exchanger (4) is unavailable and the $sCO_2$ is hindered from reaching the needed supercritical conditions. For this reason, the controller C1 which allows to choose the electrical power and then calculates automatically the fluids mass flow is switched off (it is white in this configuration). Additionally, the pressure input P1 is deactivated because there is no circulating mass flow, while temperatures in T1 and T2 are given since they are required by the software to calculate all the cycle thermodynamic parameters without errors. As in the "Evening" configuration, the switch S1 plays the key role of avoiding the circulation of a

freezing fluid: indeed, the “Storage Empty” set up performs not only the case of the night hours, when the sun is absent, but also all that situations characterized by a powerless sun radiation which is not able to heat the molten salt over 290 °C. The fundamental difference between the aforementioned configurations is the level of the hot storage tank, that at the beginning of the “Evening” simulation is full, while in the “Storage Empty” is completely vacant and hence it is uncapable of suppling the amount of molten salt to power the cycle. This configuration is used to simulate the unlucky event which urges to switch off the plant.

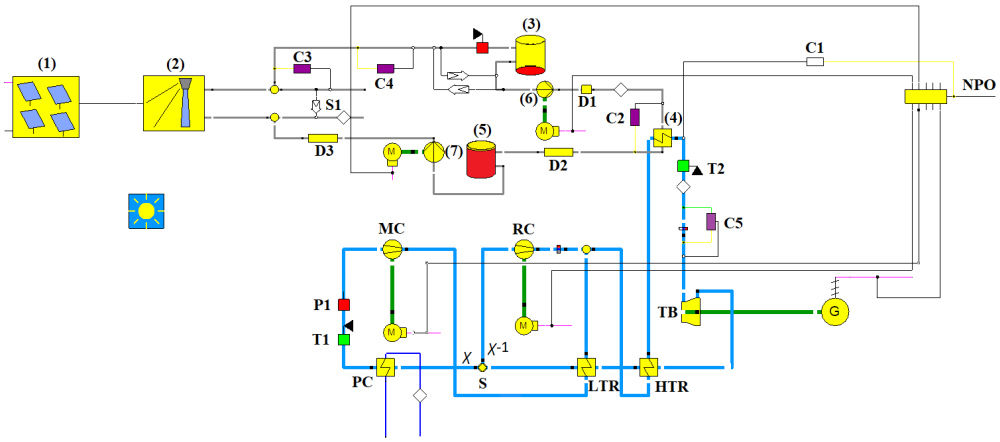


*Figure 4.7: "Storage Empty" off design configuration*

## 4.4 Seasonal and daily behaviour

The studied plant is able to supply electrical energy for the entire year. Correspondingly, the output is function of the sun radiation and, as a consequence, depends on the time of the day and the period of the year. The whole system is designed to be as flexible as possible: the net electrical power is allowed to be externally chosen and regulated and, hence, it is changed with time. For this reason, different days of the year are simulated and analysed separately as example for spring, summer, autumn and winter. The key objective is to obtain the maximum net electrical power output with the given sun radiation, ensuring an efficiency of about 33-36 %, and simultaneously to regularly provide the necessary amount of molten salt in the hot storage tank which enables the generation of the rated power also when the sun is absent, without any interruption. In fact, the production of dispatchable electrical energy is the main feature which makes CSP technology competitive and profitable, especially when coupled with a TES system, as in the proposed plant.

### 4.4.1 Summer

The design configuration represents the best operational status of the system and it is reasonably chosen to be at 12:00 on the 21st of June, during the summer solstice, when the

sun radiation is maximum. The nominal power is 45 $MW_{el}$ net, which is a larger output than the nominal one of "Gemasolar" (20 $MW_{el}$ net), and the configuration under consideration is the optimized one discussed in section 4.2. During summer, the "Day" starts at 6:00 am and ends at 19:00 pm. The time interval is not arbitrary chosen, but it is reasonably selected observing the results obtained through the Time Series of the "Daily behaviour" off design: until 5:00 am, the sun is absent and no molten salt mass flow is produced, but starting from 6:00 am the heliostats begin to concentrate the sun radiation on the receiver tower, where a larger hot Solar Salt mass flow than the amount required to produce the nominal power is produced. For this reason, the "Daily behaviour" off design starts at 6:00 am with an empty hot tank that would be filled during the successive hours. In particular, at 6:00 am the molten salt mass flow is around 438 kg/s, while the amount required for producing electricity is approximately 374 kg/s. The difference in these values is the stored amount that will be used during the night. At 7:00 pm, the hot storage tank level reaches its maximum value and starts to decrease: the "Evening" period begins and all the stored amount is used to heat the $sCO_2$ working fluid which in turn produces the nominal power of 45 $MW_{el}$. Performing the Time Teries, it is noticed that the stored Solar Salt is enough to continuously supply the necessary heat until 6:00 am, when the sun rises, the radiation is again captured by the heliostats field and the operation of the plant is simulated switching to "Day" hours. The resulting thermal efficiency is always almost around 36.5 %.

### 4.4.2 Winter

Starting from the considerations made in the subsection 4.1.2, in order to achieve a flexible plant which allows the whole-day operation, the maximum electrical power output is chosen as function of the molten salt mass flow rate which is accumulated during the day and discharged during the evening and the night, ensuring a continuous power generation. For the winter case, the maximum allowable power output that provides the whole-day operation of the plant is equal to 35 $MW_{el}$ net. It has to be reduced compared to the summer case because the available radiation from the sun is lower and at the same time the system is required to constantly generate electricity during the day. 35 $MW_{el}$ is the maximum output which allows to charge the hot tank enough to supply hot molten salt for the hours of the evening and the night. First, the same cycle used for the design during summer is simulated changing in the "Sun" component the day and set it to the 21$^{st}$ of January; then, through a series of sensitivity analyses, it has been optimized (see section 4.2) and a 35 % of thermal efficiency is reached. The plant behaviour is the same described for the summer, but in this case the hours characterized by the presence of the sun are reduced and the "Day" interval starts at 8:00 am and ends at 17:00. Once again, the time interval has been chosen according to the results given by the Time Series calculation, observing when the

hot tank level starts to increase and decrease. Given that it is allowed to accumulate molten salt for only 9 hours during the day, the output power has to be reduced in order to have the possibility of using the less amount of stored molten salts to satisfy the demand for the remaining 15 hours, without switching off the plant. This is possible with a maximum of 35 $MW_{el}$.

### 4.4.3 Spring and autumn

The main aim of this project is to obtain a plant able to operate during the whole year, without considering at this design step the stops needed for the necessary maintenance. So, also for spring and autumn days, the maximum power output which allows the continuous production during the day and the night and the correct loading and unloading process of the storage tanks has to be found. The procedure is the same discussed for the winter in the previous section and the net electrical power output for a typical mid-season day is found equal to 42 $MW_{el}$. The result is obtained through the already discussed sensitivity analyses and time series calculation on the 21st of March and 21st September: from both days, for the selected plant at the chosen latitude of 30 ° N the outputs are the same. The accumulation process starts at 7:00 and ends at 18:00, so the hot storage tank supplies the necessary molten salt flow rate for the remaining 12 hours, when the power output is constant and equal to 42 $MW_{el}$. The time interval for the charging and discharging process of the tanks is not arbitrarily chosen, but rationally selected analysing the Time Series calculation results: the accumulation starts when the Solar Salt produced exceeds the needful amount to generate the rated power; the hot tank starts to discharge the stored mass flow when the field is no longer able to produce hot Solar Salt. The reached efficiency is equal to 36.1 %, which is undoubtedly satisfying.

## 4.5 High efficiency cycle

As demonstrated, the thermal efficiency of the examined plant is always ranging almost from 32 % to 36 %, when the plant is considered to operate for the entire day. The obtained result underlines that the potential advantages of the closed supercritical $CO_2$ cycle are not exploited, since the efficiency is comparable with the efficiencies reached by typical steam Rankine power cycles (Binotti *et al.*, 2017). Indeed, the plant has been developed taking into consideration the current state of the art regarding materials and molten salts limitations, so that it could actually operate: the turbine inlet temperature is kept constant at 560 °C, the minimum and maximum pressures of the power cycle are respectively equal to 9.5 MPa and 28.0 MPa, the split ratio is equal to 0.75 and the maximum temperature of the HTF at the receiver outlet cannot exceed 565 °C. Furthermore, since one of the main objectives of the study is to reach a flexible behaviour, all these constraints are strictly

necessary in order to allow for whole-day and whole-year operation of the plant, keeping in mind that the availability of the system is not regarded at this design step, without scheduling any switching off due to the non-availability of sun radiation, but considering only the unlucky event simulated by the "Storage Empty" off design (subsection 4.3.2). In fact, with the time changing, the sun radiation varies and, consequentially, temperatures and pressures distributions differ from the optimum range for which the components are set. Hence, compromises must be found, and so the best efficiency cannot be obtained. Especially regarding the heat exchangers, pinch point problem is likely to occur when thermodynamic parameters are strongly changing.

For the purpose of highlighting and studying the strong advantages given by a recompression closed supercritical $CO_2$ cycle, a new configuration is developed and simulated in Ebsilon® Professional 13.01. The latter, which this time is considered to be the design profile, consists of a typical recompression layout and it is not integrated with the solar loop, since the software does not provide advanced fluids allowing extreme operational state. Indeed, in order to fully exploit the properties of the carbon dioxide at supercritical state, a TIT higher than the previous 560 °C is required, as well as a higher pressure ratio. Additionally, the heat source is no longer depending on the time of the day and the power output is calculated by the software, while in the actually proposed plant it is imposed by the user. In this way, constraints are eliminated, and the plant becomes free to operate at its maximum efficiency point. With the assumption of allowable operation in an intense and severe context, as the one explained in chapter 3, the solar field and the heat transfer system are replaced by a heat exchanger where air transfers the required heat to the $sCO_2$. The thermal efficiency, calculated as the ratio between the net electrical power output over the thermal input supplied in this case by the hot air, is calculated by varying one parameter over a certain range, in order to find the best efficiency point. The sensitivity analysis is carried out thanks to the possibility offered by the software to create sub-profiles, starting from the design profile. So, as already explained, first, a script has been written with the aim of creating different sub-configurations, each one characterized by a change in a single parameter. Once again, the studied parameters are:

1. the turbine inlet temperature;
2. the minimum cycle pressure;
3. the turbine inlet pressure;
4. the split ratio.

Different simulations have shown the less significant impact of the $sCO_2$ mass flow rate compared with the just-mentioned thermodynamic parameters, so it has been chosen to keep it constant and set to 500 kg/s, the same order of magnitude of the real operating plant that is object of this study. This could be explained considering that the enthalpy of

the fluid entering the turbine has already been examined by considering the TIT ($h = m \cdot c_p \cdot TIT$), thus the variation of the temperature acts to compensate the modified mass flow rate. In other words, the same fluid enthalpy can be obtained either by increasing the mass flow and reducing the TIT or vice versa. In the end, it is sufficient to study the effect of only one of these two parameters and therefore TIT is selected.

The analysed quantities are closely interrelated: the best efficiency point cannot be found by just varying one single parameter but through examining all of them simultaneously. In this case, the cycle would have more degrees of freedom since the controllers are eliminated and the heat source would allow extreme working temperatures, then the impact of the interlinked parameters on the thermal efficiency would be more evident. For this reason, first a sensitivity analysis has been carried out to understand the effect of the change in a single physical value, in order to have a reasonable range of variation. Then, thanks to another on-purpose script, 81 sub-profiles have been created, where the lowest cycle pressure, the split ratio, the inlet turbine pressure and temperature are changed simultaneously along the previously found range of variation, eliminating the values that generate errors since they cause, thermodynamically speaking, unfeasible operational conditions. The final outcome is that different combinations of the investigated parameters lead to higher efficiencies, in accordance with previous experimental studies (Luu *et al.*, 2017). Examples of the inputs and outcomes of the sensitivity analyses are shown in Table 4.4 and Table 4.5, where the influence on the system of the combination of the bounded quantities is demonstrated. The highest efficiency is 64.15 % and it is reached thanks to 0.7 as splitting ratio, maximum and minimum pressures respectively at 33.0 MPa and 8.5 MPa and at a highest examined TIT of 1,500 °C. It is worth to notice that highest efficiencies are obtained with a minimum pressure slightly higher than the critical point, in this case it is 8.5 MPa. It must be reminded again that the considered operation conditions are absolutely extreme and not allowable with the current state of the art and technology development.

*Table 4.4: Sensitivity range of variation*

| **Parameter** | **Minimum value** | **Maximum value** |
|---|---|---|
| Minimum pressure [MPa] | 7.5 | 12.5 |
| Maximum pressure [MPa] | 25.0 | 35.0 |
| Turbine inlet temperature [°C] | 700 | 1,500 |
| Split ratio [-] | 0.15 | 0.60 |

*Table 4.5: 4-parameters sensitivity results*

| **Mass flow [kg/s]** | **Split ratio [-]** | **Pmin [MPa]** | **Pmax [MPa]** | **TIT [°C]** | **Thermal input [MW]** | **Net power output [MW]** | **Thermal efficiency [%]** |
|---|---|---|---|---|---|---|---|
| 500 | 0.70 | 8.5 | 33.0 | 1,500 | 232.11 | 148.89 | 64.15 |
| 500 | 0.75 | 9.0 | 34.0 | 1,500 | 234.80 | 149.73 | 63.77 |
| 500 | 0.65 | 8.5 | 34.0 | 1,450 | 227.27 | 142.39 | 62.65 |
| 500 | 0.65 | 8.5 | 35.0 | 1,500 | 236.40 | 149.88 | 63.40 |
| 500 | 0.70 | 8.5 | 33.0 | 1,450 | 232.79 | 147.73 | 63.29 |
| 500 | 0.70 | 9.0 | 33.0 | 1,500 | 226.56 | 144.74 | 63.89 |
| 500 | 0.70 | 8.5 | 34.0 | 1,500 | 235.98 | 151.31 | 64.12 |

# 5. RESULTS

All the different plant configurations early described, together with Time Series calculations and the various sensitivity analyses, allow the estimation and computation of each parameter typical of a solar power plant, with a view to underlining the actual feasibility of the designed plant and its convenience when compared with the existing power plants.

## 5.1 Sensitivity results

The necessity to enhance the thermal efficiency without renouncing the plant flexibility and always guarantying the actual materials limitations leads to performing a group of sensitivity analyses. The examined thermodynamic quantities are:

1. the minimum cycle pressure;
2. the turbine inlet pressure;
3. the turbine inlet temperature;
4. the split ratio.

First, the influence of one single parameter on the thermal efficiency is analysed: four appropriate scripts are written, making each quantity vary individually and keeping all the other constant. Nevertheless, it is well established that all the thermodynamic properties of the fluid have a reciprocal impact and they are strictly linked in a cycle. Accordingly, after finding a feasible range of variation for each parameter through the first group of sensitivities, their interdependence is studied by means of writing a new dedicated script which makes the software create different sub-profiles where the four studied parameters vary in their range simultaneously. In particular, 162 are generated: obviously, some of them runs with errors and the given results are not reliable. For instance, the cycle with a TIT equal to 600 °C is simulated, even if it is absolutely expected not to obtain a feasible operation. However, there are also sub-profiles characterized by operating conditions slightly changed from the first-attempt cycle which give errors, as shown in Table 5.1. In

sub-profile 1, the energy balance of the cooler is violated. In sub-profile 2, on the other hand, problems arise in the heat exchanger connecting the solar loop with the power cycle, where the energy balance is violated and the hot side outlet temperature results lower that the cold side inlet. Sub-profile 3 shows the common error for $sCO_2$ cycle, that is the pinch point violation due to the change of the fluid specific heat capacity and it will be explained and shown later, in section 5.3. Errors are also present with higher pressure ratio, as in the case of sub-profiles 4, where the pinch point and the energy balance are violated in the heat exchanger between the solar loop and the power cycle, as well as the correct temperature difference between the cold and the hot side. The really small difference between the parameters of the cycles correctly running, such as the first-attempt and the optimized cycle, and of the cycles giving errors demonstrate the strong and deep interference among all the characteristic thermodynamic quantities.

*Table 5.1: Comparison between first-attempt cycle and sub-profiles from sensitivities*

| **Parameter** | **First-attempt cycle** | **Sub-profile 1** | **Sub-profile 2** | **Sub-profile 3** | **Sub-profile 4** | **Optimized cycle** |
|---|---|---|---|---|---|---|
| $p_{min}$ [MPa] | 10.0 | 10.5 | 9.5 | 10.0 | 10.5 | 9.5 |
| $p_{max}$ [MPa] | 22.0 | 22.0 | 21.0 | 22.0 | 30.0 | 28.0 |
| TIT [°C] | 525 | 500 | 550 | 500 | 550 | 560 |
| X [-] | 0.699 | 0.750 | 0.750 | 0.700 | 0.650 | 0.750 |

After reaching an operating plant which ensures a thermal efficiency equal to 36.5 %, the Time Series calculation is performed on each typical day that is representative of a particular season. Dividing the day in one-hour intervals, each output is studied and analysed so that the plant behaviour can be fully understood.

Once the optimum cycle is selected, the sensitivity analysis to show the plant flexibility is performed. The allowable variation for the net power output ranges from 10 $MW_{el}$ to 60 $MW_{el}$. After this value, in fact, the necessary mass flow rate of the cooling water is larger than 400 kg/s. Since this analysis is performed with the assumption of studying the reaction of the designed and installed system only to the variation of the output, keeping all the other parameters equal to the optimum value, it has been decided to stop the sensitivity at 60 $MW_{el}$. For electricity values higher than 60 $MW_{el}$, the software undergoes the common error of the violation of the energy balance in the primary cooler, due to the water mass flow lower than the necessary.

## 5.2 Solar loop

A central role is played by the heliostat field. The one selected for this project is HEL180_35N_100MW$_{th}$ and it has the standard features given by Deutsches Zentrum for Luft-und Raumfahrt (DLR), but the number of the heliostats has been modified in order to meet the desired plant set up and dimension. It shows a higher overall efficiency in winter than in summer for the latitude where the plant is installed (30° North). This is due to the fact that the solar field is design looking from the north side to the tower, hence it better exploits the radiation from the south. For the selected latitude, this condition is satisfied during winter, when in fact the field efficiency is the highest. Indeed, the overall efficiency is the product of four parameters:

1. reflectivity efficiency, equal to the standard of 0.8841 for all the seasons; it takes into account also the soiling;
2. focus efficiency, always equal to 1 in the designed plant because heliostats are always focusing the radiation;
3. wind efficiency, equal to 1 during the whole year since the most probable wind direction is 90° on the heliostats, so it has no impact;
4. efficiency of the full tracked and cleaned field, which has a different value for each season. In fact, the parameter is calculated by the software as a linear interpolation between the sun azimuth (Υ), which is the relative direction of the sun along the local horizon, and the sun elevation angles (α), which represents the latitude of the sun, that is the angle between the horizon and the centre of the sun (Figure 5.1). These angles are peculiar for every considered period of the year.

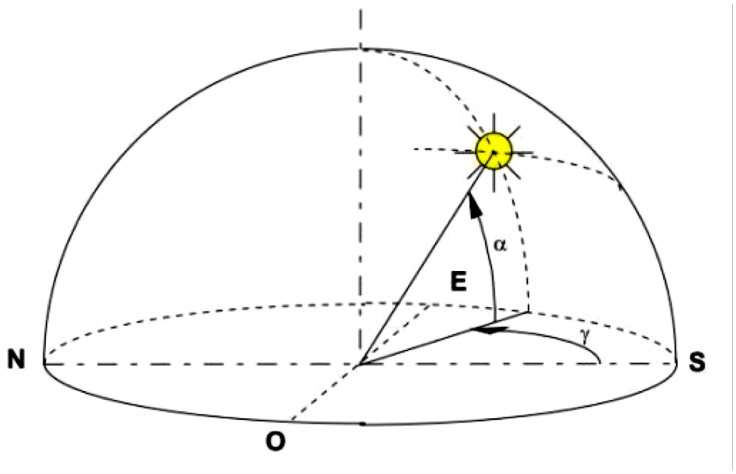


*Figure 5.1: Sun azimuth (Υ) and elevation (α) angles*

To clarify, if the same heliostat field is put at a different latitude, i.e. 60° N, the field efficiency will be strongly decreased in winter and increased in summer. For the purposes

of this project, it is accepted to have a higher field efficiency for the given latitude during the winter (0.752), since in this period the sun radiation is weaker and can be captured for a maximum of 9 hours per day, so efforts are done with a view to fully exploiting the low income in order to produce an acceptable power during the whole day. On the other hand, during the summer days, the radiation in stronger and can be focused on the receiver for 13 hours: hence, even though the lower field efficiency (0.675), it is possible to allow the generation of the rated power output, which is higher than the one producible in winter (respectively 45 $MW_{el}$ and 35 $MW_{el}$). It is definitely a compromise and it affects the produced molten salt flow rate and the behaviour of the storage in the different seasons.

From the software, the height of the receiver above the ground is equal to 127 m, so it is reasonable to use concrete to build it. The receiver view angle is equal to 180° and it is installed at a latitude of 30° N, hence the surrounded distribution of the heliostats is suggested, like in "Gemasolar" project (Figure 2.12). Better efficiencies are obtained through the minimization of the angle between the incidence beam on the mirror from the sun and the reflected towards the tower (Figure 5.2). This angle is function of the height of the tower and of the heliostats position: the higher the tower, the smaller the angle; the longer the distance, the higher the angle.

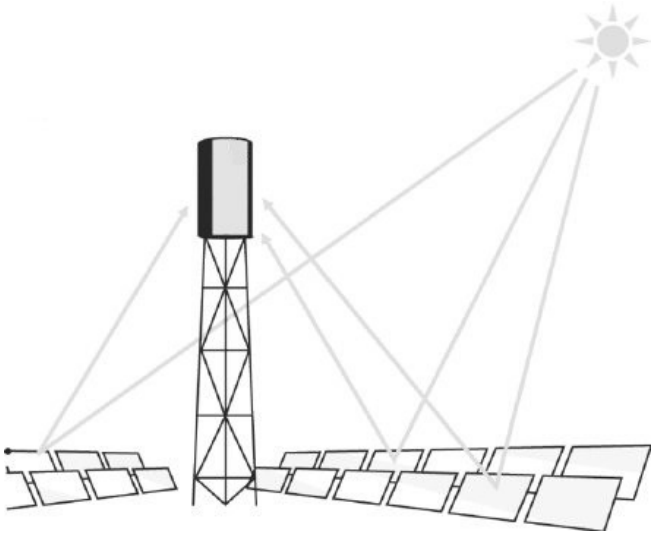

*Figure 5.2: Solar tower system principle of operation*

Now, it is possible to calculate the Concentration Ratio (CR), defined as the ratio between the collecting area and the receiver area. In this way, it is possible to have an idea of the energy density. The adopted solar tower technology allows a high CR: indeed, the huge heliostats field surrounding the tower, made up of 3,000 mirrors in this project, focuses the solar flux on the receiver, whose aperture area is equal to 247 $m^2$. It is calculated by the software as function of the chosen heliostat field connected to the solar tower and it is in line with expectations: for example, the aperture area of the "Gemasolar" receiver is equal

to 270 $m^2$ (section 2.6). The resulting CR of the proposed project is of the order of 2,000, that is an extreme condition for the receiver operation. In fact, the adopted tower is equipped with a common tubular receiver and it is fundamental not to concentrate the radiation on one single point, but to spread it on the total receiver surface, in order not to permanently damage the structure. Additionally, a too high CR usually limits the optical accuracy of the heliostats: this is a further explanation of the reduced solar field optical efficiency.

After the field, the storage system is examined. First of all, the level of the hot storage tank is investigated. This is a central and critical component on which the operation of the whole plant depends: it allows the generation of electricity even during the evening and night hours, since it accumulates the excess molten salt mass flow produced during the day. So, it is fundamental to ensure the correct and necessary amount of Solar Salt mass flow to be stored that enables the production of the rated power output for all the hours of the day. Together with reaching the flexibility and whole-day operation, additional efforts are done in order to avoid the switching off and on of the plant during the ordinary operation: in fact, each component is characterized by its own inertia and, thereby, they need a transient time to adapt to the new imposed conditions. During that period of time, the entire system is not able to work in the optimal conditions for which it is designed: hence, in the ordinary operation simulation the possibility to switch off the plant is not contemplated and it is considered only in the unfavourable event described by the "Storage Empty" sub-profile. As already said, only the normal daily operation of the plant is considered while designing the system: all the stops related to maintenance are not taken into account at this design step. Additionally, at the design step chosen for this project, the dynamic nor the transient of the components are not considered. For these reasons, the level of the hot storage tank is constantly monitored and it is ensured that the stocked mass flow is always enough to supply the power cycle. In this view, two controllers are used, as already explained, which automatically calculate the required $sCO_2$ and Solar Salt mass flow rates that exchange the necessary heat to produce the required output power. Concurrently, in the solar loop, at the outlet of the solar tower, controllers to fix the maximum and minimum operating temperatures, respectively equal to 565 °C and 290 °C, are used and the circulating molten salt flow rate is always at 565 °C. So, the heat transfer process with the power cycle is correct. Thanks to the extensive installed solar field, starting from the sunrise, when the hot storage tank is assumed to be empty, the accumulation process begins. As an example, the two opposite seasons evolutions are clarified: for the summer, analysing the results obtained through the Time Series, the initial hour of the "Day" is 6:00 am, while for the winter it is 8:00 am. At this time, the flow rate of molten salt produced by the tower exceeds the necessary amount required to heat the $sCO_2$ and to produce electricity. The excess mass flow is stored in the hot tank. During the whole day, the level of the hot storage tank is

increasing to the maximum and decreasing to the minimum level, which is reached exactly at the time when the solar field is able to start again the production of molten salt. From the Time Series, regarding the summer, the maximum is reached at 19:00, while during the winter the hot tank results full at 17:00. The mismatch between the two seasons is due to the different amount of the available sun radiation, that directly impacts on the time when the solar field starts to reflect the sun radiation on the receiver, where the molten salt is produced, and on when the radiation is too weak to heat the fluid until the needful temperature and, instead, the stored amount is used for generating electricity. As an example, the behaviour of the component during an ordinary day of the summer season is shown in Figure 5.3, together with the cold tank evolution. During the other seasons, the shape of the curve is the same, but the maximum is reached earlier, especially in winter (17:00). Moreover, accumulation process is slower in summer than in winter, since the incident radiation is available for a longer interval of time and the required output is higher, while the discharging process is faster because the hours of absent sun radiation are less than in winter.

Vice versa, the cold storage tank has an opposite behaviour (Figure 5.3): in the early morning, it is full and it starts to discharge the amount of cold Solar Salt, which is pumped back to the tower, in order to always ensure the mass balance of this component; when the available radiation is weak and the hot storage vessel begins the unloading process, it starts to be filled up. The flow rate exiting the hot tank is always equal to the one entering the cold vessel, as well as the amount entering the hot tank which equals the mass flow exiting the cold one, as clearly demonstrated by the following figure.

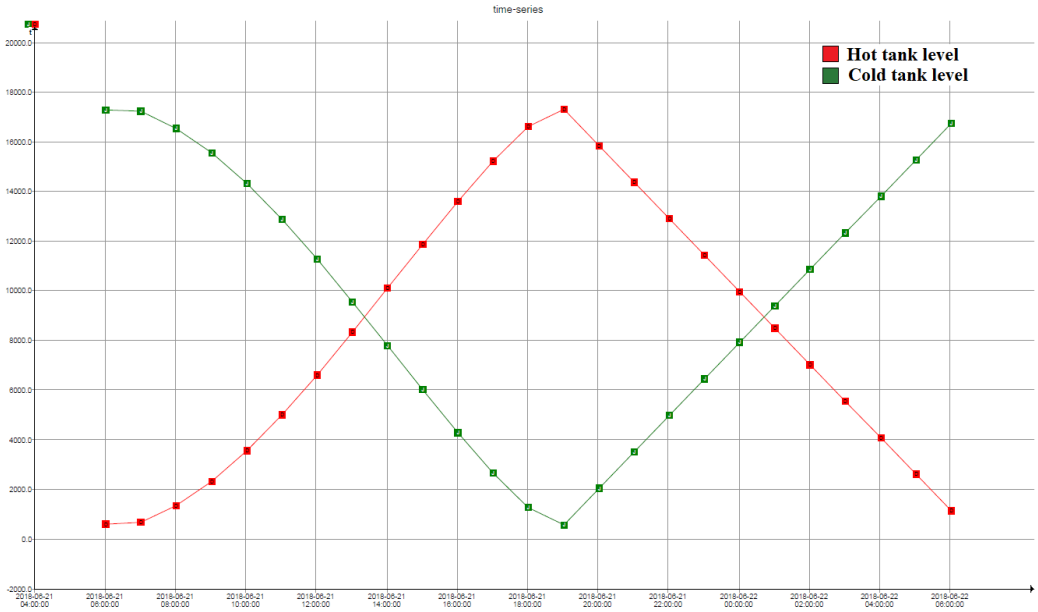


*Figure 5.3: Hot and cold storage tank behaviour during summer*

Regarding the molten salt mass flow produced by the solar field and circulating in the solar loop, it is only function of the heliostats features and the incident sun radiation. It is not affected by the operation condition of the cycle. Clearly, the influence of the time of the day and the period of the year is crucial. Hence, in the four seasons the time when the hot molten salt starts to be generated and the produced amount is different, as shown in Table 5.2. To clarify, a short comparison between winter and summer is made: during summer days, at 6:00 in the morning, the receiver starts to produce hot molten salt, while at the same time in winter the sun is not shining and no mass flow is circulating in the solar loop; instead, at 8:00 during summer, the molten salt mass flow produced by the solar field is larger than the one produced in winter at the same time. Looking at Table 5.2, it must be kept in mind that the value of the reported mass flow is the one generated in the first hour of available incident sun radiation, which is different for each season. In Figure 5.4, the behaviour of the molten salt flowing in the solar loop from the heliostat field and the receiver during the summer period is depicted in blue, while the purple line represents the necessary flow rate to produce the required power output. Obviously, during summer the hot salt is produced for a longer period, as reported in Table 5.2.

*Table 5.2: Typical daily parameters*

| Parameter | Winter | Spring | Summer | Autumn |
|---|---|---|---|---|
| Initial time ($t_i$) | 8:00 | 7:00 | 6:00 | 7:00 |
| End time ($t_e$) | 17:00 | 18:00 | 19:00 | 18:00 |
| Mass flow produced at $t_s$ | 650 kg/s | 555 kg/s | 438 kg/s | 555 kg/s |
| NPO | 35 MW | 42 MW | 45 MW | 42 MW |
| Thermal Efficiency | 35.3 % | 36.2 % | 36.5 % | 36.2 % |

On the contrary, the molten salt mass flow rate needed to satisfy the required NPO is function both of the operating conditions and, thanks to the controllers already described, of the demand. For this reason, it is automatically calculated for each time interval for the four seasons and it gives different values. This result is totally in line with the expectations: first, because the NPO is not constant during the year, but it is chosen equal to the maximum allowing continuous electricity generation; ultimately, because the operation of the plant changes according to the available radiation, which in turn is function of time. In detail, the necessary mass flow of molten salt is higher during the "Day" hours because the NPO takes into account also the auxiliaries, especially pumps employed in the solar loop that face a larger mass flow rate during the "Day" hours: consequentially, the power produced by the $sCO_2$ turbine is higher because a fraction is absorbed by the pumps working with salts. In particular, the pump after the hot tank works with almost the same flow rate during the whole day, due to the inserted controller; conversely, the one after the cold tank has to deliver quite a large mass flow during the "Day" hours, since the vessel is discharging the huge amount of molten salt stored in the night. During the "Evening", on the other hand, this pump does not work because the tank is accumulating without discharging (green line in Figure 5.3): hence the power produced by the $sCO_2$ cycle to ensure the same fixed NPO is lower and less Solar Salt flow rate is needed to supply the cycle. As an example, in Figure 5.4 the trend of the necessary molten salt amount is depicted in purple for a summer day: it can be noticed that it slightly increases when the solar field is producing hot Solar Salt, due to the work needed by the pump. To show the direct impact of the power produced by the turbine on the necessary molten salt mass flow, these two quantities are plotted together in Figure 5.5: on the x-axis there is the power produced by the turbine, expressed in kW, while on the y-axis the calculated required Solar Salt amount, expressed in kg/s. Their direct proportionality, that was expected, is therefore demonstrated. During

summer, this mass flow is of the order of 415 kg/s. From Figure 5.5, it can be notice that the necessary Solar Salt mass flow ranges, during summer, almost from 410 kg/s to 420 kg/s: this is not a big variation, as expected, since it is due only to the additional work that the turbine provides for the pump which work only during the day. Making a comparison with the antipodal situation of the winter, here the flow rate necessary to produce the rated power is clearly lower, since the required electricity is externally diminished from 45 $MW_{el}$ at summer to 35 $MW_{el}$, in order to allow production during the whole day with less hours of sun shine.

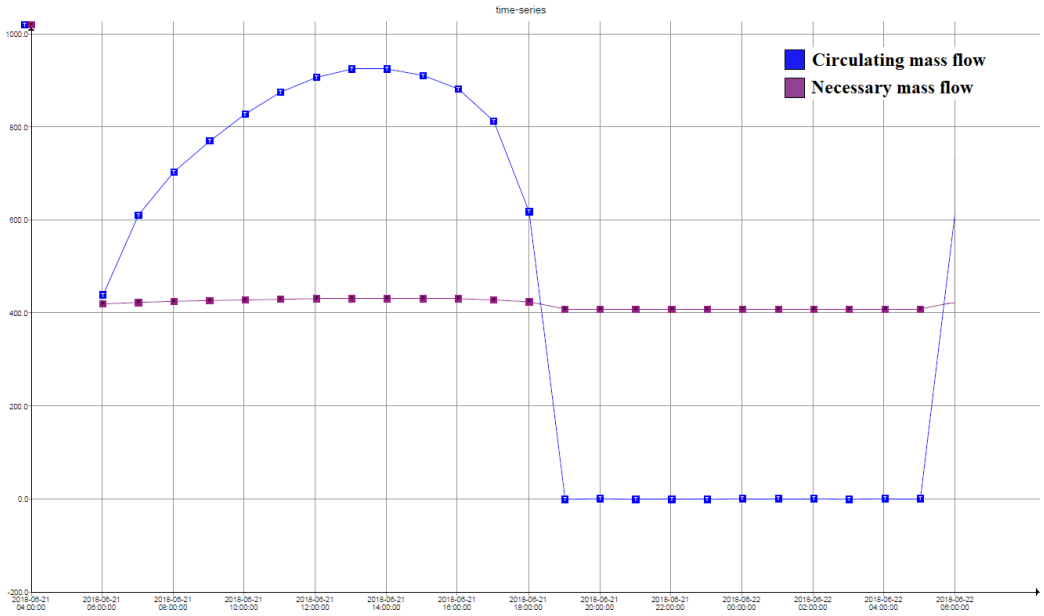


*Figure 5.4: Mass flow rates of the molten salt in the solar loop (summer)*

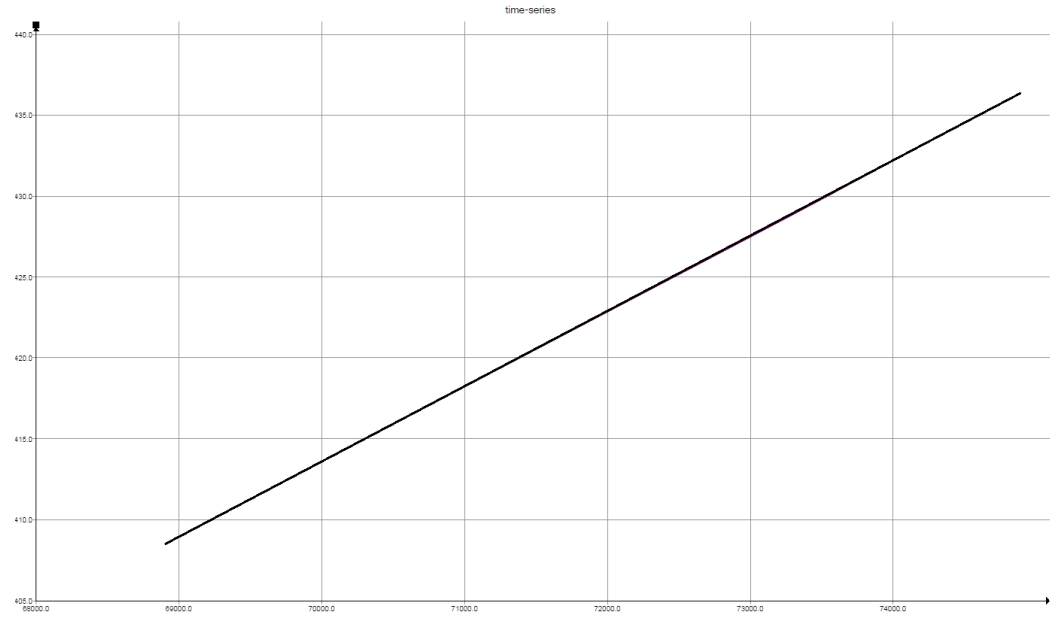


*Figure 5.5: Necessary molten salt flow rate as function of the turbine work (summer)*

Given the limitations imposed by using the Solar Salt, in the solar loop the temperature interval ranging from 290 °C to 565 °C must be ensured. For this reason, as already largely explained in section 4.3, controllers are inserted: the first prevents the cycle from working with a freezing fluid, whose temperature is lower than 290 °C, and the second one imposes the maximum operating temperature which is equal to 565 °C. During the first "Evening" hours, a small amount of Solar Salt can be produced by the field, but obviously its temperature is too low, the enthalpy negligible and its flowing in the pipes must be avoided

in order not to damage the system. Through the switch S1 (Figure 4.1), this amount of molten salt is sent back to the tower and no mass flow is circulating in the loop.

To summarize, as expected, during the whole day, in order to obtain the same net electrical power output, externally chosen by the user, the turbine is required to produce a slightly different amount of work which is function of the time being. Consequentially, the inserted controllers compute the mass flow rates of $sCO_2$ and molten salt which are necessary to supply the demand, while the molten salts mass flow produced by the solar field is not affected by the cycle evolution. This concept is well demonstrated in Figure 5.6 where, as function of the time, divided into one-hour intervals on the x-axis, four quantities are represented together in order to highlight their interdependence:

1. on the left y-axis there is the value, in kW, of the gross power produced by the turbine (light blue line);
2. the net electrical power output in kW (orange line) is plot on the left y-axis, too. It is externally set and always constant;
3. on the right y-axis, the molten salt amount (kg/s) produced by the solar tower is represented in green and it is only function of the time being and of the field features;
4. the purple line on the right y-axis represents the calculated hot Solar Salt (kg/s) necessary to supply the required power.

As foreseen and already explained, when the salt produced by the field increases, the gross power generated shows the same trend since the turbine has to provide the work absorbed by the pumps. Subsequently, a lager mass flow of molten salt is required to heat the necessary $sCO_2$ mass flow rate. Therefore, the purple line, representing the necessary amount of hot salt, and the blue one, which stands for the gross power, show the same trend of the green curve, that is the molten salt produced by the field. An ordinary summer day has been selected for instance, but the same is obtained for all the other seasons.

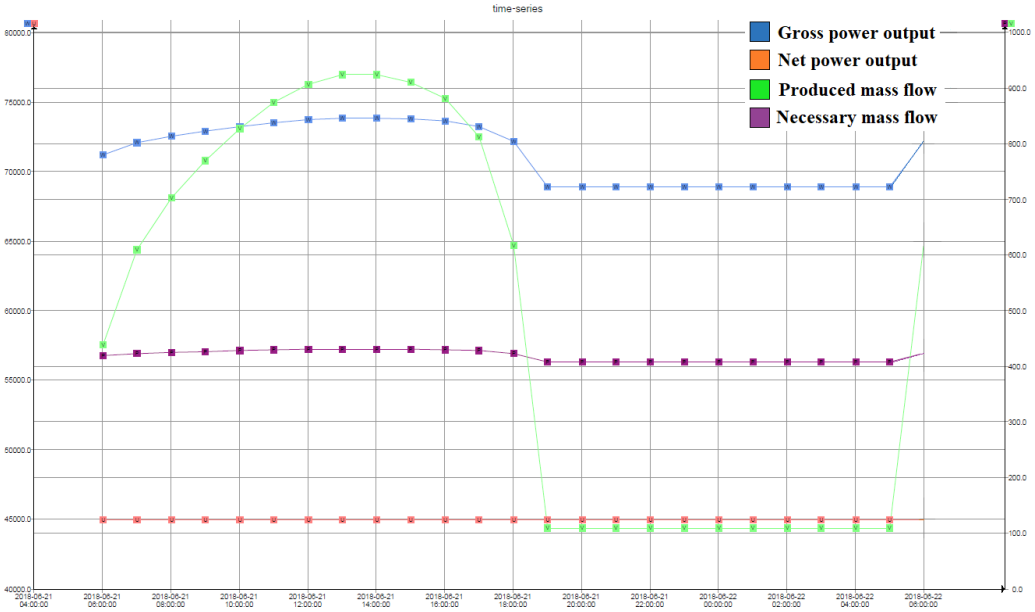


*Figure 5.6: Molten salt mass flow rates, gross and net power output (summer)*

A critical component of the system is the heat exchanger between the solar loop and the power cycle (component (4) in Figure 4.1): here, it is difficult to ensure a correct and simultaneously efficient heat transfer process, since the inlet molten salt temperature is set at 565 °C and it is not allowed to increase it, because of corrosion enhancement in pipes and components. Hence, the minimum temperature difference is chosen equal to 5 °C, in order to obtain the maximum allowable outlet temperature of the $sCO_2$ which will be expanded in the turbine and will produce work. Even though this is a quite risky situation, the heat exchanger works in the right way and the heat is properly transferred, as shown Figure 5.7. Here, the T-q diagram is obtained through the software and it shows both the design and the off-design condition, that in this project means the daily behaviour characterized by different thermodynamic quantities distributions, calculated as function of the time.

1. The blue line is the cold side in the design condition, so it is the $sCO_2$ that has to be heated;
2. the red one is the design hot side, that is the molten salt always entering with a temperature equal to 565 °C;
3. the green line is the cold side ($sCO_2$) in off-design, condition necessary for the Time Series calculation;
4. the orange one is the hot side (molten salt) of the heat exchanger in case of off-design operation.

From the figure, it can be observed that the minimum temperature difference is always guaranteed and that in both the configurations the inlet temperature of the hot side (molten

salt) and the outlet temperature of the cold side ($sCO_2$) coincide, since they are fixed. Then, the outlet molten salt temperature is specified by the controller (C2 in Figure 4.1) which computes the needed flow rate in order not to have the pinch point problem, while the inlet $sCO_2$ temperature is calculated by the software in dependence of the operating conditions. In accordance with what was forecasted, the heat transferred in the off-design operation is larger than the amount discharged in the design to obtain the same electrical power output: indeed, the latter is the optimized configuration with the highest thermal efficiency.

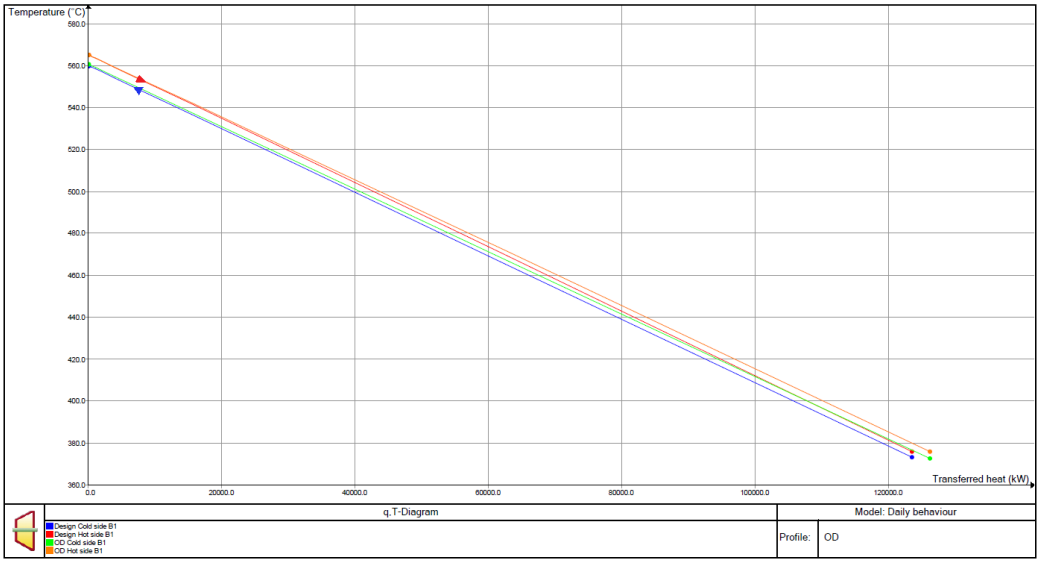


*Figure 5.7: T-q diagram of the heat exchanger between solar loop and power cycle*

## 5.3 Power cycle

A supercritical fluid is characterized by overcoming the end point of the phase equilibrium curve. At the critical point, liquid and gaseous conditions exists together, so that the advantages descending from both phases can be exploited. This is the reason why supercritical carbon dioxide has been selected as working fluid for the power cycle in this project. Indeed, it enters the main compressor near the critical point, when it behaves as a liquid and its high density (from the software, almost equal to 692 kg/m$^3$) allows a small amount of work necessary for the compression process, but it is expanded in the turbine in the supercritical region, where it shows the typical gaseous properties (from the software, density almost equal to 169 kg/m$^3$) and gives a large output. Furthermore, being the density high for all the cycle, the components are smaller and the plant footprint is reduced.

The choice of employing a close supercritical $CO_2$ cycle in a view to enhancing the efficiency of the system causes the difficulties on the design of the heat exchangers which act as recuperators and cooler in the selected recompression layout. The main problem arises from the change of specific the heat capacity of the $CO_2$ when the critical conditions are

approached, as discussed in section 2.1 and subsection 2.4.3: using supercritical carbon dioxide as working fluid implies a variation of the specific heat capacity not only as function of the pressure, but also of the temperature. The direct consequence is the probable occurrence of the pinch point violation in some parts within the heat exchangers, not only at the inlet or outlet. Hence, the sensitivity analysis to find the proper split ratio $\chi$ is a crucial step for this project, first to make the cycle run without errors and ensure the correct heat transfer process; then, to enhance the cycle efficiency, which is strongly affected by any change on the amount of mass flows passing through the heat exchangers and compressors. The result of the sensitivity analysis made varying simultaneously the split ratio, the TIT and the minimum and maximum pressures, as described in section 4.2, is shown in red in Figure 5.8, where it is compared with the first attempt cycle, depicted in green. The figure is obtained through the used software, Ebsilon® Professional 13.01. The achieved efficiency in the design condition is equal to 36.5 % when the NPO is 45 $MW_{el}$ and 36.1 % when the latter is 35 $MW_{el}$, while the first attempt cycle gives almost 33.4 % as thermal efficiency. In Table 5.3 a short comparison is made. In order to obtain reliable and consistent results from both the cycles, they are asked to produce the same electrical power output, that is 35 $MW_{el}$, because in the first attempt, given the non-optimal thermodynamic conditions, it is the maximum guarantying the continuous electricity generation, during the day and during the night.

*Table 5.3: Comparison between first attempt and optimized cycle*

| **Parameter** | **First attempt cycle** | **Optimized cycle** |
|---|---|---|
| $p_{min}$ [MPa] | 10.0 | 9.5 |
| $p_{max}$ [MPa] | 22.0 | 28.0 |
| TIT [°C] | 525 | 560 |
| $\chi$ [-] | 0.699 | 0.75 |
| Thermal Efficiency [-] | 33.4 % | 36.1 % |

Thanks to the optimization, the thermal efficiency results improved. Even if from Figure 5.8 it is evident that in the optimized cycle the turbine output increases (6 → 7) but the compressors need more work (1 → 2 and 9 → 10), as well, to compress the fluid, it is worth to notice that the rate of the turbine output increasing is not linear with the rising in the necessary compression work. This is an advantage descending from the simultaneous variation of the thermodynamic parameters in the sensitivity analysis, given their

interdependence on the overall cycle impact. Besides, the optimized power cycle is able to use more effectively the heat from the solar loop. In detail, the temperatures difference of the molten salt in the heat exchanger (11 → 12) is fixed, but the needed mass flow is calculated as function of the required power. Since the non-optimized cycle is not able to well exploit the $sCO_2$ properties, the necessary $sCO_2$ and, consequentially, Solar Salt flow rates increase: hence, the thermal power from the solar loop to the power cycle does the same, being equal to 105 $MW_{th}$. Though it is not because the outlet $sCO_2$ temperature is higher, but because the $sCO_2$ mass flow to be heated is larger. Remember that in each heat exchanger the energy balance between the two sides has to be respected ($\dot{Q} = \dot{m} \cdot cp \cdot \Delta T$). Indeed, from Figure 5.8 it is clear that the temperature in 5 is quite the same for the green (non-optimized) and the red (optimized) curve, but the value in 6 for the red is higher than for the green. This means the first attempt cycle was not able to well exploit the available heat. Concurrently, in the optimized cycle the TIT is higher, so that a smaller amount of $sCO_2$ is necessary to obtain the same power output and, consequentially, a lower amount of molten salt. Given that the molten salt temperature difference is fixed by the inserted controller, the direct consequence is that less heat is needed by the power cycle to generate the required electricity, in particular 97 $MW_{th}$. Hence, the thermal efficiency (ratio between the net power output to the heat collected by the HTF and given to the $sCO_2$) results further improved because the denominator decreases and the numerator stays the same. Additionally, the new optimum split ratio allows a better recuperation process, characterized by the correct heat transfer even with a very small minimum temperature difference that allows the operation even in tough conditions.

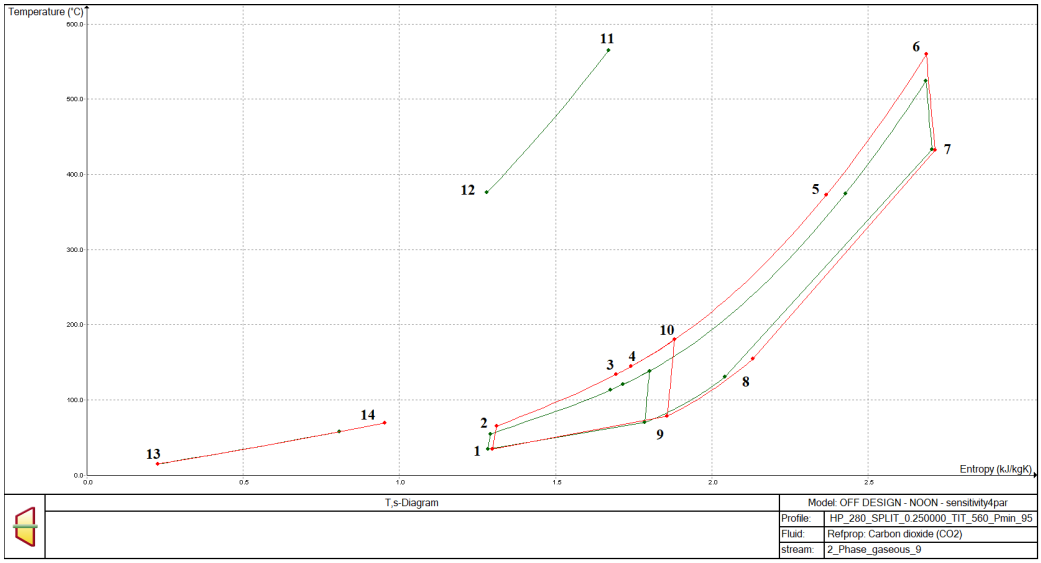


*Figure 5.8: T-s diagram of the first attempt and optimized cycle*

The optimized cycle is therefore selected and, given the better performances already discussed in subsection 4.2.2, the NPO is increased from 35 $MW_{el}$ to 45 $MW_{el}$ in the design

condition and in general for the summer days. The winter days, instead, result optimized with an NPO equal to 35 $MW_{el}$, while the mid-seasons can both continuously supply 42 $MW_{el}$.

The T-s diagram of the design condition of the optimized power cycle is better described in Figure 5.9. Comparing Figure 5.9 and Figure 5.10:

- 1 → 2: main compressor (MC);
- 2 → 3 and 8 → 9: respectively, cold side (or high pressure) and hot side (or low pressure) of the low temperature recuperator (LTR);
- 9: splitter (S);
- 9 → 10: re-compressor (RC);
- 3 → 4 and 10 → 4: mixer before the high temperature recuperator (HTR);
- 4 → 5 and 7 → 8: respectively, cold side (or high pressure) and hot side (or low pressure) of the high temperature recuperator (HTR);
- 5 → 6 and 11 → 12: respectively, cold side and hot side of the main heat exchanger between solar loop and power cycle (4); in particular, 5 → 6 is $sCO_2$ and 10 → 11 is Solar Salt;
- 6 → 7: turbine (TB);
- 9 → 1 and 13 → 14: respectively, hot side and cold side of the cooler (PC); in detail, 9 → 1 represents the $sCO_2$ that has to be cooled down, while 13 → 14 is the heated water.

Considering the design condition as example, the advantage of combining in the same cycle both the gaseous and the liquid properties, thanks to the supercritical condition of the fluid, is highlighted by the gross power produced by the turbine and the necessary compression work: the first one is almost equal to 73 $MW_{el}$, while the work needed by both the employed compressors is of the order of 24 $MW_{el}$, much more smaller than the produced. However, when the comparison is made, it is fundamental to remember that the thermodynamic features of the power cycle are the best that can be used with the studied plant equipped with all the limitations largely described and discussed. Obviously, without the constraints imposed by the actual materials, such as the maximum Solar Salt temperature not to have corrosion, the TIT could be increased and the potential of the closed supercritical $CO_2$ cycle could be better and fully exploited.

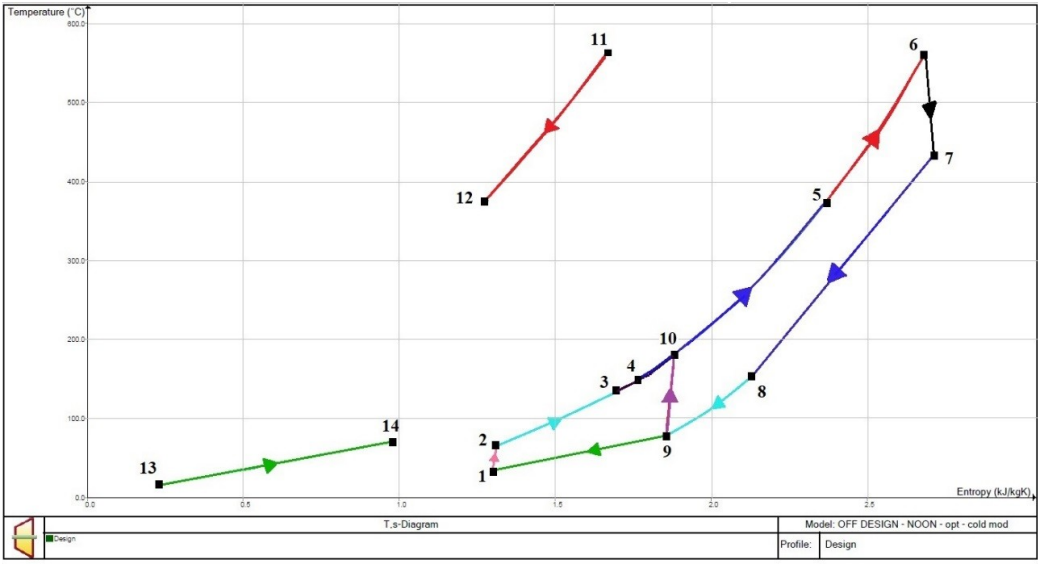


*Figure 5.9: T-s diagram of the optimized cycle*

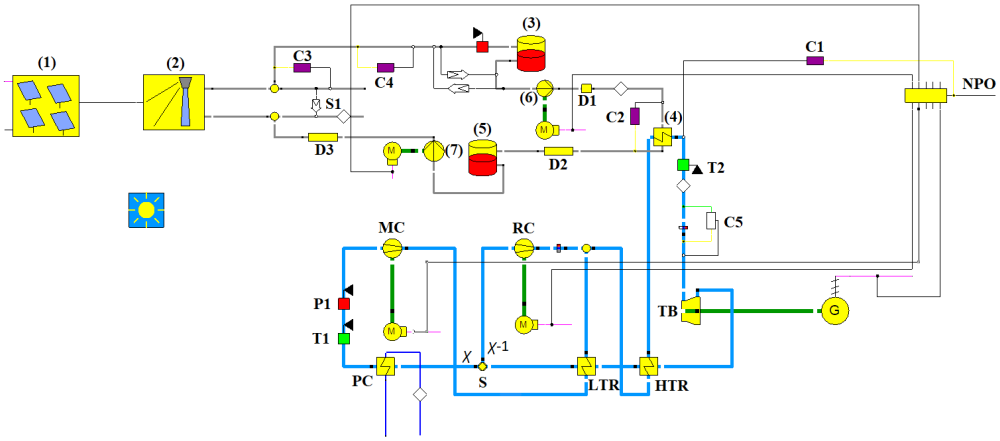


*Figure 5.10: Plant layout*

The split ratio which allows the appropriate transfer of the heat and, at the same time, the maximum thermal efficiency is found equal to 0.75. This can be a risky situation for the cooler, but it has been decided to accept it because it gives the highest thermal efficiency. The correct heat transfer process in both the recuperators is shown in

Figure 5.11, while the T-q diagram of the cooler is presented in Figure 5.12. In

Figure 5.11, the red line represents the hot side of the recuperators, that is the $sCO_2$ exiting the turbine and entering first the HTR (1 → 2) and then the LTR (2 → 3), which in off-design condition is depicted in orange, while the blue line (green one in off-design) is the $sCO_2$ that has to be heated: in the LTH (4 → 5) the 75 % of the total mass flow from the main compressor (MC) is heated; this amount is then mixed with the remaining 25 % from the re-compressor (RC) and they enter together the LTR (6 → 7). The difference between

point 5 and 6 in due to the mixing process. On the other hand, from Figure 5.12, the uncommon behaviour of the carbon dioxide approaching the critical conditions becomes evident: indeed, the red curve for the design and the orange for the off-design condition perform the response of the $sCO_2$ (1 → 2) to the cooling process, done by water (3 → 4) (blue line in design and green in off-design). This diagram results totally in line with what was described in subsection 2.4.3 and shown in Figure 2.10, where deep the change of the specific heat capacity near the critical conditions is represented. The $sCO_2$ exiting the cooler and entering the main compressor is characterized by a pressure equal to 9.5 MPa and a temperature of 35 °C, very close to the critical point (around 7.4 MPa and 31 °C). The change in the specific heat capacity absolutely affects the heat transfer process and this justifies the shape of the red curve in Figure 5.12. All the heat exchangers undoubtedly exhibit the possible occurrence of the pinch point violation if some quantity is slightly changed, since the minimum temperature difference is very small, of the order of 5 °C. The off-design configuration is the most sensitive and delicate because the temperature distribution is not set and fixed but computed in the simulation for each time span. Nonetheless, given that from the Time Series calculation results that the correct heat transfer process is ensured also in this uncertain situation, it has been decided to keep all the thermodynamic parameters obtained through the sensitivity analyses which allow the maximum thermal efficiency, because the pinch point of 5 °C is always guaranteed. It is important to notice that, given the selected layout of recompression and the 75 % of splitting optimized with a minimum and maximum cycle pressures of respectively 9.5 MPa and 28.0 MPa and a TIT equal to 560 °C, a quite regular behaviour of the $sCO_2$ is obtained and the pinch point problem is always avoided in each component.

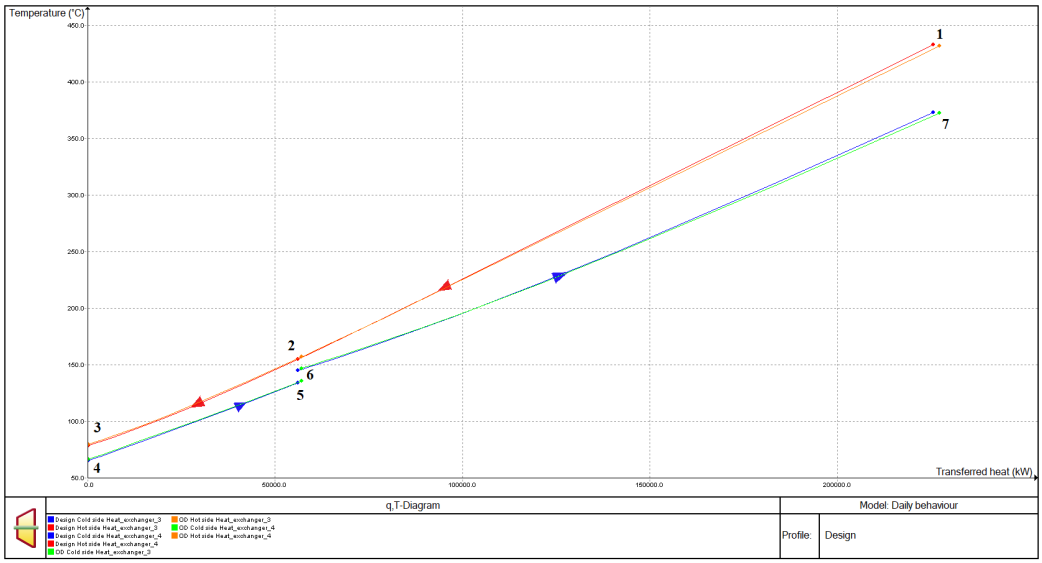


*Figure 5.11: T-q of the HTR and LTR*

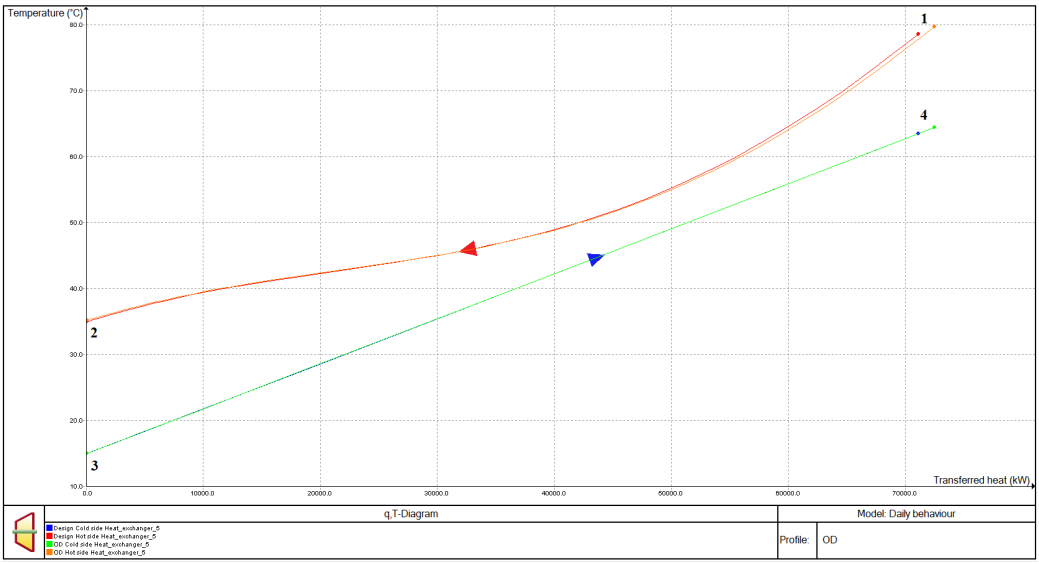


*Figure 5.12: T-q diagram of the cooler*

In order to understand what an error in the pinch point violation is, performing the sensitivity analysis a sub-profile with a lowest cycle temperature equal to 31 °C is created, keeping all the other thermodynamic quantities from the optimized design condition. The software advises about an occurring error on the pinch point due to the change on the fluid specific heat capacity curve in the cooler. Obviously, when the cycle runs with some error, the results are no longer stable nor reliable. Decreasing the minimum temperature from 35 °C to 31 °C, with the same minimum pressure equal to 9.5 MPa, means getting closer and closer to the $sCO_2$ critical conditions. Hence, the change in the specific heat capacity of the fluid is so strong that the pinch point inside the cooler is luckily to be violated and in the T-q diagram of the component the lines representing the cold (water) and the hot ($sCO_2$) side are expected to overlap. Moreover, problems related with the reduced approaching temperature difference between the inlet temperature of the power cycle fluid and outlet temperature of the cooling one are absolutely foreseen. These issues are well demonstrated in Figure 5.13, where the cooling water is represented in blue (3 → 4) and the $sCO_2$ in red (1 → 2). From the inlet condition of around 72 °C to reach a temperature equal to 31 °C, the red curve changes its slope and intersects the straight blue line, causing the pinch point violation. Further, the point 1, that is the $sCO_2$ inlet temperature, is very close to the point 4, outlet water temperature: their difference is less than 1 °C. This is a too extreme and risky condition that could not be accepted. In point of fact, the minimum temperature of the operating designed cycle never goes under 35 °C, neither when the plant works in off-design, no matter the season is. In these conditions, as largely explained in subsection 4.3.1, the maximum and minimum temperatures of the cycle are no longer externally given, like in design operation, but automatically calculated by the software as function of the heat transfer process, in order to obtain the convergence of all the thermodynamic quantities in

the close power cycle. This is a further confirmation of the reliability of the achieved plant results.

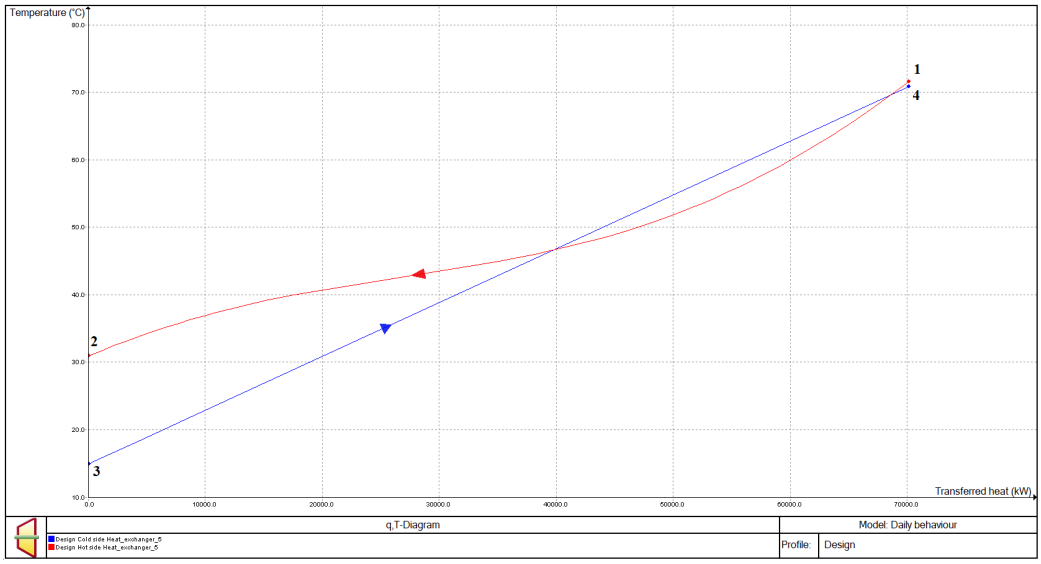


*Figure 5.13: T-q diagram of the cooler with pinch point violation*

After the group of sensitivities to optimize the cycle, as already mentioned, a further analysis is performed to demonstrate that the inserted controllers coupled with the scripts allow a flexible plant operation. The gained flexibility is important since, if a different output is desired, it is necessary only to choose this value and to put it on the appropriate controller (C1 in Figure 5.10). Then, the software automatically calculates the necessary flow rates of Solar Salt and $sCO_2$ as function of the externally chosen demand, inserted in C1. The sensitivity analysis produces the result of an improved thermal efficiency when the demand increases, but, after a net electrical power of 60 $MW_{el}$, a huge mass flow rate of water is necessary, larger than 400 kg/s. Of course, the plant is dimensioned for 45 $MW_{el}$ for the summer, 35 $MW_{el}$ for the winter and 42 $MW_{el}$ for the mid-seasons, that are the power allowing the continuous generation for the different seasons. So, the considered range of regulation regards only a temporary operation, even if the dynamic is not an object of this study, which runs without errors and without any change in the system thermodynamic inputs, apart from the required power output that is obviously externally chosen. The designed system could correctly work in a wide range of outputs, from 10 $MW_{el}$ to 60 $MW_{el}$, with acceptable thermal efficiencies: the flexibility is demonstrated to be reached thanks to the controllers and the on-purpose written scripts. From Figure 5.14, the impact of the NPO on the thermal efficiency is evident: when the required output is decreased, the resulting thermal efficiency is lowered and the slope of curve is very steep; after an NPO of 35 $MW_{el}$, the rate of change is smoother. This is in line with the expectations, since the plant is optimized for a net electricity of 45 $MW_{el}$: changing the output, keeping the same TIT and pressure ratio, affects the efficiency of the system, whose

best operational point is found as the combination of the thermodynamic quantities and the NPO. So, in the neighbourhood of the design output, the obtained values of the thermal efficiencies are comparable; at lower NPOs, the resulting efficiencies are penalized. Given the aim of regulating the plant without any manual change, apart from the demand, and the assumption of working at partial load for a short time interval, it is accepted to deal with lower efficiencies than in the design case.

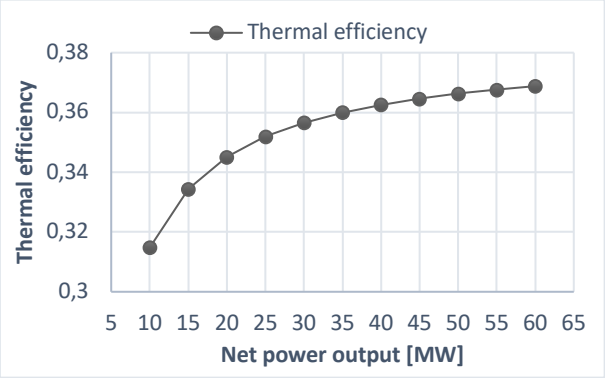


*Figure 5.14: Thermal efficiency as function of the NPO*

## 5.4 System Performance

### 5.4.1 Solar-to-electric efficiency

Solar-to-electric efficiency represents the overall efficiency of the plant. It is the ratio between the net electrical power output to the input from the solar field, taking into account the optical and thermal efficiencies of the solar field, losses in the pipes and the efficiency of the power block. When a storage system is included in the plant, employed in order to increase the operating hours of the system, there is a considerable thermal energy stored in the tanks, too. In literature, there is no unique indication to calculate the overall efficiency of a plant equipped with a storage system. Since the simulation is performed in one-hour intervals with a view to see the variation of each parameter as function of the time and of the available irradiation, it would not be precise nor accurate to estimate the tanks thermal energy making the day average of the stored mass flow and considering this energy as a useful output. Hence, two procedures are presented:

1. create a new cycle with a smaller solar field producing exactly the Solar Salt flow rate necessary to supply the rated power, without including any storage system;
2. neglect the presence of the storage system when a long period of time is considered.

Regarding the first procedure, the new cycle is depicted in Figure 5.15 and it is simulated on the 21st of June, in the usual design condition. The system is made up of a smaller

heliostat field (1) which is coupled with the same solar tower (2) as before. The is dimensioned in order to generate exactly the flow rate necessary to produce the rated power of 45 $MW_{el}$, which results equal to 407 kg/s. This value is slightly lower than the typical one for the complete system, integrated with the storage, since now pumping work in solar loop is reduced and hence the resulting necessary Solar Salt flow rate is reduced, too, as explained in section 5.2. Notice that the controller which allowed the automatic calculation of the molten salt flow rate, set on both sides of the primary heat exchanger (3), has been eliminated: the aim of this cycle is no longer to study the variation of all the parameters as function of time, but to dimension a plant which can only supply the rated power in the design operation. Component (5) pumps the molten salt back to the solar tower (2) to close the loop. Through component I1, the maximum temperature withstood by the Solar Salt is given, always equal to 565 °C, while through the components I2 and I3 the minimum temperature and pressure and the maximum temperature, respectively, are given as input and they are equal to 35 °C, 9.5 MPa and 560 °C, as previously assessed. The turbine maximum pressure is set again equal to 28.0 MPa. The controller C1 allows the automatic calculation of the necessary $sCO_2$ mass flow rate as function of the required power, equal to 45 $MW_{el}$. Hence, in accordance with the proposed methodology, this power cycle is entirely equal to the one designed for the real design plant. Component number (4) is inserted in order to highlight the correctness of the procedure and of the results: indeed, it is always in the same unchanged state, it never accumulates nor discharges, in line with this study objective. However, it ensures the minimum temperature of 290 °C.

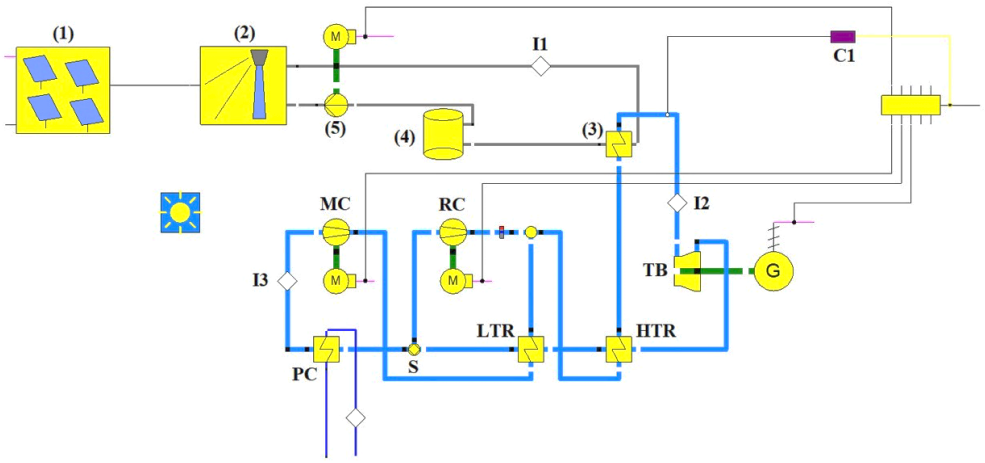


*Figure 5.15: Plant layout without accumulation*

Once the heliostat field (1) is dimensioned to obtain a power cycle exactly equal to the real system one, it is possible to take advantage of the definition of solar-to-electric efficiency, which is the ratio of the net electric power output to the input given by the solar field. Since this cycle grants only the generation of the rated power, without accumulating, all the

energy from the solar field (276 $MW_{th}$) is totally used to produce the electric power. Hence, the solar-to-electric efficiency results equal to 16.30 % (Eq. 5.1).

$$Solar - to - electric\ efficiency = \frac{Produced\ electrical\ power}{Produced\ thermal\ power} = \frac{45\ MW}{276\ MW} = 16.30\ \% \qquad Eq.\ 5.1$$

Concurrently, the second procedure is an average calculation which is based on the idea that the storage tanks are loading and unloading during the day, reaching the maximum and then getting empty. There is always an average stored mass flow in the hot or cold vessel. If it could be possible to consider a long period of time, the molten salt mass flow produced by the solar field would be extremely higher than the amount stored in the tanks, since this is always the same on average during all days of the considered season. Remember that the employed storage is a daily system. In other words, considering one day (24 hours), the thermal energy of the storage has a strong impact on the overall efficiency. But, considering three months of the same season, the thermal energy of the storage system is always equal to the thermal energy of one single day and, being orders of magnitude smaller than the produced and used thermal energy, it is allowed to neglect it. Hence, three months of summer are considered and the solar to electric efficiency is calculated first taking advantage of Eq. 5.2, through which the produced electrical power during three months is calculated, considering the continuous power supply of 45 $MW_{el}$; then, through Eq. 5.3, the produced thermal power during the 13 hours of sun radiation in summer (13 hours is the time interval in which the sun is shining during summer, obtained through the Time Series calculation) is computed; finally, in Eq. 5.4 the ratio between the previous results is made and the solar-to-electric efficiency effectively calculate.

$$Produced\ electrical\ energy = 24\frac{hours}{day} \cdot 30\frac{days}{month} \cdot 3\ months \cdot 45\ MW = 97{,}200\ MWh \qquad Eq.\ 5.2$$

$$Produced\ thermal\ energy = 13\frac{hours}{day} \cdot 30\frac{days}{month} \cdot 3\ months \cdot 510\ MW = 596{,}700\ MWh \qquad Eq.\ 5.3$$

$$Solar - to - electric\ efficiency = \frac{Produced\ electrical\ energy}{Produced\ thermal\ energy} = 16.29\ \% \qquad Eq.\ 5.4$$

The results obtained through the proposed procedure give the same result, hence it is reliable and the presented procedures are both correct. In particular, the second procedure gives a result (16,29 %) lower than the first one (16,30 %) of 0.0001 because in this case the small daily contribution of the energy stored in the tank is neglected. Moreover, the result lies in the range given by IRENA when solar tower is coupled with superheated steam cycle, for both power plants in operation and under research and construction, that is from 15 % to 17 %, with the aim to reach the 20 % (IRENA, 2012a, 2012b).

### 5.4.2 Storage Equivalent hours

In order to have an idea of the production of the proposed plant granted by the storage system, the storage equivalent hours are calculated. They are defined as the hours in which the nominal power can be produced thanks to the storage system. Indeed, it is used in a view to increase the operating hours of the plant, since it permits the generation of electricity also during the hours of absent radiation. The calculation is performed firstly by averaging the mass flow of molten salt stored in one day. Then, the average energy of the tanks is computed using Eq. 5.5 and, dividing it by the thermal power that the Solar Salt transfers to the power cycle according to Eq. 5.6, the equivalent hours of the storage system are obtained. The stored mass flow is obtained through the Time Series calculation, where it is calculated over a one-hour interval, together with all the other cycle parameters of interest. From the literature, the specific heat capacity of the Solar salt is equal to 1.5 $kJ \cdot kg^{-1} \cdot °C^{-1}$ and the maximum and minimum solar loop temperatures are respectively 565 °C and 290 °C. In the proposed plant, the net electrical power output is different for each season, since it is the maximum which allows to accumulate enough molten salt mass flow in order to ensure the continuous power supply. Accordingly, the stored mass flow rate is not constant during different periods of the year, but it is function first of the necessary amount to supply the power cycle and then of the field efficiency as well. As already discussed in section 5.2, the field efficiency results higher in winter than in summer, because of the non-optimal latitude where it is installed. Hence, it is expected that, on average, the stored mass flow of Solar Salt will be slightly higher in winter than in summer: in this period, the demand is higher, and equal to 45 $MW_{el}$, than during winter, where 35 $MW_{el}$ are produced, leading primarily to a reduction of the excess molten salt amount stored in the hot tank to supply the rated power for the few hours of night; secondly, it provokes an increase of the heat exchanged between the Solar Salt and the $sCO_2$ to produce the large required power output. In consideration of this, the number of equivalent hours obtained through the winter time series outputs is predicted to be bigger than the number for the summer case, since the decreased demand (35 $MW_{el}$), in turn, affects the thermal power needed by the power cycle to supply the rated power which will be decreased as well. The same considerations, for the field efficiency and the necessary heat to be stored and discharged, justify the higher molten salt average mass flow during spring and autumn with respect to summer: this time, the demand equal to 42 $MW_{el}$ is comparable with the summer case (45 $MW_{el}$), but the field efficiency is higher and so it is able to produce a larger molten salt flow rate, which in part is used to directly supply the power cycle and in part is stored. In particular, the sun shines for 11 hours, value found through the Time Series calculation, and the heliostat field efficiency is equal to 0.732, higher than the summer value (0.675). So, it is foreseen to obtain, on average, a higher stored mass flow. However, since in the mid-seasons the thermal power transferred from the solar loop to the power cycle is higher

than the winter case, when the maximum field efficiency is registered equal to 0.753, and lower than the summer one, it is reasonable to forecast a value of the storage equivalent hours lower than the one obtainable in winter, but higher than in summer. Logically speaking, the plant and, in particular, the storage system are sized in order to supply electrical power with absent radiation for a longer period in winter, that is from 18:00 to 8:00, than in summer, when the radiation is focused for 13 hours and the "Evening" period lasts from 19:00 to 6:00. Results are summarized in Table 5.4 and they are in accordance with expectations, where the dependence of the accumulated thermal power on the required output is evident.

$$Accumulated\ energy = \dot{m} \cdot cp \cdot \Delta T \qquad Eq.\ 5.5$$

$$Equivalent\ storage\ hours = \frac{Accumulated\ energy}{Nominal\ thermal\ power} \qquad Eq.\ 5.6$$

*Table 5.4: Daily equivalent hours*

| **Season** | **NPO [$MW_{el}$]** | **Average mass flow rate $\dot{m}$ [tons/s/day]** | **Accumulated energy [MWh/day]** | **Nominal thermal power [$MW_{th}$]** | **Equivalent hours [hours/day]** |
|---|---|---|---|---|---|
| Summer | 45 | 8,485.35 | 972.28 | 123.41 | 7.87 |
| Winter | 35 | 8,581.33 | 983.28 | 97.88 | 10.05 |
| Spring and Autumn | 42 | 9,054.06 | 1,037.45 | 116.62 | 8.90 |

At this point, the operating hours of the designed plant are estimated. In order to perform this calculation, the daily sunshine hours, when a part of the produced hot molten salt is directly used to generate electricity, are added up to the just calculated storage equivalent hours for each season. Then, they are multiplied by the number of days composing the seasons and added up, so that the yearly operating hours of the plant are obtained, according to Eq. 5.7, equal 7,451 hours per year. All the yearly results are corrected by a factor 365/360, since each month is assumed to be made up of 30 days. Given the way they are computed, they represent the hours in which the plant is able to provide the maximum rated power output for which it has been designed.

*Yearly operating hours*

$$= \left[\left(13\frac{hours}{day} + 7.87\frac{hours}{day}\right) \cdot 90\frac{days}{year} + \left(9\frac{hours}{day} + 10.05\frac{hours}{day}\right)\right. \quad \textit{Eq. 5.7}$$
$$\left. \cdot 90\frac{days}{year} + \left(12\frac{hours}{day} + 8.90\frac{hours}{day}\right) \cdot 180\frac{days}{year}\right] \cdot \frac{365}{360} = 7{,}451\frac{hours}{year}$$

In order to have an idea of the daily equivalent storage hours during the year, a weighted average calculation is performed, in accordance with Eq. 5.8.

*Daily equivalent storage hours*

$$= \frac{7.87\frac{hours}{day} \cdot 1\frac{season}{year} + 10.05\frac{hours}{day} \cdot 1\frac{season}{year} + 8.90\frac{hours}{day} \cdot 2\frac{seasons}{year}}{1\frac{season}{year} + 1\frac{season}{year} + 2\frac{seasons}{year}} = 8.93\frac{hours}{day} \quad \textit{Eq. 5.8}$$

The result of 8.93 hours/day of full load production is a good indication of the proposed plant performance. However, it is only an indication because the presented plant produces maximum power all-over the year which ensures production during the entire day, without any interruption due to the unavailable sun radiation. So, the power output has been chosen different for each season, causing different values of equivalent hours. In fact, the focal point of this study is the whole-day plant operation and the possibility to easily change the production according to the demand, designing a flexible plant which is able to adapt to different required power output. But it is important to remember that all the simulations have been performed with maximum output ensuring continuous daily power supply. Hence, it is plausibly expected that reducing the required electricity, allowed by the plant flexibility, the equivalent hours will surely increase. In other words, imposing a diminished output and maintaining the same solar field, a larger amount of Solar Salt would be stored in the tanks and less thermal power would be consumed by the $sCO_2$ power cycle. Looking at Eq. 5.5, the numerator would result increased and the denominator decreased, obtaining a higher number of equivalent hours. In addition, asking the plant the same power output during the whole year, the nominal thermal power transferred from the solar loop to the power cycle would be the same for all the seasons and the consequent equivalent hours calculation would be more precise. In this case, the tanks are assumed bigger in order to allow the storage of the mass flow unnecessary to generate electricity. As an example, the assumption of 35 $MW_{el}$ continuous power during the entire year is made. The results of the Time Series calculations are shown in Table 5.5.

*Table 5.5: Equivalent hours obtained with the same power output*

| Season | NPO [$MW_{el}$] | Average mass flow rate $\dot{m}$ [tons/s/day] | Accumulated energy [MWh/day] | Nominal thermal power [$MW_{th}$] | Equivalent hours [hours/day] |
|---|---|---|---|---|---|
| Summer | 35 | 11,444.99 | 1,311.40 | 97.88 | 13.40 |
| Winter | 35 | 8,581.33 | 983.28 | 97.88 | 10 |
| Spring and Autumn | 35 | 11,138.67 | 1,276.31 | 97.88 | 13.04 |

Taking advantage of Eq. 5.8, assuming a constant required electricity during the year, the average daily equivalent hours are 12.4. Now, it is evident how the required output strongly impacts on the offered equivalent hours: even though the heliostat efficiency is the lowest during the summer months, more Solar Salt mass flow is stored thanks to the largest number of available sun irradiation, which is powerful. Hence, as logically thought and expected, the highest number of equivalent hours is provided in summer. The equivalent hours would increase more if, obviously, the electricity was further reduced. However, the aim of the presented study is to design a plant equipped with a daily storage system ensuring the continuous supply of the maximum power which allows the production of the rated power also when the sun is absent. The storage tanks are designed to be empty in the early morning and full when the radiation is no longer available, therefore the maximum power is selected different for each season. The performed calculation is used to underline the feasibility of the plant and the advantages deriving from its flexibility, in terms of easy regulation and equivalent hours. Indeed, the already described controllers and switches make the external variation of the required electricity unsophisticated and they automatically and simultaneously calculate the $sCO_2$ and HTF mass flow rate of the new system, characterized by different thermodynamic parameters distribution that has changed as function of the different output.

The same considerations and calculations could be done to estimate the yearly equivalent hours, referring to the hours in which the plant can operate at full load during the year. The calculation is performed averaging the mass flow of molten salt stored in one day and multiplying it times 360 days per year, in order to obtain a value for the yearly mass flow rate accumulated in the storage tanks. This estimation is legitimated by the fact that the proposed plant is designed to accumulate every day of the year, neglecting at this design step the availability of the plant (Table 5.6).

*Table 5.6: Storage system equivalent hours for different seasons*

| Season | NPO [$MW_{el}$] | Average mass flow rate $\dot{m}$ [tons/s/day] | Accumulated energy [MWh/year] | Nominal thermal power [$MW_{th}$] | Equivalent hours [hours/year] |
|---|---|---|---|---|---|
| Summer | 45 | 8,485.35 | 350,021 | 123.41 | 2,836 |
| Winter | 35 | 8,581.33 | 353,980 | 97.88 | 3,616 |
| Spring and Autumn | 42 | 9,054.06 | 373,480 | 116.62 | 3,202 |

With the hypothesis that the plant behaves for 90 days as simulated for the summer, for 90 days as simulated for the winter and for 180 as simulated for the mid-seasons, the weighted average of the seasonal equivalent hours is done and the yearly storage system equivalent hours are equal to 3,258 hours per year (Eq. 5.9). Again, the result is corrected by 365/360, as earlier explained, to consider the real duration of the year.

$$\begin{aligned} &Equivalent\ storage\ hours \\ &= \frac{2{,}836\,\frac{hours}{year}\cdot 90\,\frac{days}{year} + 3{,}616\,\frac{hours}{year}\cdot 90\,\frac{days}{year} + 3{,}202\,\frac{hours}{year}\cdot 180\,\frac{days}{year}}{90\,\frac{days}{year} + 90\,\frac{days}{year} + 180\,\frac{days}{year}} \cdot \frac{365}{360} \\ &= 3{,}258\,\frac{hours}{year} \end{aligned} \qquad Eq.\ 5.9$$

This result demonstrates the important benefit introduced by the storage system: it enables the additional generation of full load electricity for 3,258 hours per year. Without the storage system, when the peak power is fixed, the abundant molten salt mass flow rate produced during the hours of higher radiation would simply be wasted and rejected to the environment as wasted heat.

All these results are obtained from full sunny days simulations. Obviously, during the year there are some cloudy or partly cloudy days, when the direct normal irradiance is reduced or absent. In order to have a more realistic estimation of the behaviour and performance of the designed system, the daily and yearly average DNI is extrapolated from the Solar Global Atlas (Solargis, 2018), where it is calculated based on the last decades trend. Given the latitude and longitude chosen for the plant, it is placed near Alexandria and Cairo, in Egypt (Figure 5.15

Figure 5.17 (Solargis, 2018)). From the Atlas, the DNI results yearly almost equal to 2,250 kWh/m$^2$ and daily equal to 6.075 kWh/m$^2$.

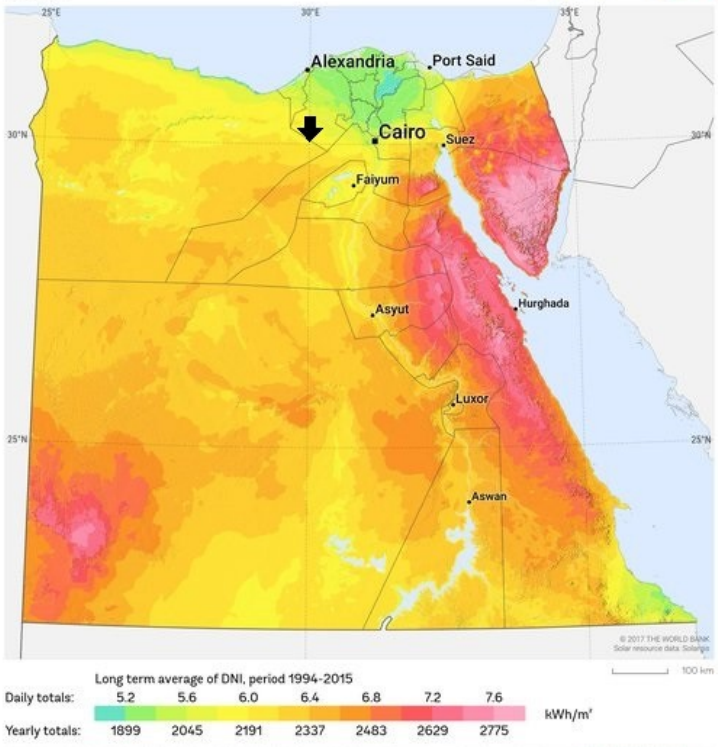


*Figure 5.16: Egypt average daily and yearly DNI (Solargis, 2018)*

At this point, the objective is to find a factor representing the overestimation of the production achieved by the calculations made with the assumption of all clear sky days. Unfortunately, the software does not provide directly the variation of the DNI during the different time intervals of the day, but it assumes it to be constant. The value which changes during the day and the year is the heat between the heliostat field and the solar tower, computed by the software as function of the sun angles. Therefore, it is necessary to go back to the DNI variation through the heat exchanged between the aforementioned components, which in turn is function of the sun angles and, accordingly, of time. The result is a daily average of the DNI, affected by the actual reduced and absent available sun irradiation during the early morning, the evening and the night. So, for each season, firstly the sum of the heat transferred from the heliostats to the tower is computed and it is divided by 24 hours per day. Obviously, it results higher for summer than for the other seasons. In the second place, it is necessary to break free from the efficiency of the heliostat field, since it clearly affects the amount of heat flowing from the mirrors to the receiver and at this point the aim is to find the variation of the direct incident irradiation on the heliostats, which is not function of the field properties (Eq. 5.10). Additionally, the software provides the heat captured by the field, defined as the product of the DNI and the mirrored area and, given

its definition, it is constant for the whole day and cannot be used to find the irradiation available from the sun. So, the average DNI is estimated dividing the average hourly exchanged heat just calculated by the total area of the solar heliostats, equal to 600,000 m² (Eq. 5.11). The results, shown in Table 5.7, demonstrate the dependence on the time: the daily average DNI is much lower than the nominal, set to 850 W/m², because it takes into account the hours of low and absent sun radiation that are present every day. Ultimately, the average DNI for the entire year is calculated and, through a series of equivalences, the necessary value for calculations is reached, in accordance with Eq. 5.12, where again each season is assumed to last for 30 days and the correction for considering the real duration of the year is applied (365/360).

$$Average\ hourly\ exchanged\ heat = \frac{\sum(Heat\ from\ field\ to\ tower)}{24\ \frac{hours}{day} \cdot \eta_{field}} \qquad Eq.\ 5.10$$

$$Avrage\ daily\ DNI = \frac{Average\ hourly\ exchanged\ heat}{Field\ area} \qquad Eq.\ 5.11$$

*Table 5.7: Average daily and yearly DNI values*

| **Season** | **Average hourly exchanged heat [$MW_{th}$]** | **Average daily DNI [$W/m^2$]** |
|---|---|---|
| Summer | 229.21 | 382.02 |
| Winter | 168.01 | 280.01 |
| Spring and Autumn | 202.21 | 337.03 |

$$Average\ DNI = \frac{382.02\frac{W}{m^2 \cdot day} \cdot \frac{90days}{year} + 280.01\frac{W}{m^2 \cdot day} \cdot \frac{90days}{year} + 337.03\frac{W}{m^2 \cdot day} \cdot \frac{180days}{year}}{360\frac{days}{year}} \cdot \frac{365}{360} = 335.68\ \frac{W}{m^2} \cdot 24\frac{hours}{day} \cdot \frac{10^{-3}kW}{W} \cdot \frac{360days}{year} = 2{,}900\frac{kWh}{year \cdot m^2} \qquad Eq.\ 5.12$$

Once the actual average DNI is computed for the proposed system, considering the hours of low of absent radiation typical of the evening and early morning, the comparison between this and the value found in the Atlas for the same place is made. In fact, in the presented study all the calculations are based on total clear sky days, while the DNI value from the Atlas considers also the partly or totally cloudy days in a statistical way. The ratio of the aforementioned quantities is the factor representing the overestimation made

because of the hypothesis of all fully sunny days, as in Eq. 5.13: in particular, the storage equivalent hours early found will be multiplied by this factor in order to have a more realistic estimation of the plant and, according to Eq. 5.14, they are equal to 7 hours/day.

$$f = \frac{Atlas\ DNI}{Average\ DNI} = \frac{2{,}250 \frac{kWh}{year \cdot m^2}}{2{,}900 \frac{kWh}{year \cdot m^2}} = 0.78 \qquad \textit{Eq. 5.13}$$

$$\begin{aligned} Actaul\ daily\ storage\ equivalent\ hours &= Daily\ storage\ equivalent\ hours \cdot f \\ &= 8.93\ \frac{hours}{day} \cdot 0.78 = 7 \frac{hours}{day} \end{aligned} \qquad \textit{Eq. 5.14}$$

From this estimation, the actual daily storage equivalent hours are reduced, as expected, and equal to 7 hours per day. However, this result is satisfying and still in line with the expectations: it indicates that the plant ensures the rated production for additional 7 hours every day, thanks to the integration with the thermal storage system. Once again, it is not a precise value but an average indication of the system performance, since it is obtained first averaging the optimistic equivalent hours among the seasons, each one different from the others due to the distinctive NPO and consequent different thermal power accumulated, and then multiplying it times an estimated factor which indicates the real atmospheric conditions in the plant location. In addition, it must be highlighted once again that the result is obtained asking the system for the maximum power output and that, as already demonstrated, it could be definitely increased if a diminished NPO is required. As an example, the previous case of constant 35 $MW_{el}$ during the whole year is considered: the number of equivalent storage hours, reduced by *f* accounting for actual sky conditions, is equal to 9.8 hours per day, that are additional hours of full load (35 $MW_{el}$) guaranteed by the storage system.

The actual operating hours can be estimated, as well, with the same previous hypothesis, considering the reduction of the operating hours due to the real sky conditions through the early calculated factor *f*, which is equal to 0.78 (Eq. 5.15). The result is lower than the previously found (7,451 hours per year from Eq. 5.7), as foreseen.

$$\begin{aligned} &Actual\ yearly\ operating\ hours \\ &= \left[\left(13 \frac{hours}{day} + 7.87 \frac{hours}{day}\right) \cdot f \cdot 90 \frac{days}{year} + \left(9 \frac{hours}{day} + 10.05 \frac{hours}{day}\right)\right. \\ &\left. \cdot f \cdot 90 \frac{days}{year} + \left(12 \frac{hours}{day} + 8.90 \frac{hours}{day}\right) \cdot f \cdot 180 \frac{days}{year}\right] \cdot \frac{365}{360} \\ &= 5{,}894 \frac{hours}{year} \end{aligned} \qquad \textit{Eq. 5.15}$$

### 5.4.3 Capacity Factor

Another strong motivation that suggests the convenience of the storage system employment is the Capacity Factor (CF), defined as the energy actually produced in one year divided by the product between the nominal full capacity of the plant and the number of hours in a year. Several reasons which could cause a CF lower than 100 % exists. First of all, the routine maintenance or the unlucky failures cause a direct reduction of the output. Then, if the maximum power is not required or the price of electricity is too low to make the production convenient, the generated output is decreased. The first reason is the most influencing on the capacity factor reduction of baseload power plants, as the one proposed in this study: indeed, they are designed to always work at their maximum output. The latter, on the contrary, is the main cause affecting the CF of peak-power plants, which are modelled to work for only small interval of time or up to a limited number of hours. Concerning renewable energy, another unavoidable source influencing the reduction of the CF arises, which has actually a key role: the unavailability and the intermittence of the source used as fuel. This is helpful not to misunderstand the capacity factor and the availability factor: indeed, the last indicator is not affected by such a possible zero production period, but it is mainly influenced by reliability and required periodic maintenance. The difference lies in the definition: the capacity factor is the ratio between produced and nominal power, while the availability is the time in which the plant produces electricity over a certain period divided by that period. To clarify, the fact that a plant is available does not imply that it can operate at its maximum nameplate. For renewable energy, given the strong dependence on the availability of the source, the capacity factor could result much lower than the availability factor, causing a consequent decrease on the economic interests. However, the plant proposed in this study has the fundamental potential of increasing the capacity factor thanks to the integration with a thermal energy storage system, which easily and efficiently decouples the availability of the sun irradiation from the electricity production, ensuring dispatchability and baseload supply in such a way that the intermittence of the source is no longer an issue. According to IRENA (IRENA, 2012b), adding 15 hours of thermal energy storage the capacity factor could reach the 80 %, while without the storage system it ranges from 20 to 25 %. The fundamental role of the increased CF lies in the potential reduction of the LCOE. The proposed plant offers, during winter, the possibility of storing the necessary amount of hot Solar Salt to supply the required electrical power for 15 hours during the night, while the average storage equivalent hours are 7 hours per day (8.9 h/day in the optimistic case of clear sky). Thereby, it is reasonable to foresee a capacity factor ranging from 0.6 to 0.8, which indicates that the presented system is able to supply the 60-80 % of the nameplate capacity during the yearly operation. Applying the definition, the CF of the presented power plant is calculated in Eq. 5.18. Given the fact that the presented plant is design to generate a different electrical

output on each season, for the reasons largely discussed, it is first necessary to estimate the annual production. The plant produces 45 $MW_{el}$ during summer, 35 $MW_{el}$ in winter and 42 $MW_{el}$ during spring and autumn. The operating hours typical of each season are calculated by summing up the earlier computed storage equivalent hours plus the sun shining hours. So, the production of each season is derived from the product of the seasonal operating hours and the chrematistic power output. Ultimately, the annual production is the sum of the just calculated production of all the four seasons, as in Eq. 5.16, corrected by 365/360. Here, the *f* factor reducing the operating hours is considered, in order to have a realistic estimation of the actual behaviour of the system. On the other hand, the nominal producible energy is considered as the sum of the nominal output chosen for every season, each one multiplied by the number of hours in which the plant is assumed to behave in that way, corrected by 365/360, according to Eq. 5.17.

$$\begin{aligned} &Energy\ produced\ in\ a\ year \\ &= \left[\left(13\frac{hours}{day} + 7.9\frac{hours}{day}\right)\cdot f \cdot 90\frac{days}{year}\cdot 45\ MW\right. \\ &+ \left(9\frac{hours}{day} + 10.05\frac{hours}{day}\right)\cdot f \cdot 90\frac{days}{year}\cdot 35\ MW \\ &\left. + \left(12\frac{hours}{day} + 8.90\frac{hours}{day}\right)\cdot f \cdot 180\frac{days}{year}\cdot 42\ MW\right]\cdot\frac{365}{360} \\ &= 242{,}421\frac{MWh}{year} = 242.42\frac{GWh}{year} \end{aligned} \qquad \textit{Eq. 5.16}$$

$$\begin{aligned} &Nominal\ producible\ energy \\ &= \left[24\frac{hours}{day}\cdot 90\frac{days}{year}\cdot 45\ MW + 24\frac{hours}{day}\cdot 90\frac{days}{year}\cdot 35\ MW\right. \\ &\left. + 24\frac{hours}{day}\cdot 180\frac{days}{year}\cdot 42\ MW\right]\cdot\frac{365}{360} = 359.15\frac{GWh}{year} \end{aligned} \qquad \textit{Eq. 5.17}$$

$$CF = \frac{Energy\ produced\ in\ a\ year}{Nominal\ producible\ energy} = \frac{242.42\frac{GWh}{year}}{359.15\frac{GWh}{year}} = 0.68 \qquad \textit{Eq. 5.18}$$

The result of a capacity factor equal to 0.68 makes the proposed plant a very interesting competitor for fossil fuel power plants, whose capacity factor is summarized in Table 5.8 (EIA, 2018) and it could well penetrate the market. It is absolutely in line with literature and experimental studies and it underlines the considerable advantages gained by the integration of the plant with a thermal energy storage, which, as demonstrated, enables the additional production of the nominal electrical power for more than 7 storage hours per day when the maximum NPO is requested.

*Table 5.8: Capacity Factors for Utility Scale Generators Primarily Using Fossil Fuels in USA (EIA, 2018)*

| Year 2018 | Coal | Natural gas fired combined cycle | Natural gas fired combustion turbine | Natural gas steam turbine | Petroleum steam turbine | Petroleum liquids fired combustion turbine |
|---|---|---|---|---|---|---|
| January | 64.2 % | 54.0 % | 11.9 % | 13.1 % | 19.0 % | 5.0 % |
| February | 49.3 % | 55.1 % | 6.9 % | 6.5 % | 11.8 % | 0.9 % |
| March | 43.9 % | 51.5 % | 9.3 % | 8.4 % | 10.9 % | 1.4 % |
| April | 41.7 % | 48.0 % | 11.4 % | 8.5 % | 12.7 % | 1.9 % |
| May | 47.0 % | 52.3 % | 11.8 % | 16.7 % | 9.2 % | 2.3 % |
| June | 58.4 % | 61.9 % | 12.0 % | 17.7 % | 15.2 % | 3.0 % |
| July | 64.3 % | 73.0 % | 18.9 % | 25.5 % | 14.3 % | 3.6 % |
| August | 64.3 % | 72.2 % | 18.9 % | 22.3 % | 15.8 % | 2.6 % |

## 5.4.4 Solar Multiple

The main drawback coming from the TES system is the rise of the plant costs: the solar field has to be over-dimensioned in order to allow the production of the excess mass flow to be thermally stored, in addition to the amount necessary to directly generate the electricity; components which compose the storage system cause a direct increase in the investment costs. This represents the biggest reason why investors could be discouraged: historically, despite the possibility to be integrated with a storage system which easily allows dispatchability, CSP has always been seen as an expensive technology. However, the choice to select a CSP power plant and to employ a thermal energy storage system is justified by the possible economical reduction of the LCOE and the advantages on the O&M costs deriving from the economy of scale (Dunham and Iverson, 2014; IRENA, 2012b). In order to have an indication of the over-sizing of the solar field, the Solar Multiple (SM) index is calculated. The solar field of a plant equipped with a TES system, as a matter of fact, is over-dimensioned, with the aim of producing more molten salt than the necessary, so that it could be accumulated. The solar multiple is the actual dimension of the real solar field referred to the solar field extension that would be required by a plant designed only to

produce the rated electrical power in the on-design, without any accumulation process. Regarding the plant presented in this project, the SM is calculated taking advantage of the system simulated to estimate the solar-to-electric efficiency (Figure 5.15). Sure enough, this cycle is comprised of a smaller heliostat field which allows only the production of the exact Solar Salt mass flow to supply the rated power, as described in subsection 5.4.1. So, according to Eq. 5.19, the solar multiple is equals to 1.85.

$$SM = \frac{Thermal\ energy\ of\ the\ actual\ solar\ field}{Thermal\ energy\ of\ the\ solar\ field\ withouth\ storage} = \frac{510\ MW}{276\ MW} = 1.85 \qquad Eq.\ 5.19$$

The result is in line with the estimations done by IRENA (IRENA, 2012b), where a SM up to 2 is proposed when the storage system exceeds 6 hours. The equivalent storage hours of the proposed plant are earlier estimated almost equal to 7, when the atmospheric conditions are taken into account, while they are 8.9 assuming always clear sky. Both results are satisfied by a solar multiple of 1.85.

### 5.4.5 Water consumption

The cooling system plays a key role on the efficiency of the plant. The solar source for the CSP technology is usually available in desert regions, where the lack of fresh water for the cooling system is a common issue. The main advantage of dry-cooling systems arises: water consumption could be reduced by 90 % compared to a power plant equipped with wet cooling, where about 3 $m^3$/MWh of water are required. Nonetheless, if a dry (air) cooling tower is employed, the plant efficiency is reduced, 4-9 % of annual electricity is lost and the capital costs increases simultaneously. But only 10 % of the water required by a wet cooling tower is necessary, hence is it employed especially in desert zones. However, the increase of cost is not negligible: dry cooling system are 3.3 times more expensive than wet ones. Additionally, dry towers suffer from the variation of the ambient temperature and their performance is strongly affected by off-design operation (Dunham and Iverson, 2014; IRENA, 2012b). The efficiency penalization due to the employment of a dry cooling system is shown in

Figure 5.17 and compared with the wet cooling tower system (Dunham and Iverson, 2014).

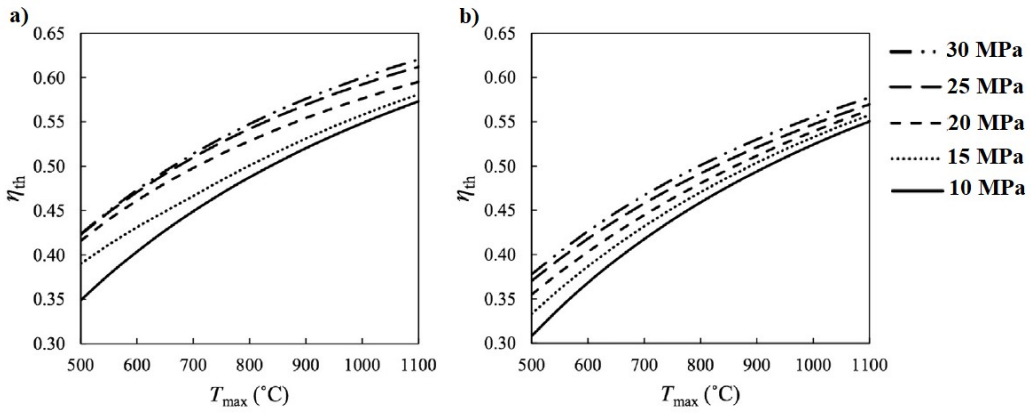


*Figure 5.17: Thermal efficiency of $sCO_2$ cycle under a) wet and b) dry cooling system (Dunham and Iverson, 2014)*

Therefore, the proposed plant is designed with a wet cooling system in order to enhance the overall efficiency and because the returning temperature of the water is already almost equal to 70 °C during the whole year. This value is calculated by the software as function of the operating conditions and of the heat transfer process. Hence, it is reasonable to use this hot water for CHP application, such as heating purposes for buildings.

Given the fact that the presented plant provides a different electrical output on each season, the yearly plant production is calculated in accordance with Eq. 5.16. The yearly water consumption of the presented plant is calculated in accordance with Eq. 5.20, while through Eq. 5.21, Eq. 5.22 and Eq. 5.23 an indication of the daily water consumption for the different seasons is provided, because daily results are easier to be understood and compared. The operating hours are reduced by the earlier calculated *f* factor, indicating the real atmospheric conditions, since the necessary water is directly function of the actual operating hours of the plant. Additionally, the water consumption is calculated with the maximum amount, that is 3 m³/MWh (worst case scenario of water consumption), while it ranges between 2.5 m³/MWh and 3 m³/MWh: therefore, an overestimation of the necessary water is probable to result from this calculation.

$$Yearly\ water\ consumption = Yearly\ production \cdot\ 3{,}000 \frac{m^3}{GWh} \cdot 1 \frac{kg}{m^3} \qquad Eq.\ 5.20$$

$$= 242.42 \frac{GWh}{year} \cdot\ 3{,}000 \frac{kg}{GWh} \cdot \frac{10^{-3} t}{kg} = 727.26 \frac{t}{year}$$

*Daily summer water consumption*

$$= \left(13\frac{hours}{day} + 7.9\frac{hours}{day}\right) \cdot f \cdot 45\ MW \cdot 3\frac{m^3}{MWh} \cdot 1\frac{kg}{m^3} \cdot \frac{10^{-3}t}{kg} \qquad \textit{Eq. 5.21}$$

$$= 2.23\frac{t}{day}$$

*Daily winter water consumption*

$$= \left(9\frac{hours}{day} + 10.05\frac{hours}{day}\right) \cdot f \cdot 35\ MW \cdot 3\frac{m^3}{MWh} \cdot 1\frac{kg}{m^3} \cdot \frac{10^{-3}t}{kg} \qquad \textit{Eq. 5.22}$$

$$= 1.58\frac{t}{day}$$

*Daily mid − seasons water consumption*

$$= \left(12\frac{hours}{day} + 8.90\frac{hours}{day}\right) \cdot f \cdot 42\ MW \cdot 3\frac{m^3}{MWh} \cdot 1\frac{kg}{m^3} \cdot \frac{10^{-3}t}{kg} \qquad \textit{Eq. 5.23}$$

$$= 2.08\frac{t}{day}$$

## 5.5 High efficiency cycle results

Up to now, the obtained outputs are comparable with operating solar tower power plants which are coupled with steam Rankine power cycles. This result clearly highlights that the potential advantages of the adopted closed supercritical $CO_2$ cycle are not fully exploited. To clarify, the high operating pressures and consequent high density of the working fluid allows first of all the overall employment of smaller components; in the second place, the less corrosiveness of the fluid with respect to steam extends components and pipes life-time; thirdly, its high molecular mass reduces the risk of leakage; ultimately, $sCO_2$ is stable over a wide range of pressure, it is not toxic, it is abundant and quite available. However, the high temperatures which could permit to obtain a greatly boosted thermal efficiency are not yet reached at the presented power plant. It is designed considering all the actual material limitations and employing the current commercial Solar Salt as heat transfer fluid, where the highest allowable temperature is equal to 565 °C, so the maximum $sCO_2$ which ensures a correct heat transfer between the solar loop and the power cycle is 560 °C, much lower than temperatures at which the $sCO_2$ power cycles experience highest efficiencies. Unfortunately, the current state of the art regarding HTF does not offer different molten salt compounds which can be used in the Ebsilon simulation, since they are not commercially available, but only studied and investigated in test-labs with advanced materials (see sections 3.2 and 3.5). For these reasons, in order to demonstrate the strongly

enhanced thermal efficiency that a fully exploited $sCO_2$ power cycle could reach with respect to a steam Rankine cycle (Dunham and Iverson, 2014), it has been chosen to neglect the solar loop, which is clearly the strongest limitation due to the temperature range and the corrosion on the employed materials. So, only the power cycle is simulated, under the assumption that the turbine inlet temperature is reached thanks to the correct heat transfer between a novel molten salt compound ensuring stability at higher temperatures, delivered in pipes which do not suffer of corrosion problems related with the boosted operation conditions.

The cycle components are the same employed for the power plant earlier presented in this study, so the effectiveness of the heat exchangers and the efficiencies of the turbine and compressors are assumed, same as summarized in

Table 4.1. But the thermodynamic quantities are pushed towards the allowable maximum in order to obtain a higher thermal efficiency. The studied parameters are the same as before:

1. the turbine inlet temperature;
2. the minimum cycle pressure;
3. the turbine inlet pressure;
4. the split ratio.

The procedure to optimize the cycle is the same adopted for the proposed plant and consists in finding a proper range of variation for each parameter, keeping all the other constant, and then varying simultaneously the chosen four quantities in the just found values interval, since they are intermeshed and contribute together to reach better performances. Once again, the procedure is conducted creating sub-profiles which work according to on-purpose written scripts. The results obtained through the first group of sensitivity analysis are shown in Figure 5.18. They are all conducted starting from the same cycle, characterized by a mass flow rate equal to 500 kg/s, a minimum and maximum pressure respectively of 9.0 and 32.0 MPa, a turbine inlet temperature equal to 700 °C and a splitting ratio of 0.75. Then, each of the four parameters is varied while all the others are kept unchanged.

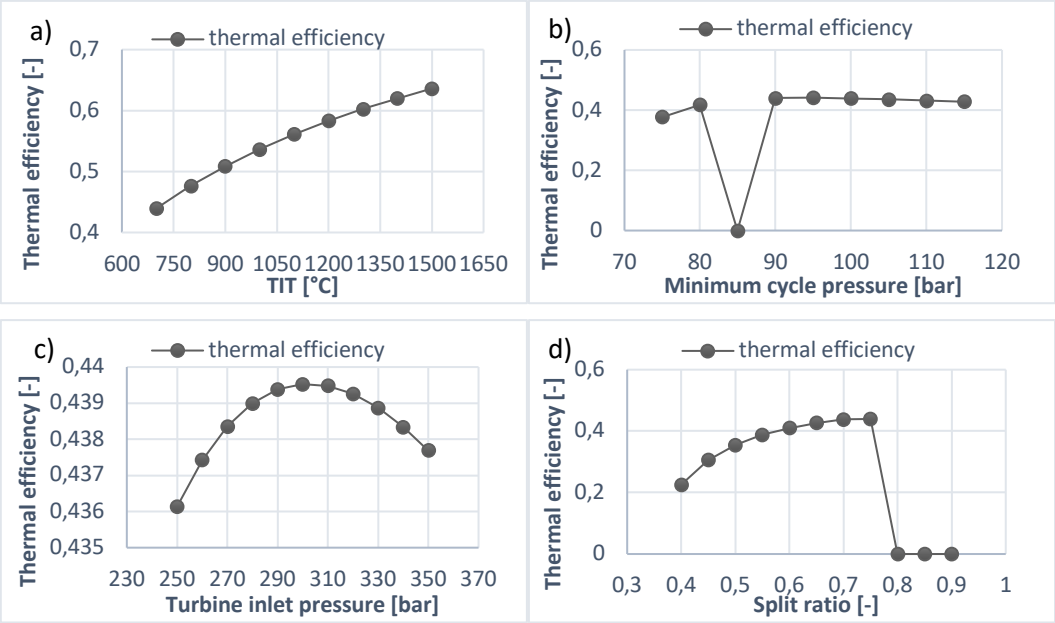


*Figure 5.18: First sensitivity analysis results*

The influence of the increasing turbine inlet temperature on the thermal efficiency is undoubtedly positive: as expected, the thermal efficiency tends to reach Carnot efficiency (Eq. 5.24), which is improved by increasing the maximum cycle temperature. The best minimum pressure value, instead, is again lightly higher than the critical one and this is a result already obtained for the presented plant equipped with the storage system and the solar loop. In the graph representing the minimum pressure influence (Figure 5.18), however, there is a point characterized by zero efficiency. Actually, it corresponds to the minimum pressure value, in particular 8.5 MPa, where the primary cooler (PC) undergoes a pinch point violation, so the software experiences an error and the calculated cycle features are absolutely not reliable. Hence, it is totally incorrect to calculate the thermal efficiency, which is set equal to zero for the sake of visual clearness. This result clearly demonstrates how a small change in a single parameter could jeopardize the correct operation of the whole cycle: in fact, the nearest points with a pressure slightly higher and lower than the one resulting in error make the plant correctly operate and give a thermal efficiency higher than 40 %. In contrast, Figure 5.18 demonstrates that the turbine inlet pressure positively impacts on the thermal efficiency until 30.0 MPa, after which the performance is penalized. At this point, it is crucial to fully understand the extrapolated results and not to misunderstand them: this group of sensitivity analyses is conducted varying only the examined parameter and keeping constant all the others. Hence, the deducted outcome that the best maximum cycle pressure is 30.0 MPa is improper. The correct conclusion to be drawn is that, once the minimum pressure is set at 9.0 MPa and the TIT at 700 °C with 0.75 as splitting ratio, the thermal efficiency is optimized at a maximum pressure of 30.0 MPa and it results almost equal to 44 %. The interdependence

of the thermodynamic quantities must always be considered. Obviously, if one or some of these parameters change, the maximum efficiency does the same and the best point operation is different from the one previously found. The last graph of Figure 5.18 shows the strong influence of the split ratio on the thermal efficiency: it is, in fact, a crucial parameter which has to be accurately chosen. The thermal efficiency equal to zero for splitting of 0.80, 0.85 and 0.90 is due to the pinch point problem occurrence (hence errors and unreliability of cycle results) on the primary cooler, where the $sCO_2$ is very sensitive to any parameter change and its specific heat capacity deeply varies near the critical conditions.

$$\eta\_Carnot = 1 - \frac{Tmin}{Tmax} \qquad Eq.\ 5.24$$

After having understood the trend of the thermal efficiency as function, separately, of each of the four examined thermodynamic parameters, the necessity to enhance the cycle performance leads to perform the final sensitivity analysis where their influence is studied simultaneously, so that a set of optimizing values is found. In this way, it is easy to perceive how each parameter has to be matched with a feasible value of the others in order to obtain first a cycle running free of errors and, ultimately, with the best thermal efficiency. For example, if 1,000 °C of TIT is coupled with a maximum pressure of the order of 20.0 MPa, the resulting thermal efficiency is much lower than the one obtained when setting the inlet turbine pressure and temperature respectively at 30.0 MPa and 1,000 °C, given the same split and minimum pressure. The same considerations can be done regarding also the split ratio and the minimum cycle pressure. In order to have a wide range of variation for the thermal efficiency, each parameter is varied within the just found values interval simultaneously with all the others, resulting in a huge number of sub-profiles running according to a script. Looking at Figure 5.18, the direct proportionality of the TIT and the thermal efficiency is evident: in other words, the increase in TIT has always a positive impact on the power cycle performance, which would be further improved by the correct choice of all the other parameters. For this reason, from the sensitivity analysis the best efficiency is reached at really high TITs. Another interesting outcome is the fact that with a minimum pressure equal to 8.5 MPa the pinch point is very probable to occur, even with an increase in the maximum cycle pressure. It is important to underline how the previous results must be taken together with the imposed non-varying parameters: from Figure 5.18, the best efficiency point corresponds to a maximum pressure of 30.0 MPa, when the TIT, the splitting and the minimum pressure are fixed and respectively equal to 700 °C, 9.0 MPa and 0.75. Now, thanks to the analysis including all the parameters, when the TIT is boosted up to 1,400-1,500 °C, the thermal efficiency is no longer maximized by a maximum pressure of 30.0 MPa, but at 33.0-35.0 MPa. However, it is not true that the highest the

parameters, the best the performance is: the cycle results optimized by a maximum pressure of 33.0 MPa with a TIT equal to 1,500 °C, reaching 64.15 % of thermal efficiency, while the sub-profile of 1,500 °C and 35.0 MPa shows a one percentage point lower efficiency, obviously choosing the split ratio and the minimum pressure that better fits the cycle on each configuration. To conclude, a thermal efficiency higher than 60 % could be obtained by optimizing the cycle to be capable of operating at very high temperatures and pressures (see again Table 4.5 for additional values). Results are in line with recent studies (Dunham and Iverson, 2014), where different cycles are compared. The most important outcome is that, increasing inlet turbine temperature and pressure, the recompression $sCO_2$ cycle ensures a thermal efficiency higher than the one reachable using the common-used Rankine cycle, whilst under 600 °C of TIT the obtained thermal efficiencies are comparable (Figure 5.19 (Dunham and Iverson, 2014)). Indeed, the corrosiveness of steam at boosted operation conditions strongly and negatively affects the Rankine cycle efficiency, while $sCO_2$ does not experience such problems.

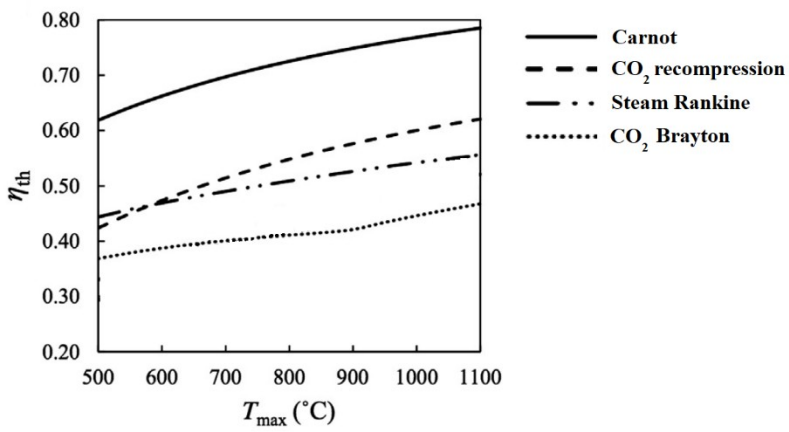


*Figure 5.19: Different cycles efficiency as function of the TIT (Dunham and Iverson, 2014)*

One of the aims of this study, however, is not to demonstrate only the potential performance of the $sCO_2$ cycle compared to the commonly-used Rankine cycle, but to show the improvements projected from coupling a CSP technology to a $sCO_2$ cycle. In this view, even if the used software does not allow the employment of molten salt compounds different from the Solar Salt, because they are not actually commercially available, it is important to do some considerations about the feasibility of the just presented optimized high-efficiency cycle and its integration with a solar tower.

First of all, it must be considered that a working fluid at 1,500 °C surely results in high stresses on pipes and components, especially when the pressure reaches and overcomes 30.0 MPa. Ni-base superalloys could be used, but the expensiveness makes them less interesting from an economic point view, so that usually Ni-base alloys are employed (see previous section 3.5). When the TIT is higher than the limit that the material can withstand,

the turbine undergoes an extreme operation condition which will permanently damage it, so it must be cooled down. From Brayton cycle well-established technology, solutions could be found. One possibility is represented by internal convection cooling, where some compressed cold gas from the compressor is sent inside the first stage of the turbine. Since the pressure inside the blades is higher than the one outside, the cooling process is promoted and the turbine works at a safer condition. As a strong disadvantage, the cooling gas has to be at a high pressure, at the expense of the compressor efficiency, surely jeopardizing the performance. In addition to this system, a film cooling improvement could be adopted: it is based on ejecting a cold gas film (at 400–500 °C, hence colder than the working fluid) along the blade, making some holes. Attention must be paid on the design and dimension of the holes, because especially at the blade suction side the pressure is low and there is the risk that all the mass flow could pass through the holes designed for the cooling system. What is undoubted is that cooling ensures safer operation conditions, but creates perturbations during the expansion process, since some cold gas is interacting with the hot stream, and the turbine efficiency is lowered.

Even if it could be accepted to employ expensive superalloys or to use a cooling system for the turbine, working at very boosted TIT, its effect on the solar loop must be carefully considered. When a CSP technology is equipped with a power cycle, the thermodynamic condition surely will influence the performance of the solar loop. In particular, considering the promising thermal efficiency allowed by a TIT higher than 700–800 °C, it has to balance the strong repercussions on the efficiency of the solar tower and on the HTF behaviour. In order to transfer the necessary amount of heat to the power cycle, the temperature of the HTF has to increase, keeping always a minimum temperature difference with the $sCO_2$ to ensure a correct process. Hence, as already mentioned, a compound different from the Solar Salt has absolutely to be used, guaranteeing stability above the limit it imposes (565 °C), and avoiding corrosion on the pipes and components. Then, the receiver thermal efficiency has a key role on the overall plant performance: increasing the HTF temperature, the solar tower efficiency first shows an improvement because the flux increases (denominator in Eq. 5.25), but later the losses become more dominant and efficiency decreases. Furthermore, the receiver is a component experiencing variable temperatures and fluxes during the day, even in different position. So, it is constantly under thermal stresses.

$$\eta_{th} = \frac{\dot{Q}_{rec} - \dot{Q}_{heat\ loss}}{\dot{Q}_{rec}} = 1 - \frac{\sigma \cdot E \cdot A_{rec} \cdot (T_{rec}^4 - T_{amb}^4) + h \cdot A_{rec} \cdot (T_{rec} - T_{amb})}{Flux \cdot A_{rec}} \qquad \textit{Eq. 5.25}$$

$$\eta_{opt} = \frac{\dot{Q}_{rec}}{\dot{Q}_{sun}} \qquad \textit{Eq. 5.26}$$

$$\eta_{rec} = \eta_{opt} \cdot \eta_{th} \qquad \textit{Eq. 5.27}$$

- $\eta_{th}$: receiver thermal efficiency;
- $\eta_{opt}$: receiver optical efficiency, function of the absorbance (α) and transmissivity (τ) of the material;
- $\eta_{rec}$: receiver efficiency;
- $\sigma$: Stefan–Boltzmann constant, equal to $5.67 \cdot 10^{-8}$ W/(m² K⁴);
- $E$: receiver emissivity;
- $h$: heat transfer coefficient for convection;
- $A_{rec}$: receiver area;
- $T_{rec}$: receiver temperature;
- $T_{amb}$: ambient temperature;

Consequently, with a view to optimizing the whole system made up of the power cycle and the solar loop, the best temperatures for the HTF and the $sCO_2$ have to be found together, ensuring such compromise. This is well explained by an experimental study showing different power cycles performance when coupled to a solar tower (Dunham and Iverson, 2014) which is shown in Figure 5.20. The system efficiency, in this case, is function of the TIT at a maximum pressure set equal to 30 MPa.

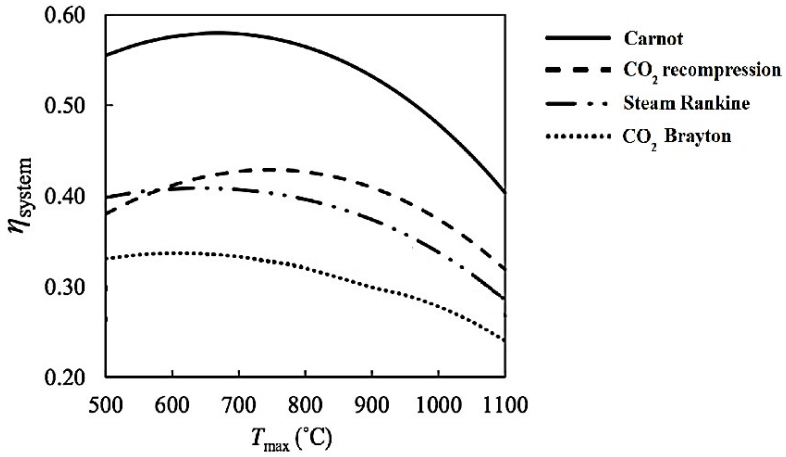


*Figure 5.20: System efficiency for different power cycles coupled with a solar tower (Dunham and Iverson, 2014)*

The interesting outcome is that, after a TIT equal to 600 °C, the system efficiency reached through a $sCO_2$ cycle is always higher than the one obtained with a Rankine cycle. However, a peak efficiency exists, after which the plant performances are jeopardized, as foreseen and expected. This means that if the power cycle operation conditions are required to be boosted, efforts have to be directed towards improving the receiver performances,

otherwise the overall efficiency will for sure decrease. As observed and demonstrated, the recompression $sCO_2$ cycle could reach a thermal efficiency at the order of 60 %, but the necessary TIT will increase the receiver losses and reduce the system efficiency. A more realistic range of TIT for $sCO_2$ power cycles integrated with solar tower CSP is between 700-800 °C, as shown in Figure 5.20: sensitivity analyses performed within this range of temperatures show a cycle thermal efficiency of the order of 44-50 %, when minimum and maximum pressure are respectively equal to 9.5 and 30.0 MPa and the split ratio is equal to 0.75.

# CONCLUSION AND FUTURE WORK RECOMMENDATIONS

The proposed plant is designed with the aim to generate electricity exploiting the direct irradiation of the sun. It is composed of a heliostat field focusing the radiation on the top of a solar tower where the receiver, which heats the molten salt, is placed. In the solar loop, a thermal energy storage system is integrated. The heat collected by the heliostats is then transferred through the primary heat exchanger to the power cycle. The latter is a closed recompression supercritical carbon dioxide cycle: the working fluid is $CO_2$ above its critical conditions and the compression process is performed by two different compressors, working at variable amount of fluid and inlet operating conditions, in order to increase the cycle efficiency taking advantage from the behaviour of the $sCO_2$ near its critical point. A key point is to determine the correct split ratio according which the compressors work: it is necessary to be found in order to prevent the cycle heat exchangers (recuperators and cooler) from the common pinch point problem widely mentioned in literature.

The core of this project is to study the possibility to ensure a baseload power thanks to the integration of a thermal energy storage system, that guarantees the correct supply of the necessary molten salt amount during the hours of absent sun radiation. This is the main reason pushing towards the choice of a solar tower configuration, to be able to reach high efficiencies, since it could be easily integrated with a TES system.

In order to demonstrate the feasibility of the designed system, the most sever conditions have been selected: the maximum power which allows continuous generation of electricity is chosen as output. Given the varying availability of radiation during the year, the simulation is done selecting a particular net power output for each season. Using the software Ebsilon® Professional 13.01, the plant is simulated as a subsequence of steady-state conditions during the whole day, dividing it in one-hour intervals. This is possible thanks to an on-purpose script developed and inserted in the software, which makes the plant working based on the different amounts of available radiation, that is obviously

function of time. In this way, all the characteristic parameters of the plant are constantly monitored and studied. In particular, the level of the hot and cold tanks is analysed, in order to be sure that they provide the necessary amount of molten salt to continuously generate electricity on demand. From the Time Series outputs, the estimation and computation of the cycle performance are conducted.

Given that a primary objective of the presented study is to design an actual feasible power plant that could operate using current state of the art, the molten salt playing the role of the heat transfer fluid and, simultaneously, of the storage fluid is the commonly used Solar Salt. Here, the first and the strongest system limitation arises: the temperature to avoid solidification and ensure thermal stability ranges from 290 °C to 565 °C. This deeply penalizes the efficiency of the power cycle, since it imposes a maximum TIT at 560 °C, and does not allow to fully exploit the advantageous properties of the $sCO_2$ working at high temperatures.

The actual proposed system is designed with a view to reaching maximum flexibility, despite the constraints imposed by the Solar Salt. For this reason, controllers are used which make the regulation of the externally required power absolutely simple and immediate, without considering any transient behaviour of the system components at this design step. Additionally, the inserted switches and controllers enable automatic calculation of all thermodynamic quantities not imposed by any material limitations as function of the heat exchange process. In particular, the mass flow rate of both the Solar Salt and the $sCO_2$ is automatically computed by the software program: so, in order to regulate the output, only the required electricity has to be externally modified, while the cycle is able to consequentially adapt to the different imposed conditions. Once the minimum and maximum temperature and pressures are given to the software as an input, in order to respect the imposed limitations, the distribution of the typical cycle thermodynamic parameters is calculated by the software as function of the heat exchange process.

As starting point, operating conditions are taken from literature and experimental studies, in order to design a realistic and feasible plant. The thermodynamic quantities of the power cycle impact together and simultaneously on each other and on the overall efficiency: for this reason, a group of sensitivity analyses is performed to find out the best operating point of the plant, without exceeding the discussed constraints. It is done with writing Pascal scripts and inserting them within the software, so that it accordingly changes the analysed parameters. The resulting best thermal efficiency is 36.46 % when the TIT is 560 °C, the minimum and maximum power cycle pressures respectively are 9.5 MPa and 28.0 MPa and the split ratio is 0.75. This result is totally satisfying and in line with experimental studies. However, when the TIT is lower than 700 °C, a Rankine cycle could reach comparable

efficiencies, so that the advantages of a recompression $sCO_2$ cycle are not visible. With a view to demonstrating the convenience of employing a closed recompression $sCO_2$ increasing the TIT, the power cycle is then designed in Ebsilon® Professional 13.01 decoupled from the solar loop and analysed through a series of sensitivity analyses, given to the software through some Pascal dedicated scripts. Accordingly, the best compromise of maximum and minimum pressures, split ratio and TIT is found also for this configuration. The gained results clearly demonstrate that the cycle efficiency definitely increases when the conditions at the turbine inlet are pushed toward higher pressure and temperature values: it is higher than 60 % with a TIT of 1,500 °C. Clearly, material limitations, stresses on components and cooling issues must be considered, as well as the successive connection with a solar tower configuration, whose efficiency, up to now, is jeopardized by extreme temperatures. A more realistic range of TIT for $sCO_2$ power cycles integrated with solar tower CSP is between 700-800 °C, where the cycle thermal efficiency could reach up to 50 %, with minimum and maximum pressure respectively equal to 9.5 and 30.0 MPa and split ratio equal to 0.75. In this interval of temperatures, receiver performance could be maximized, as well, if an efficient molten salts compound, allowing high temperatures operation, is used.

Moreover, sensitivity analyses are carried on in order to study the flexibility of the system and to show that the thermal efficiency is improved when the required electricity increases, while it is penalized by the reduction of the NPO. This is in line with the main analysis hypothesis of varying only the output, keeping the system dimension and thermodynamic parameters unchanged: in fact, the proposed plant is designed with a view to obtaining a high electrical power and it is not optimized to provide a lower output. However, flexibility is reached since it is allowed to work in non-optimal conditions, once lower efficiencies are accepted to be obtained.

The Time Series calculations done on the real designed and proposed plant show feasible operating conditions and high efficiencies. From the outputs, the storage equivalent hours, the operating hours, the solar multiple and the capacity factor are calculated: all the results are in line with the experimental studies available in literature and expectations. In particular, the storage equivalent hours are firstly estimated directly from the Time Series outcomes and they are equal to 8.9 hours per day. Then, with the aim of considering the real sun radiation on the selected site, combination of cloudy and sunny days, the DNI from the Global Solar Atlas is obtained and compared with the one used in the software simulations: a factor *f* equal to 0.78 is found from their ratio which is multiplied by the previously found equivalent hours, in order to obtain a more realistic estimation. In this way, the storage equivalent hours are equal to 7 hours per day, which is still a satisfying result. In the first place, the operating plant hours are estimated equal to 7,451 hours per year. Then, in consideration of the aforementioned factor *f*, whose role is to diminish the

plant performance in accordance with actual sky conditions and make it more realistic, the operating hours of the plant are found equal to 5,894 hours per year and the capacity factor is calculated equal to 68 %, perfectly in line with the number of storage equivalent hours. For the sake of clearness, a short comparison with "Gemasolar" is made: its CF is 55 % and the yearly production is equal to 110 GWh/year, whilst the proposed plant reaches 242 GWh/year, without jeopardizing thermal (36.5 %) nor solar-to-electric (16.3 %) efficiencies. The high capacity factor undoubtedly shows the importance of integrating the plant with a TES system, even if it requires the necessity of an indirect configuration. As already explained, all these results are obtained from a plant operating with the actual commercially available technologies, such as the well-known Solar Salt with its temperature limitations. Therefore, it is expected to obtain further improvements with the use of more performing salt compounds pushing towards higher temperatures.

On the contrary, using a direct configuration with a supercritical $CO_2$ receiver, the withstood fluxes would be surely higher, as well as the TIT. Therefore, the thermal and the solar-to-electric efficiencies would be definitely improved. But, as a disadvantage, the storage system is very difficult to be integrated, since it would deal with a gaseous fluid, and so the possibility of a continuous production during the whole day would be lost or and indirect TES system should be adopted.

To have a complete picture of the situation, the dynamic study of the components should be performed in future works, in order to understand how the plant is effectively able to adapt to different conditions imposed by system regulation and partial load. Moreover, in this study it is assumed to work with the Solar Salt, which is the actual well-known salt compound commonly used for heat transfer fluid and storage system. It is strongly suggested to work with different compounds of molten salts that would allow for higher temperature ranges, so that the power cycle performance would consequently increase. The proposed plant thermal efficiency, in fact, results slightly higher than the one obtainable through a steam Rankine cycle: in fact, in this study it has been demonstrated that an enhancement of the thermal efficiency could be reached through a TIT increase, forbidden by the Solar Salt maximum temperature in the presented plant. The solar-to-electric efficiency is similar to the Gemasolar one, as well. Anyhow, the latter is a plant producing 20 $MW_{el}$, while the one proposed in this study is able to produce up to 45 $MW_{el}$ without any stop, apart from the scheduled ones for maintenance. Even if not fully exploited, the advantages in terms of compactness of the whole system, availability, non-toxicity, stability, high density of $sCO_2$ still play a fundamental role, especially regarding the faster expected response to transients, thanks to the smaller size of components. Powerful molten salts are recommended also because they can handle higher fluxes in the receiver (concentration ratio is very high), decreasing thermal losses and leading to better performance. Nevertheless, materials used for pipelines and components must have the

adequate properties to handle them, such as higher mechanical strength, corrosion resistance etc. Another good option could be the use of liquid metals, but they are not suitable to the role of heat storage fluid, so that an indirect TES system should be adopted, causing additional investment costs.

A deep limitation of the proposed plant is the use of an improper solar field for the selected latitude, as demonstrated by the field efficiencies for the different seasons. It is undoubtedly suggested to employ the correct field designed for the latitude where it is placed and the correct heliostats orientation. Then, a fluid dynamic study would be necessary to fully assess the plant, studying in detail the behaviour of the fluids and the dynamic of the components, and a mechanical analysis of the stresses on the components. Ultimately, an economic analysis is suggested to optimize the proposed system and to see how the increased costs caused by the TES storage system could be balanced by the reduction of the components dimension, the increased equivalent hours, the beneficial effect of the economy of scale and the enhancement of the efficiency.

# BIBLIOGRAPHY


Ahn, Yoonhan; Bae, Seong Jun; Kim, Minseok; Cho, Seong Kuk; Baik, Seungjoon; Lee, Jeong Ik; Cha, Jae Eun (2015): Review of supercritical CO2 power cycle technology and current status of research and development. In: Nuclear Engineering and Technology n. 6, 47, pp. 647–661. DOI: 10.1016/j.net.2015.06.009.

Alkholidi, Abdulsalam Ghalib; Altowij, Khaleel Saeed (2014): Free Space Optical Communications — Theory and Practices. In: Mutamed Khatib: Contemporary Issues in Wireless Communications: InTech.

Alva, Guruprasad; Lin, Yaxue; Fang, Guiyin (2018): An overview of thermal energy storage systems. In: Energy, 144, pp. 341–378. DOI: 10.1016/j.energy.2017.12.037.

Angelino, G. (1968a): Carbon dioxide condensation cycles for power production. New York, N.Y.: ASME (American Society of Mechanical Engineers (Series), 68-GT-23).

Angelino, G. (1968b): Carbon Dioxide Condensation Cycles For Power Production. In: J. Eng. Gas Turbines Power n. 3, 90, p. 287. DOI: 10.1115/1.3609190.

Angelino, G. (1969): Real gas effects in carbon dioxide cycles. New York, N.Y.: ASME (American Society of Mechanical Engineers (Series), 69-GT-102).

Azoumah, Y.; Ramdé, E. W.; Tapsoba, G.; Thiam, S. (2010): Siting guidelines for concentrating solar power plants in the Sahel: Case study of Burkina Faso. In: Solar Energy n. 8, 84, pp. 1545–1553. DOI: 10.1016/j.solener.2010.05.019.

Barlev, David; Vidu, Ruxandra; Stroeve, Pieter (2011): Innovation in concentrated solar power. In: Solar Energy Materials and Solar Cells n. 10, 95, pp. 2703–2725. DOI: 10.1016/j.solmat.2011.05.020.

Bauer, Matthew L.; Vijaykumar, Rajgopal; Lausten, Mark; Stekli, Joseph (2016): Pathways to cost competitive concentrated solar power incorporating supercritical carbon dioxide power cycles. The 5th International Symposium - Supercritical CO2 Power Cycles. San Antonio, Texas, March 28-31, 2016.

Bauer, Thomas; Pfleger, Nicole; Breidenbach, Nils; Eck, Markus; Laing, Doerte; Kaesche, Stefanie (2013): Material aspects of Solar Salt for sensible heat storage. In: Applied Energy, 111, pp. 1114–1119. DOI: 10.1016/j.apenergy.2013.04.072.

Bauer, M., Vijaykumar, R., Lausten, M. & Stekli, J., 2016. Pathways to cost competitive concentrated solar power incorporating supercritical carbon dioxide power cycles.

Bauer, M.L. et al. (2016) Pathways to cost competitive concentrated solar power incorporating supercritical carbon dioxide power cycles. The 5th International Symposium - Supercritical CO2 Power Cycles. San Antonio, Texas, March 28-31, 2016. (2016).

Benoit, H.; Spreafico, L.; Gauthier, D.; Flamant, G. (2016): Review of heat transfer fluids in tube-receivers used in concentrating solar thermal systems: Properties and heat transfer coefficients. In: Renewable and Sustainable Energy Reviews, 55, pp. 298–315. DOI: 10.1016/j.rser.2015.10.059.

Binotti, Marco; Astolfi, Marco; Campanari, Stefano; Manzolini, Giampaolo; Silva, Paolo (2017): Preliminary assessment of sCO 2 cycles for power generation in CSP solar tower plants. In: Applied Energy, 204, pp. 1007–1017. DOI: 10.1016/j.apenergy.2017.05.121.

Blanc, P.; Espinar, B.; Geuder, N.; Gueymard, C.; Meyer, R.; Pitz-Paal, R. et al. (2014): Direct normal irradiance related definitions and applications: The circumsolar issue. In: Solar Energy, 110, pp. 561–577. DOI: 10.1016/j.solener.2014.10.001.

Camporeale, S., Ciliberti, P. & Pantaleo, A., (2015): Thermoeconomic analysis and fluid selection of the bottoming ORC cycle coupled with an externally fired gas turbine. Napoli, Italy, 17 – 20 May, 2015

Canada, S.; Cohen, G.; Cable, R.; Brosseau, D.; Price, H. (2004): Parabolic Trough Organic Rankine Cycle Solar Power Plant, 25 - 28 October. Denver, Colorado.

Carling, R.; Kramer, C.; Bradshaw, R.; Nissen, D.; Goods, S.; Mar, R. et al. (1981): Molten nitrate salt technology development status report.

Carter, N.T. and Campbell, R.J. (2009) Water Issues of Concentrating Solar Power (CSP) Electricity in the U.S. Southwest. CongressionalResearchService, 8 June 2009.

Chung-Ling Chien, John; Lior, Noam (2011): Concentrating solar thermal power as a viable alternative in China's electricity supply. In: Energy Policy n. 12, 39, pp. 7622–7636. DOI: 10.1016/j.enpol.2011.08.034.

Cordaro, Joseph G.; Rubin, Nicholas C.; Bradshaw, Robert W. (2011): Multicomponent Molten Salt Mixtures Based on Nitrate/Nitrite Anions. In: J. Sol. Energy Eng. n. 1, 133, p. 11014. DOI: 10.1115/1.4003418.

Crespi, Francesco; Gavagnin, Giacomo; Sánchez, David; Martínez, Gonzalo S. (2017): Supercritical carbon dioxide cycles for power generation: A review. In: Applied Energy, 195, pp. 152–183. DOI: 10.1016/j.apenergy.2017.02.048.

DeBarbadillo, J.J. et al. (2018) Properties of INCONEL alloy 740H for high pressure steam and supercritical CO2 applications. Proceedings of the ASME 2018 Symposium on Elevated Temperature Application. ETAM2018. Seattle, WA, USA, 3-5 April. (2018).

Dieckmann, Simon; Dersch, Jürgen; Giuliano, Stefano; Puppe, Michael; Lüpfert, Eckhard; Hennecke, Klaus et al. (2017): LCOE reduction potential of parabolic trough and solar tower CSP technology until 2025. In: SOLARPACES 2016: International Conference on Concentrating Solar Power and Chemical Energy Systems. Abu Dhabi, United Arab Emirates, 11–14 October 2016: Author(s) (AIP Conference Proceedings), p. 160004.

Directive 2004/8/EC of the European Parliament and of the Council of 11 february 2004 on the promotion of cogeneration based on a useful heat demand in the internal energy market and amending directive 92/42/EEC 2004. (2004).

Dostal, Vaclav; Hejzlar, Pavel; Driscoll, Michael J. (2006): The Supercritical Carbon Dioxide Power Cycle: Comparison to Other Advanced Power Cycles. In: Nuclear Technology n. 3, 154, pp. 283–301. DOI: 10.13182/NT06-A3734.

Dostál, Václav (2004): Advanced nuclear power technology program a supercritical carbon dioxide cycle for next generation nuclear reactors. Massachusetts Institute of Technology.

Dunham, Marc T.; Iverson, Brian D. (2014): High-efficiency thermodynamic power cycles for concentrated solar power systems. In: Renewable and Sustainable Energy Reviews, 30, pp. 758–770. DOI: 10.1016/j.rser.2013.11.010.

Dunn, Rebecca I.; Hearps, Patrick J.; Wright, Matthew N. (2012): Molten-Salt Power Towers: Newly Commercial Concentrating Solar Storage. In: Proc. IEEE n. 2, 100, pp. 504–515. DOI: 10.1109/JPROC.2011.2163739.

Dunn, R., Hearps, P. & Wright, M., (2012): Molten-salt power towers: newly commercial concentrating solar storage. Proc IEEE, Volume 100, p. 504–15.

E, Cohen Gilbert; Kearney, David W.; KOLB, GREGORY J. (1999): Final Report on the Operation and Maintenance Improvement Program for Concentrating Solar Power Plants.

EIA (2018a): Electric Power Monthy.

El Chammas, Rody; Clodic, Denis (2005): Combined Cycle for Hybrid Vehicles. In:. SAE 2005 World Congress & Exhibition, APR. 11, 2005: SAE International400 Commonwealth Drive, Warrendale, PA, United States (SAE Technical Paper Series).

Endo, T.; Kawajiri, S.; Kojima, Y.; Takahashi, K.; Baba, T.; Ibaraki, S. et al. (2007): Study on Maximizing Exergy in Automotive Engines. In:. SAE World Congress & Exhibition, APR. 16, 2007: SAE International400 Commonwealth Drive, Warrendale, PA, United States (SAE Technical Paper Series). Available at https://www.eia.gov/electricity/monthly/epm_table_grapher.php?t=epmt_6_07_b.

Energy Solutions Center (2016): Gas turbines. Available at https://understandingchp.com/chp-applications-guide/4-3-gas-turbines/.

Ercole, D., Manca, O. & Vafai, K., 2017. An investigation of thermal characteristics of eutectic molten salt-based nano fluids. Int Commun Heat Mass Tran, Volume 87, pp. 98-104. (2017).

Eurekalert (2018): DOE to cut solar tower costs by pairing novel techs with sCO2 loop. How three innovative technologies will compete to make cheaper 24-hour solar. Available at https://www.eurekalert.org/pub_releases/2018-06/s-dtc061418.php, modified on 14 giugno 2018.

Feher, E. G. (1968): The supercritical thermodynamic power cycle. In: Energy Conversion n. 2, 8, pp. 85–90. DOI: 10.1016/0013-7480(68)90105-8.

Feher, E., 1967. The Supercritical Thermodynamic Power Cycle. Miami Beach (FL), (1967).

Fernández-García, A.; Zarza, E.; Valenzuela, L.; Pérez, M. (2010): Parabolic-trough solar collectors and their applications. In: Renewable and Sustainable Energy Reviews n. 7, 14, pp. 1695–1721. DOI: 10.1016/j.rser.2010.03.012.

Gil, Antoni; Medrano, Marc; Martorell, Ingrid; Lázaro, Ana; Dolado, Pablo; Zalba, Belén; Cabeza, Luisa F. (2010): State of the art on high temperature thermal energy storage for power generation. Part 1—Concepts, materials and modellization. In: Renewable and Sustainable Energy Reviews n. 1, 14, pp. 31–55. DOI: 10.1016/j.rser.2009.07.035.

Gilbert; Cohen for ACCIONA (2010): Nevada Solar One - Case Study. A Brief History & Status of the First CSP Operating Solar Energy Power Plant in Nevada. CSP today Conference. San Francisco, CA, 24.06.2010. Available at http://www.csptoday.com/usa2010/assets/pdf/slides/day_2_track_1/Parabolic%20Trough%20collectors.pdf.

Giostri, Andrea; Binotti, Marco; Astolfi, Marco; Silva, Paolo; Macchi, Ennio; Manzolini, Giampaolo (2012): Comparison of different solar plants based on parabolic trough technology. In: Solar Energy n. 5, 86, pp. 1208–1221. DOI: 10.1016/j.solener.2012.01.014.

González-Roubaud, Edouard; Pérez-Osorio, David; Prieto, Cristina (2017): Review of commercial thermal energy storage in concentrated solar power plants: Steam vs. molten

salts. In: Renewable and Sustainable Energy Reviews, 80, pp. 133–148. DOI: 10.1016/j.rser.2017.05.084.

Goods, S. H.; Bradshaw, R. W. (2004): Corrosion of Stainless Steels and Carbon Steel by Molten Mixtures of Commercial Nitrate Salts. In: Journal of Materials Engineering and Performance n. 1, 13, pp. 78–87. DOI: 10.1361/10599490417542.

Green, Martin A.; Hishikawa, Yoshihiro; Warta, Wilhelm; Dunlop, Ewan D.; Levi, Dean H.; Hohl-Ebinger, Jochen; Ho-Baillie, Anita W.H. (2017): Solar cell efficiency tables (version 50). In: Prog Photovolt Res Appl n. 7, 25, pp. 668–676. DOI: 10.1002/pip.2909.

Green Rhino Energy Ltd (2016): The sun's observed position. Available at http://www.greenrhinoenergy.com/solar/radiation/geometry.php.

Grirate, H.; Zari, N.; Elamrani, Iz.; Couturier, R.; Elmchaouri, A.; Belcadi, S.; Tochon, P. (2014): Characterization of Several Moroccan Rocks Used as Filler Material for Thermal Energy Storage in CSP Power Plants. In: Energy Procedia, 49, pp. 810–819. DOI: 10.1016/j.egypro.2014.03.088.

Hanania, Jordan; Stenhouse, Kailyn; Donev; Jason (2015): P-n junction. Available at https://energyeducation.ca/encyclopedia/P-n_junction.

Heier, Johan; Bales, Chris; Martin, Viktoria (2015): Combining thermal energy storage with buildings – a review. In: Renewable and Sustainable Energy Reviews, 42, pp. 1305–1325. DOI: 10.1016/j.rser.2014.11.031.

Heimsath, A.; Cuevas, F.; Hofer, A.; Nitz, P.; Platzer, W. J. (2014): Linear Fresnel Collector Receiver: Heat Loss and Temperatures. In: Energy Procedia, 49, pp. 386–397. DOI: 10.1016/j.egypro.2014.03.042.

Ho, Clifford K.; Iverson, Brian D. (2014): Review of high-temperature central receiver designs for concentrating solar power. In: Renewable and Sustainable Energy Reviews, 29, pp. 835–846. DOI: 10.1016/j.rser.2013.08.099.

Holbert, Keith E.; Haverkamp, Colin J. (2009 - 2009): Impact of solar thermal power plants on water resources and electricity costs in the Southwest. In: 41st North American Power Symposium. 2009 North American Power Symposium - NAPS. Starkville, MS, USA, 04/10/2009 - 06/10/2009: IEEE, pp. 1–6.

Holcomb, Gordon R.; Carney, Casey; Doğan, Ömer N. (2016): Oxidation of alloys for energy applications in supercritical CO 2 and H 2 O. In: Corrosion Science, 109, pp. 22–35. DOI: 10.1016/j.corsci.2016.03.018.

International Energy Agency (2017a) Key World Energy Statistics. Available at: http:// www.iea.org/statistics/. (2017). Available at in www.iea.or.

International Energy Agency (2017b) World Energy Outlook 2017. Available at: https://www.iea.org/weo2017/. Available at www.iea.or.

Iodice, Paolo; Langella, Giuseppe; Amoresano, Amedeo; Senatore, Adolfo (2017): Comparative Exergetic Analysis of Solar Integration and Regeneration in Steam Power Plants. In: J. Energy Eng. n. 5, 143, p. 4017042. DOI: 10.1061/(ASCE)EY.1943-7897.0000477.

IRENA (2012a): CSP Summary Charts. Available at http://www.irena.org/costs/Charts/CSP.

IRENA (2012b): Concentrating Solar Power. RENEWABLE ENERGY TECHNOLOGIES: COST ANALYSIS SERIES. Available at file:///C:/Users/tomal/Downloads/re_technologies_cost_analysis-csp.pdf.

IRENA (2012c): Concentrating Solar Power. Technology Brief. Available at file:///C:/Users/tomal/Downloads/re_technologies_cost_analysis-csp.pdf.

Irwin, Levi; Le Moullec, Yann (2017): Turbines can use CO2 to cut CO2. In: Science (New York, N.Y.) n. 6340, 356, pp. 805–806. DOI: 10.1126/science.aam8281.

Iverson, Brian D.; Conboy, Thomas M.; Pasch, James J.; Kruizenga, Alan M. (2013): Supercritical CO2 Brayton cycles for solar-thermal energy. In: Applied Energy, 111, pp. 957–970. DOI: 10.1016/j.apenergy.2013.06.020.

Kearney, D.; Kelly, B.; Herrmann, U.; Cable, R.; Pacheco, J.; Mahoney, R. et al. (2004): Engineering aspects of a molten salt heat transfer fluid in a trough solar field. In: Energy n. 5-6, 29, pp. 861–870. DOI: 10.1016/S0360-5442(03)00191-9.

Kribus, A.; Zaibel, R.; Carey, D.; Segal, A.; Karni, J. (1998): A solar-driven combined cycle power plant. In: Solar Energy n. 2, 62, pp. 121–129. DOI: 10.1016/S0038-092X(97)00107-2.

Kulhánek, Martin; Dostál, Václav (2010): Supercritical carbon dioxide cycles thermodynamic analysis and comparison.

La Casinière, A. de; Bokoye, A. I.; Cabot, T. (1997): Direct Solar Spectral Irradiance Measurements and Updated Simple Transmittance Models. In: J. Appl. Meteor. n. 5, 36, pp. 509–520. DOI: 10.1175/1520-0450(1997)036<0509:DSSIMA>2.0.CO;2.

Ladislav, Vesely; Vaclav, Dostal; Ondrej, Bartos; Vaclav, Novotny (2016): Pinch Point Analysis of Heat Exchangers for Supercritical Carbon Dioxide with Gaseous Admixtures in CCS Systems. In: Energy Procedia, 86, pp. 489–499. DOI: 10.1016/j.egypro.2016.01.050.

LAZARD (2017) Lazard's Levelized Cost of Energy Analysis -Version 11.0. Available at: https://www.lazard.com/media/450337/lazard-levelized-cost-of-energy-version-110.pdf. (2017).

Lee, Ho Jung; Kim, Hyunmyung; Jang, Changheui (2014): Compatibility of candidate structural materials in high-temperature S-CO2 environment. The 4th International Symposium - Supercritical CO2 Power Cycles. Pittsuburgh, Pennsylvania, 9-10 September 2014.

Lee, H.J., Kim, H. and Jang, C. (2014) Compatibility of candidate structural materials in high-temperature S-CO2 environment. The 4th International Symposium - Supercritical CO2 Power Cycles. Pittsuburgh, Pennsylvania, 9-10 September 2014.

Lehar, M. & Michelassi, V., 2013. System and Method for Recovery of Waste Heat from Dual Heat Sources. (2013).

Luu, Minh Tri; Milani, Dia; McNaughton, Robbie; Abbas, Ali (2017): Analysis for flexible operation of supercritical CO 2 Brayton cycle integrated with solar thermal systems. In: Energy, 124, pp. 752–771. DOI: 10.1016/j.energy.2017.02.040.

Manzolini, Giampaolo; Giostri, Andrea; Saccilotto, Claudio; Silva, Paolo; Macchi, Ennio (2011): Development of an innovative code for the design of thermodynamic solar power plants part A: Code description and test case. In: Renewable Energy n. 7, 36, pp. 1993–2003. DOI: 10.1016/j.renene.2010.12.027.

Mecheri, Mounir; Le Moullec, Yann (2016): Supercritical CO2 Brayton cycles for coal-fired power plants. In: Energy, 103, pp. 758–771. DOI: 10.1016/j.energy.2016.02.111.

Mittelman, Gur; Epstein, Michael (2010): A novel power block for CSP systems. In: Solar Energy n. 10, 84, pp. 1761–1771. DOI: 10.1016/j.solener.2010.06.004.

Mohammadi, Amin; Kasaeian, Alibakhsh; Pourfayaz, Fathollah; Ahmadi, Mohammad Hossein (2017): Thermodynamic analysis of a combined gas turbine, ORC cycle and absorption refrigeration for a CCHP system. In: Applied Thermal Engineering, 111, pp. 397–406. DOI: 10.1016/j.applthermaleng.2016.09.098.

Moisseytsev, A. & Sienicki, J., 2009. Analysis of Supercritical CO2 Cycle Control Strategies and Dynamic Response for Generation IV Reactors. [On line] (2009).

Moisseytsev, A. & Sienicki, J., June 2013. Extension of the supercritical carbon dioxide Brayton cycle for application to the Very High Temperature Reactor. San Diego (CA), (2013).

Morin, G. y otros, 2012. Comparison of linear fresnel and parabolic trough collector power plants. Sol Energy, Volume 86, pp. 1-12. (2012).

Moroz, L., Burlaka, M. and Rudenko, O. (2014): Study of a Supercritical CO2 Power Cycle Application in a Cogeneration Power Plant. Supercritical CO2 Power Cycle Symposium. Pittsburg, Pennsylvania USA, 9-10 September 2014

Moser, Massimo; Trieb, Franz; Fichter, Tobias (2013): Potential of Concentrating Solar Power Plants for the Combined Production of Water and Electricity in MENA Countries. In: J. sustain. dev. energy water environ. syst. n. 2, 1, pp. 122–140. DOI: 10.13044/j.sdewes.2013.01.0009.

National Technology and Engineering Solutions of Sandia, LLC (2015): National Solar Thermal Test Facility. Available at https://energy.sandia.gov/energy/renewable-energy/solar-energy/csp-2/nsttf/.

NIST (2013a): STANDARD REFERENCE DATA. NIST Reference Fluid Thermodynamic and Transport Properties Database. Available at https://www.nist.gov/srd/refprop.

Pacio, J.; Wetzel, Th. (2013): Assessment of liquid metal technology status and research paths for their use as efficient heat transfer fluids in solar central receiver systems. In: Solar Energy, 93, pp. 11–22. DOI: 10.1016/j.solener.2013.03.025.

Pantaleo, Antonio M.; Ciliberti, Patrizia; Camporeale, Sergio; Shah, Nilay (2015): Thermo-economic Assessment of Small Scale Biomass CHP: Steam Turbines vs ORC in Different Energy Demand Segments. In: Energy Procedia, 75, pp. 1609–1617. DOI: 10.1016/j.egypro.2015.07.381.

Pelay, Ugo; Luo, Lingai; Fan, Yilin; Stitou, Driss; Rood, Mark (2017): Thermal energy storage systems for concentrated solar power plants. In: Renewable and Sustainable Energy Reviews, 79, pp. 82–100. DOI: 10.1016/j.rser.2017.03.139.

Peng, Qiang; Ding, Jing; Wei, Xiaolan; Yang, Jianping; Yang, Xiaoxi (2010): The preparation and properties of multi-component molten salts. In: Applied Energy n. 9, 87, pp. 2812–2817. DOI: 10.1016/j.apenergy.2009.06.022.

Peng, Qiang; Wei, Xiaolan; Ding, Jing; Yang, Jianping; Yang, Xiaoxi (2008): High-temperature thermal stability of molten salt materials. In: Int. J. Energy Res. n. 12, 32, pp. 1164–1174. DOI: 10.1002/er.1453.

Pihl, Erik; Kushnir, Duncan; Sandén, Björn; Johnsson, Filip (2012): Material constraints for concentrating solar thermal power. In: Energy n. 1, 44, pp. 944–954. DOI: 10.1016/j.energy.2012.04.057.

Quoilin, S.; Orosz, M.; Hemond, H.; Lemort, V. (2011): Performance and design optimization of a low-cost solar organic Rankine cycle for remote power generation. In: Solar Energy n. 5, 85, pp. 955–966. DOI: 10.1016/j.solener.2011.02.010.

Quoilin, Sylvain; van den Broek, Martijn; Declaye, Sébastien; Dewallef, Pierre; Lemort, Vincent (2013): Techno-economic survey of Organic Rankine Cycle (ORC) systems. In: Renewable and Sustainable Energy Reviews, 22, pp. 168–186. DOI: 10.1016/j.rser.2013.01.028.

Raade, Justin W.; Padowitz, David (2011): Development of Molten Salt Heat Transfer Fluid With Low Melting Point and High Thermal Stability. In: J. Sol. Energy Eng. n. 3, 133, p. 31013. DOI: 10.1115/1.4004243.

Reddy, Vundela Siva; Kaushik, Subash Chndra; Tyagi, Sudhir Kumar; Panwar, Narayanlal (2010): An Approach to Analyse Energy and Exergy Analysis of Thermal Power Plants: A Review. In: SGRE n. 03, 01, pp. 143–152. DOI: 10.4236/sgre.2010.13019.

Relloso, S.; García, E. (2015): Tower Technology Cost Reduction Approach after Gemasolar Experience. In: Energy Procedia, pp. 1660–1666. DOI: 10.1016/j.egypro.2015.03.125.

Relloso, S. & Delgado, E. (2009). Experience with molten salt thermal storage in a commercial parabolic trough plant. Andasol-1 commissioning and operation, 2009

Rochau, Gary E. (2014): Supercritical CO2 Brayton Cycle: The DOE Program. Supercritical CO2 Power Cycle Symposium. Pittsuburgh, Pennsylvania, 9-10 September. Available at http://www.sco2powercyclesymposium.org/resource_center/development_priorities/supercritical-co2-brayton-cycle-the-doe-program.

Rochau, G., 2011. Supercritical CO2 Brayton cycle. The DOE program. Supercritical CO2 power cycle Symposium. (2011).

Rochau, G.E. (2014) Supercritical CO2 Brayton Cycle: The DOE Program. Supercritical CO2 Power Cycle Symposium. Pittsuburgh, Pennsylvania, 9-10 September. Available at: http://www.sco2powercyclesymposium.org/resource_center/development_priorities/ supercritical-co2-brayton-cycle-the-doe-program. (2014). Available at www.sco2powercyclesymposium.or.

Rodríguez-Sanchez, M., Venegas, M., Marugan-Cruz, C. & Santana, D., March, 2013. Thermal mechanical and hydraulic analysis to optimize the design of molten salt central receivers of solar tower. (2013).

Romero, Manuel; Steinfeld, Aldo (2012): Concentrating solar thermal power and thermochemical fuels. In: Energy Environ. Sci. n. 11, 5, p. 9234. DOI: 10.1039/C2EE21275G.

Rosen, Julia; Egger, Anne E. (2016): Factors that Control Earth's Temperature. Available at https://www.visionlearning.com/es/library/Ciencias-de-la-Tierra/6/Factors-that-Control-Earths-Temperature/234.

Schramek, Philipp; Mills, David R. (2003): Multi-tower solar array. In: Solar Energy n. 3, 75, pp. 249–260. DOI: 10.1016/j.solener.2003.07.004.

Shipley, Anna; Hampson, Anne; Hedman, Bruce; Garland, Patti; Bautista, Paul (2009): DOE Report: Combined Heat and Power: Effective Energy Solutions for a Sustainable Future. In: Cogeneration & Distributed Generation Journal n. 2, 24, pp. 71–74. DOI: 10.1080/15453660909509010.

Solar Millenium AG (2008): The parabolic trough power plants Andasol 1 to 3. Available at http://large.stanford.edu/publications/power/references/docs/Andasol1-3engl.pdf.

Solar Millenium AG, 2008. The parabolic trough power plants Andasol 1 to 3, 2008

Solargis (2018): Global Solar Atlans. Available at https://globalsolaratlas.info/?c=29.67546,27.514881,6&s=30,30.

Sprouse, Charles; Depcik, Christopher (2013): Review of organic Rankine cycles for internal combustion engine exhaust waste heat recovery. In: Applied Thermal Engineering n. 1-2, 51, pp. 711–722. DOI: 10.1016/j.applthermaleng.2012.10.017.

Sullivan, S.; Vollnogle, E.; Kesseli, J.; Nash, J. (a cura di) (2013): High-efficiency low-cost solar receiver for use in a supercritical-CO2 recompression cycle. SunShot Concentrating Solar Power Program Review 2013. Phoenix, Arizona, 23-25 April. Available at https://www.nrel.gov/docs/fy13osti/58484.pdf.

Sullivan, S. et al. (2013) High-efficiency low-cost solar receiver for use in a supercritical-CO2 recompression cycle. SunShot Concentrating Solar Power Program Review 2013. Phoenix, Arizona, 23-25 April. Available at: https://www.nrel.gov/docs/fy13osti/58484.pdf. (2013)

Temple, J., 2017. HeliosCSP. [On line] (2017).

Turchi, W., Ma, Z. & Neises, T., 2013. Thermodynamic study of advanced supercritical carbon dioxide power cycles for high performance concentrating solar power systems. J Sol Energy Eng, Volume 41007, p. 135. (2013).

U.S. Department of Energy (2016) Combined Heat and Power Technology Fact Sheet Series. Available at: https://www.energy.gov/sites/prod/files/2016/09/f33/CHP-Steam%20Turbine.pdf.

Vignarooban, K.; Xu, Xinhai; Arvay, A.; Hsu, K.; Kannan, A. M. (2015): Heat transfer fluids for concentrating solar power systems – A review. In: Applied Energy, 146, pp. 383–396. DOI: 10.1016/j.apenergy.2015.01.125.

Wang, Kun; He, Ya-Ling (2017): Thermodynamic analysis and optimization of a molten salt solar power tower integrated with a recompression supercritical CO 2 Brayton cycle

based on integrated modeling. In: Energy Conversion and Management, 135, pp. 336–350. DOI: 10.1016/j.enconman.2016.12.085.

Wang, Kun; He, Ya-Ling; Zhu, Han-Hui (2017): Integration between supercritical CO 2 Brayton cycles and molten salt solar power towers: A review and a comprehensive comparison of different cycle layouts. In: Applied Energy, 195, pp. 819–836. DOI: 10.1016/j.apenergy.2017.03.099.

Wang, Ning; Xu, Guoying; Li, Shuhong; Zhang, Xiaosong (2017): Thermal Properties and Solar Collection Characteristics of Oil-based Nanofluids with Low Graphene Concentration. In: Energy Procedia, 105, pp. 194–199. DOI: 10.1016/j.egypro.2017.03.301.

Was, G. S.; Ampornrat, P.; Gupta, G.; Teysseyre, S.; West, E. A.; Allen, T. R. et al. (2007): Corrosion and stress corrosion cracking in supercritical water. In: Journal of Nuclear Materials n. 1-3, 371, pp. 176–201. DOI: 10.1016/j.jnucmat.2007.05.017.

Yan, J. & Zhao, C., 2016. Experimental study of CaO/Ca(OH)2 in a fixedebed reactor for thermochemical heat storage. Appl Energy, Volume 175, pp. 277-284. (2016).

Yang, Cheng; Huang, Zhifeng; Ma, Xiaoqian (2018): Comparative study on off-design characteristics of CHP based on GTCC under alternative operating strategy for gas turbine. In: Energy, 145, pp. 823–838. DOI: 10.1016/j.energy.2017.12.145.